AD-A114 808 TORONTO UNIV DOWNSVIEW (ONTARIO) INST FOR AEROSPACE --ETC F/G 20/14
ON THE PASSAGE OF A SHOCK WAVE THROUGH A DUSTY-GAS LAYER,(U)
JAN 82 H MIURA, I I GLASS AFOSR-77-3303
UNCLASSIFIED UTIAS-252 AFOSR-TR-82-0374 NL

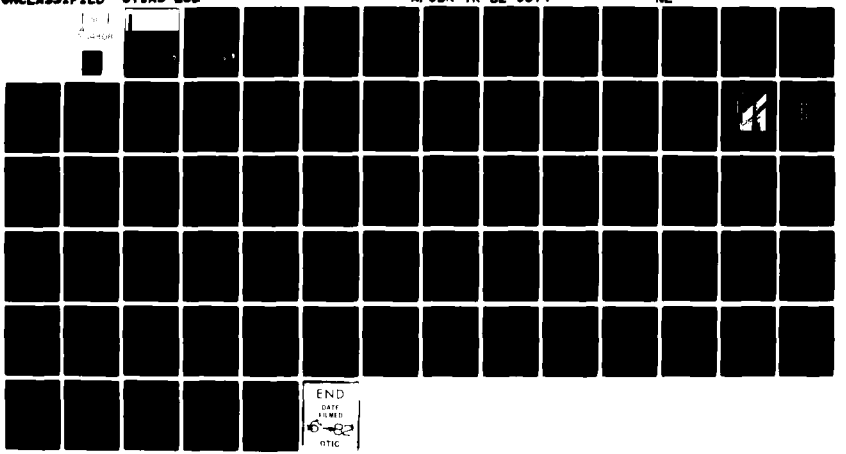

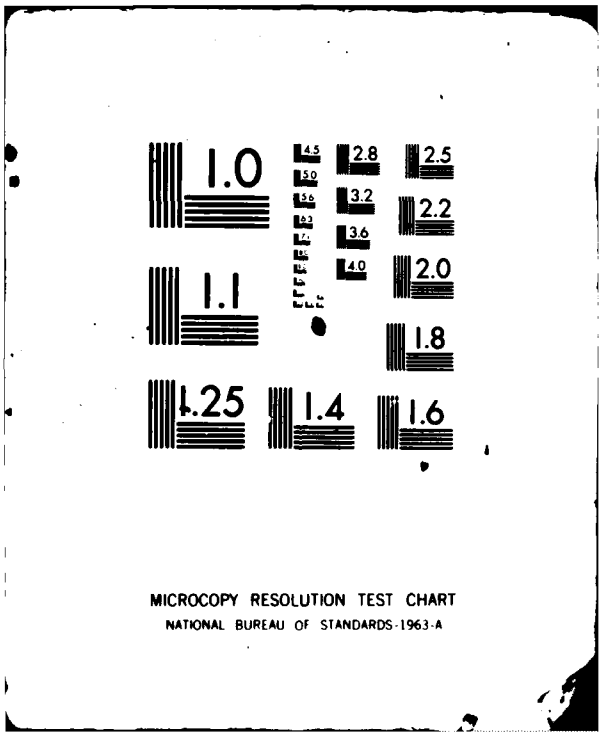
1.0
1.1
1.25
1.4
1.6
1.8
2.0
2.2
2.5
2.8
3.2
3.6
4.0
4.5
5.0
5.6
6.3
MICROCOPY RESOLUTION TEST CHART
NATIONAL BUREAU OF STANDARDS-1963-A

INSTITUTE
FOR
AEROSPACE STUDIES

UNIVERSITY OF TORONTO

AFOSR-TR- 82-0374

(12)

ON THE PASSAGE OF A SHOCK WAVE THROUGH A DUSTY-GAS LAYER

BY

H. MIURA AND I. I. GLASS

JANUARY, 1982

UTIAS REPORT NO. 252
CN ISSN 0082-5255

ON THE PASSAGE OF A SHOCK WAVE THROUGH A DUSTY-GAS LAYER

BY

H. MIURA AND I. I. GLASS

SUBMITTED SEPTEMBER, 1981

JANUARY, 1982

UTIAS REPORT NO. 252
CN ISSN 0082-5255

Acknowledgements

One of us (H. Miura) is grateful to the University of Osaka Prefecture, Sakai, Japan, for making possible his leave at UTIAS.

The financial support received from the Natural Sciences and Engineering Research Council of Canada, the U.S. Air Force under Grant AF-AFOSR-77-3303, the U.S. Army Research Office, and the Defence Research Establishment, Suffield, is acknowledged with thanks.

Summary

The flow resulting from the passage of a shock wave through a dusty-air layer is studied analytically and numerically. For the cases treated here, a shock wave is always reflected at the first contact surface separating the pure gas from the dusty layer and a shock wave is transmitted into the dusty layer. The transmitted shock wave is stronger. The criteria for the reflected wave in terms of the properties of the air and dusty layer are obtained based on an idealized equilibrium-gas approximation. Working curves are presented showing the effects of the suspended particles on the resulting flow. Similarly, at the second contact front of the dusty layer, a rarefaction wave is reflected and the transmitted shock wave transmitted into the air is weakened by this nonlinear interaction. The rarefaction wave reflects at the first contact front as a compression wave and proceeds through the layer to refract at the second contact surface where it reflects as a rarefaction wave and a transmitted compression wave. This wave overtakes the transmitted shock wave in air and produces the final transmitted wave, a new contact surface and a weak reflected rarefaction wave. This final emergent shock wave from the dusty air has almost the same strength as the original shock wave entering the layer. A particular case for an initial shock wave pressure ratio of 5 has been chosen to illustrate this type of interaction in detail.

Finally, the time-dependent transition properties through the shock waves, contact surfaces and rarefaction waves were found by solving the equations of motion numerically using a modified random-choice method with an operator-splitting technique. This provides the details for the formation of the idealized equilibrium flows in the dusty-air layer and the reflected and transmitted shock waves in the air surrounding the dusty-air layer.

CONTENTS

Notation

a_e	equilibrium speed of sound
C_m	specific heat of solid material
C_p	gas specific heat at constant pressure
C_v	gas specific heat at constant volume
C_{ve}	specific heat at constant volume of idealized equilibrium gas
D	drag force acting on a particle
d	particle diameter
k	gas thermal conductivity
m	mass of a particle
p	gas pressure
Q	rate of heat transfer to a particle
R	gas constant
T	gas temperature
t	time from shock penetration across a contact surface
u	gas velocity
u_s	propagation velocity of shock wave
v	velocity of particles
x	space coordinate measured from a contact surface
δ	shock transition thickness
ϑ	temperature of particles
μ	gas viscosity
ρ	gas density
ρ_p	density of solid material
σ	mass concentration of particles

Dimensionless Quantities

C_D	drag coefficient of a particle
M_s	shock Mach number
Nu	Nusselt number of a particle
P	normalized pressure
Pr	gas Prandtl number
Re	particle Reynolds number
T	normalized temperature
U	normalized velocity
X	normalized space coordinate
α	mass concentration ratio σ/ρ
β	specific heat ratio of two phases C_m/C_v
γ	gas specific heat ratio
γ_e	specific heat ratio of idealized equilibrium gas
Γ	normalized mass concentration

1. INTRODUCTION

High-speed flows of a mixture of a gas and small solid particles are encountered in several branches of engineering and science (Refs. 1-6). Shock waves in such a dusty gas exhibit relaxation features typical of two-phase flow. For sufficiently strong shock waves, a discontinuous jump in the gas phase precedes a thick transition region. A nonequilibrium state of the mixture gives way gradually to an equilibrium transition through the transfer of momentum and heat between the gas and the particles. This feature was utilized in experimental studies, using a shock tube, for an understanding of the basic mechanisms of the interaction between the two phases (Refs. 7-9). For example, effective drag coefficients of the particles were deduced from the experimental results,but their values cannot as yet be considered as definitive.

Some experiments used a shock tube in which only a limited portion of the channel was filled with a dusty gas (Refs. 10-14). Apparently a uniform dusty gas is easier to produce in such a configuration. It also has the advantage that disturbances arising from diaphragm rupture are avoided. In this case, a shock wave initially propagating in a pure gas then penetrates the dusty-gas layer and gives rise to a refraction problem.

A numerical analysis of this type of flow was done by Outa, Tajima and Morii (Ref. 12), using the method of characteristics. However, they made an error in calculating the dusty-gas flow by assuming that the mass concentration of the particles vanishes along the boundary particle path. There must be a discontinuity in the mass concentration at the boundary of the particles, since diffusion was not considered. Recently, Marconi, Rudman and Calia (Ref. 15) solved a problem of shock induced flow in a dusty-gas layer using a characteristic-based finite-difference method. This was a less practical case since the incident shock wave was produced by a moving piston and a subsequent reflected shock wave at the piston affected the flow.

In the present analysis the basic features are studied of the flow induced by a shock wave as it penetrates into a dusty-air layer. The transient-flow behaviour is clarified by solving the equations of motion using a modified random-choice method (Ref. 16) together with an operator-splitting technique. Discussions based upon the idealized-equilibrium-gas approximation are also made for a more complete understanding of the flow characteristics. The inverse problem is also considered as the shock wave leaves the dusty-air layer again into free air. The strengths of the initial shock wave as it penetrates the layer and the emergent shock wave as it leaves the layer are compared and discussed. It is shown that the analysis reduces to the case of a gaseous layer embedded in air in a shock-tube channel, very similar to the case studied by Glass and co-workers (Refs. 17-20) nearly three decades ago. The case of a shock wave passing through a helium layer embedded in a channel containing air is illustrated in the time-distance plane on Plate 1 and its explanatory sketch. In this case a rarefaction wave is reflected at the first contact surface and a shock wave at the second contact surface, unlike the passage through a dusty layer where the reverse happens. Had argon or carbon-dioxide been used, then it would have been similar to the dusty-gas layer.

Finally, it is worth noting that in the present analysis the overtaking of the emergent shock wave by the refracted compression wave is also considered in order to give a definite answer as to whether or not the emergent shock wave is weaker than the initial shock wave entering the dusty-air layer. In the particular illustrative examples treated here for an incident shock pressure ratio of 5, the final transmitted shock wave after the nonlinear wave interactions ultimately comes out with almost the same strength as the incident one. Of course, other examples may be treated by the reader following the methods outlined in this report.

2. REFRACTION OF A SHOCK WAVE AT AN AIR/DUSTY-AIR CONTACT FRONT FOR EQUILIBRIUM FLOWS

In this section, we consider the variation of a shock wave when it passes across the contact surface separating a pure gas and a dusty gas of semi-infinite length. This corresponds to the case when the thickness of the dusty-gas layer is much longer than a characteristic relaxation length. As time elapses after the shock wave passes across the contact surface, the particles become in equilibrium with the gas except for the transition region of the shock wave. The dusty gas can be treated effectively as a perfect gas if we neglect, from a large-scale point of view, this nonequilibrium region together with a contact region of finite thickness, which may arise as in the case of a dusty-gas shock tube (Ref. 16). The specific heat at constant volume, the specific heat ratio and the speed of sound of the idealized equilibrium gas are given by (Ref. 4)

$$C_{ve} = \frac{1 + \alpha\beta}{1 + \alpha} C_v \tag{1}$$

$$\gamma_e = \frac{\gamma + \alpha\beta}{1 + \alpha\beta} \tag{2}$$

$$a_e = \sqrt{\frac{\gamma + \alpha\beta}{(1+\alpha)(1+\alpha\beta)} \cdot \frac{p}{\rho}} \tag{3}$$

A shock wave or a rarefaction wave is reflected at the contact surface separating perfect gases of different kinds when an incident shock wave is transmitted (Ref. 19, see Fig. 1). The type of reflected wave, i.e., shock wave, Mach wave or rarefaction wave, is determined according to the conditions (Ref. 17),

$$\left(\frac{\gamma_1+1}{\gamma_1-1} \cdot \frac{p_4}{p_5} + 1\right)\left(\frac{\gamma_5+1}{\gamma_5-1} \cdot \frac{p_4}{p_5} + 1\right)^{-1} - \frac{C_{v1}T_1}{C_{v5}T_5} \gtreqless 0 \tag{4}$$

respectively. This is identical to $p_2/p_4 \gtreqless 1$.

First, we consider a shock wave transmitted from a pure gas to a dusty gas. For this case, we have (see Fig. 1),

$$\gamma_1 = \gamma_e, \qquad C_{v1} = C_{ve}$$
$$\gamma_5 = \gamma, \qquad C_{v5} = C_v \tag{5}$$

If we assume that the temperatures are the same in both gases, the left-hand side of Eq. (4) is calculated as follows:

$$\left(\frac{\gamma_1+1}{\gamma_1-1}\cdot\frac{p_4}{p_5}+1\right)\left(\frac{\gamma_5+1}{\gamma_5-1}\cdot\frac{p_4}{p_5}+1\right)^{-1}\frac{C_{v1}}{C_{v5}}$$

$$=\frac{\alpha}{1+\alpha}\left(\frac{\gamma+1}{\gamma-1}\cdot\frac{p_4}{p_5}+1\right)^{-1}\left\{\left(\frac{2\alpha\beta}{\gamma-1}+\frac{\gamma+1}{\gamma-1}-\beta\right)\frac{p_4}{p_5}-(\beta-1)\right\} \tag{6}$$

Three cases can be found from the above expression according to the value of β:

(i) For $\beta \leqq \gamma/(\gamma-1)$, the right-hand side of Eq. (6) is positive independent of the values of α and p_4/p_5. Therefore, the reflected wave is a shock wave.

(ii) For $(\gamma+1)/(\gamma-1) \geqq \beta > \gamma/(\gamma-1)$, two cases exist depending on the value of α:

(a) For $\alpha \geqq \gamma-1-\gamma/\beta$, the last factor of Eq. (6) is positive because p_4/p_5 is greater than unity. Therefore, the reflected wave is a shock wave independent of the strength of the incident shock wave.

(b) For $\alpha < \gamma-1-\gamma/\beta$, there exists a critical pressure ratio $p_4/p_5 = (\beta-1)[(2\alpha\beta/\gamma-1) + (\gamma+1/\gamma-1) - \beta]^{-1}$ for which the last factor of Eq. (6) vanishes. If the incident shock wave is stronger than this critical one, the reflected wave is a shock wave. On the other hand, a rarefaction wave is reflected if the incident shock wave is weaker than the critical one.

(iii) For $\beta > (\gamma+1)/(\gamma-1)$, three cases exist depending on the value of α:

(a) For $\alpha \geqq \gamma-1-\gamma/\beta$, the reflected wave is a shock wave independent of the strength of the incident shock wave as in (iia).

(b) For $\gamma-1-\gamma/\beta > \alpha \geqq (\gamma-1)/2-(\gamma+1)/2\beta$, a critical pressure exists as in (iib). A shock wave or a rarefaction wave is reflected according to the strength of the incident shock wave.

(c) For $\alpha < (\gamma-1)/2-(\gamma+1)/2\beta$, the last factor of Eq. (6) is negative independent of p_4/p_5. Therefore, the reflected wave is a rarefaction wave for any incident shock wave.

When a shock wave is transmitted into the dusty gas, the gas is decelerated by the particles of large inertia. This deceleration tends to raise the pressure. On the other hand, the particles absorb heat from the gas at high temperature. This absorption of heat or cooling of the gas reduces the pressure. Thus, if the specific heat of the particles is so small that the absorbed heat is sufficiently small, the pressure of the dusty gas becomes higher than that of the pure gas. As a result, a reflected shock wave is induced, for example, as for case (i). Conversely, for particles of large specific heat, a rarefaction wave appears as for case (iiic).

Generally, the specific heat ratio of the two phases β is not so high and case (i) becomes practical, that is, a shock wave is reflected at the contact surface in most cases. However, case (iii) can exist. For example, consider a mixture of argon and polystyrene-particles, for which $\gamma = 1.67$ and $\beta = 4.4$. For this mixture, we can have the three cases: (iiia) for $\alpha \geqq 0.29$, (iiib) for $0.29 > \alpha \geqq 0.032$, and (iiic) for $\alpha < 0.032$. Although the case of a reflected rarefaction wave is interesting, we have found that the rarefaction wave is very weak for this mixture and it will not be discussed further.

For the case of a reflected shock wave, the pressure behind the wave $p_3(=p_2)$ is given by (Refs. 17, 19)

$$\left(\frac{\gamma_1+1}{\gamma_1-1}+\frac{p_5}{p_3}\right)\left(1-\frac{p_5}{p_3}\right)^{-2}\left(\frac{\gamma_5+1}{\gamma_5-1}\cdot\frac{p_5}{p_4}+1\right)\left(\frac{\gamma_5+1}{\gamma_5-1}+\frac{p_5}{p_4}\right)^{-1}$$

$$\times\left[\left(1-\frac{p_5}{p_4}\right)\left(\frac{\gamma_5+1}{\gamma_5-1}\cdot\frac{p_5}{p_4}+1\right)^{-\frac{1}{2}}\left(\frac{p_4}{p_3}\right)^{\frac{1}{2}}+\left(\frac{p_4}{p_3}-1\right)\left(\frac{\gamma_5+1}{\gamma_5-1}+\frac{p_4}{p_3}\right)^{-\frac{1}{2}}\right]^2$$

$$-\frac{C_{v1}}{C_{v5}}=0 \qquad (7)$$

Several working curves for the mixture of air ($\gamma = 1.4$) and glass particles ($\beta = 1$) are presented illustrating the effect of the existence of particles upon the uniform states between the transmitted shock wave, the contact surface and the reflected shock wave. Figure 2 shows the variations of $p_3/p_5(=p_2/p_1)$ with the pressure ratio of the incident shock wave p_4/p_5 for values of α over the range $0 \leqq \alpha \leqq 2$. The pressure p_3 increases with α for a fixed p_4/p_5, that is, the reflected shock wave and transmitted shock wave are stronger for larger mass concentration of particles.

Other flow quantities are calculated from the Rankine-Hugoniot relations (see Appendix A). The variations of the velocity of the fluid between the reflected and transmitted shock waves u_2/a_5 with the incident shock pressure ratio are shown in Fig. 3. The particles decelerate the gas and therefore the mixture velocity reduces with α for a fixed p_4/p_5. The temperature behind the transmitted shock wave T_2 decreases as a result of absorption of energy by the particles (Fig. 4), but the pure gas is heated by the reflected shock wave

(Fig. 5). The density ratios $\rho_2/\rho_5(=\sigma_2/\sigma_1)$ and ρ_3/ρ_5 are raised by the deceleration of the gas due to the existence of the particles and by the induced reflected shock wave, respectively (Figs. 6, 7). The former is larger than the latter, as expected. A contact region separates these layers of different densities and temperatures.

Figure 8 shows the variations of the transmitted shock Mach number based on the frozen speed of sound equal to a_5. The presence of the particles reduces the speed of propagation of the transmitted shock wave. For sufficiently high mass concentration of the particles, the transmitted shock wave propagates at a lower velocity than the frozen speed of sound so that it must be fully dispersed.

3. REFRACTION OF A SHOCK WAVE AT A DUSTY-AIR/AIR CONTACT FRONT FOR EQUILIBRIUM FLOWS

Next, we consider a shock wave transmitted from a dusty gas to a pure gas. For this case, we have

$$\gamma_1 = \gamma, \qquad C_{v1} = C_v$$
$$\gamma_5 = \gamma_e, \qquad C_{v5} = C_{ve} \tag{8}$$

The left-hand side of Eq. (4) is calculated with these values in a similar way to Eq. (6). The same factor as the last one on the right-hand side of Eq. (6) also appears, but with a changed sign. Therefore, the criteria (i), (ii) and (iii) explained above still holds for this case, although the reflected shock wave should now read as the reflected rarefaction wave and vice versa. Thus, a rarefaction wave is reflected generally at the contact surface.

When a rarefaction wave is reflected at the contact surface, the pressure behind the wave $p_3(=p_2)$ is given by (Refs. 17, 19)

$$\left(\frac{p_3}{p_4}\right)^{\frac{\gamma_5-1}{2\gamma_5}} + \left(\frac{\gamma_5+1}{\gamma_5-1} + \frac{p_5}{p_4}\right)^{\frac{1}{2}} \left(\frac{\gamma_5+1}{\gamma_5-1}\cdot\frac{p_5}{p_4} + 1\right)^{-\frac{1}{2}} \left(\frac{p_3}{p_4} - \frac{p_5}{p_4}\right)$$
$$\times \left(\frac{\gamma_5-1}{2\gamma_5}\cdot\frac{C_{v1}}{C_{v5}}\right)^{\frac{1}{2}} \left(\frac{\gamma_1+1}{\gamma_1-1}\cdot\frac{p_3}{p_4} + \frac{p_5}{p_4}\right)^{-\frac{1}{2}} - \left(1 - \frac{p_5}{p_4}\right)$$
$$\times \left(\frac{\gamma_5-1}{2\gamma_5}\right)^{\frac{1}{2}} \left(\frac{\gamma_5+1}{\gamma_5-1}\cdot\frac{p_5}{p_4} + 1\right)^{-\frac{1}{2}} - 1 = 0 \tag{9}$$

We now present the working curves showing the variations of the flow quantities with the incident shock pressure ratio p_4/p_5 for the mixture of air and glass-particles. The pressure behind the transmitted shock wave p_2 is smaller than p_4 behind the incident shock wave in the dusty gas (see Fig. 9) and a rarefaction wave is reflected.

Variations of the velocity in the region between the transmitted and the reflected waves normalized by the frozen speed of sound equal to a_1 are shown in Fig. 10. The values of the velocity u_4 of the dusty gas behind the incident shock wave are also shown by the thin lines for comparison. The gas in state (3) is accelerated to a higher velocity after it is released from the restraints of the dust particles. The temperature of the gas behind the transmitted shock wave becomes higher than that behind the incident shock wave (Fig. 11). On the other hand, the dusty gas cools after the reflected rarefaction wave passes through (Fig. 12). Larger changes in temperature are produced for larger mass concentrations of particles. The densities of the gases behind the transmitted and the reflected waves are smaller than that behind the incident shock wave (Figs. 13, 14). Comparing these two figures, we see that the gas behind the reflected rarefaction wave is denser than the gas behind the transmitted shock wave.

Variations of the transmitted shock Mach number with the incident shock pressure ratio are shown in Fig. 15. It is seen that the transmitted shock wave propagates at higher speed than the propagation velocity of the incident shock wave in the dusty gas. It is seen that there is a region where a fully dispersed shock wave in the dusty gas can eventually become a sharp fronted transition in air. That is the reverse of the case of refraction from air into a dusty gas.

4. TIME-DEPENDENT NONEQUILIBRIUM REFRACTION AT AN AIR/DUSTY-AIR CONTACT FRONT

The transient flow induced after a shock wave passes across a contact surface is discussed in this section. The dusty gas is assumed to consist of a perfect gas and a lot of solid spheres of uniform size. The viscosity and thermal conductivity of the gas are taken into account only for the interaction between the gas and the particles. We consider the cases when the mass concentration of the particles is comparable to the density of the gas. The volume occupied by the particles is negligible because the density of the solid particle is much larger than that of the gas.

The equations of continuity, momentum and energy for either the gas or the particles are given by (Refs. 1-6)

$$\frac{\partial \rho}{\partial t} + \frac{\partial}{\partial x}(\rho u) = 0 \tag{10}$$

$$\frac{\partial \sigma}{\partial t} + \frac{\partial}{\partial x}(\sigma v) = 0 \tag{11}$$

$$\frac{\partial}{\partial t}(\rho u) + \frac{\partial}{\partial x}(\rho u^2) + \frac{\partial p}{\partial x} = -\frac{\sigma}{m} D \tag{12}$$

$$\frac{\partial}{\partial t}(\sigma v) + \frac{\partial}{\partial x}(\sigma v^2) = \frac{\sigma}{m} D \tag{13}$$

$$\frac{\partial}{\partial t}\left\{\rho\left(C_v T + \tfrac{1}{2}u^2\right)\right\} + \frac{\partial}{\partial x}\left\{\rho u\left(C_p T + \tfrac{1}{2}u^2\right)\right\} = -\frac{\sigma}{m}(vD+Q) \tag{14}$$

$$\frac{\partial}{\partial t}\left\{\sigma\left(C_m\theta + \tfrac{1}{2}v^2\right)\right\} + \frac{\partial}{\partial x}\left\{\sigma v\left(C_m\theta + \tfrac{1}{2}v^2\right)\right\} = \frac{\sigma}{m}(vD+Q) \tag{15}$$

where p, ρ, T, u are the pressure, density, temperature and velocity of the gas and σ, θ, v are the mass concentration, temperature and velocity of the particles, respectively. The equation of state for the thermally perfect gas is given by

$$p = \rho RT \tag{16}$$

The gas and the particles interact with each other through the drag force D and the heat transfer rate Q experienced by a particle in nonequilibrium with the gas. We take in the present study (Refs. 21, 22)

$$D = \frac{\pi}{8} d^2 \rho (u-v)|u-v| C_D$$

$$= \frac{\pi}{8} d^2 \rho (u-v)|u-v|(0.48 + 28\mathrm{Re}^{-0.85}) \tag{17}$$

$$Q = \pi d \mu C_p \mathrm{Pr}^{-1}(T-\theta)\mathrm{Nu}$$

$$= \pi d \mu C_p \mathrm{Pr}^{-1}(T-\theta)(2.0 + 0.6\mathrm{Pr}^{\frac{1}{3}}\mathrm{Re}^{\frac{1}{2}}) \tag{18}$$

where Re is the Reynolds number based upon the diameter of the particle and the relative velocity of the particle to the gas,

$$\mathrm{Re} = \rho|u-v|d/\mu \tag{19}$$

and Pr is the Prandtl number of the gas,

$$\mathrm{Pr} = \mu C_p/k \tag{20}$$

The viscosity and the thermal conductivity of the gas vary with the temperature. We consider air in this section, for which (Ref. 23)

$$\mu = 1.71\times10^{-4} \times \left(\frac{T}{273}\right)^{0.77} \text{ poise} \tag{21}$$

and

$$\mathrm{Pr} = 0.75 \tag{22}$$

While the equations governing the motion of the dusty gas have been described, the pure gas obeys Eqs. (10), (12) and (14) with $\sigma = 0$, and Eq. (16).

The numerical method applied to the present problem is the same as in Ref. 16, that is, a modified random-choice method together with an operator-splitting technique as follows. Two sets of equations derived from Eqs. (10)-(15) are considered. One set is obtained by omitting the inhomogeneous terms on the right-hand sides. The other set is obtained by omitting the terms differentiated with respect to x. Solving these two sets of equations alternately for each time step results in the solution of the problem.

The former set of homogeneous equations is solved by the random-choice method (Refs. 16, 24-27). In this method discontinuities can be described definitively, as artificial viscosity is not required. The elementary calculation of the random-choice method is to determine by random sampling the solutions at the mid-point between two adjacent points, where the solution is known at a previous time. The equations for the gas are not coupled with those for the particles in this set of equations. Taking step-like initial conditions for the gas phase in the elementary calculation, one obtains classical shock-tube solutions (Refs. 25-27). On the other hand, one assumes initially a linear distribution of particles in order to avoid the difficulty that the solution becomes multivalued for step-like conditions. A step-like initial condition is taken only at a boundary of the particles for the boundary to be definite. Further details are given in Ref. 16.

Numerical calculations were done for the mixture of air ($\gamma = 1.4$) and glass-particles ($\beta = 1$) of 10 μm diameter with a mass concentration ratio $\alpha = 1$. A space mesh size of $\Delta X = 0.1$ was used in most cases and a time step was taken as the Courant-Friedrichs-Lewy condition allowed.

The transition of the flow occurring when the incident shock wave of $p_4/p_5 = 5$ in a pure gas penetrates into a semi-infinite dusty-gas region is shown in Figs. 16-19. The dusty gas was assumed initially to be at atmospheric pressure and room temperature. In all figures, the distance from the initial contact surface is measured in units of $4\rho_p d/3\rho_1 = 2.72$ cm. Thermodynamic quantities are normalized by the corresponding values of the dusty gas before the shock transmission. The velocities are measured in the speed of sound for the pure gas $(\gamma p_1/\rho_1)^{\frac{1}{2}} = 350$ m/sec.

Flow structures arising when a small time ($t = 0.78\times10^{-4}$ sec) has elapsed after the shock penetrates the dusty layer are shown in Fig. 16. The particles cannot respond quickly enough to the abrupt change in the state of the gas at the shock front, but are gradually accelerated and heated by the gas around them (Figs. 16c, d). On the other hand, the temperature and velocity of the gas in the dusty-gas region are reduced from the values for the incident shock wave. This interaction of the two phases reduces the frozen shock jump at the shock front. The gas is compressed as a result of deceleration. Figures 16a and b show that the pressure and density of the gas in the dusty-gas region are raised higher than the incident values. They take on maxima at the boundary

of the particles at this stage. The compression of the gas results in a shock wave that is reflected back into the pure gas. Its initial formation can be seen in Fig. 16. It is noted in Fig. 16b that the particle concentration rises gradually behind the shock front, reaches a maximum and then drops suddenly to zero.

Subsequent transitional behaviours of the flow are shown in Fig. 17 ($t = 1.56 \times 10^{-4}$ sec) and Fig. 18 ($t = 3.12 \times 10^{-4}$ sec). The differences in temperature and velocity between the gas and the particles behind the transmitted shock wave diminish with time. While the discontinuous jump in the gas phase at the transmitted shock front decays, the formation of the reflected shock wave in the pure gas becomes more distinguished. It can be seen from Figs. 17b and c that a contact region including the boundary of theparticles begins to form.

The variations of flow quantities at $t = 2.81 \times 10^{-3}$ sec are shown in Fig. 19. The exact solution for the idealized equilibrium gas is also presented for comparison. The present results agree well with the idealized solution. The reflected shock wave in the pure gas is almost steady, although it is still followed by a weak compressive part. Its position is a little behind that for the idealized solution. This difference is brought about by a delay in response of the particles when the incident shock wave penetrated into a dusty gas. The reflected shock wave moves at a small speed in the laboratory frame, since the induced velocity of the gas behind the incident shock wave is fairly large. A stationary structure of the contact region is seen in Figs. 19b and c, where the particles are in equilibrium with the gas. The mass concentrations and temperatures of the two phases vary smoothly in the region and change discontinuously at the boundary of the particles. The structure of the contact region reflects the history of the interaction which the particles experienced so far. An almost stationary structure of the transmitted shock wave in the dusty gas has developed, which consists of an initial frozen shock front followed by the relaxation region. The particles are in nonequilibrium with the gas in the transition region. The particles and the gas interact with each other to establish an equilibrium profile.

The shock pressure ratio p_2/p_1 is found to be 6.09, from Eq. (7). The stationary structure of the transmitted shock wave can be obtained separately by solving the set of ordinary differential equations for a coordinate system moving steadily with the shock wave. Figure 20 shows the results for the transition region obtained by making use of the Runge-Kutta method. Comparing Figs. 19 and 20, we see the structure of the transmitted shock wave in the nonstationary solution is close to that of the stationary shock wave. It should be noted that the temperature of the gas exhibits an overshoot in the transition region.

Next, we consider a case when the incident shock pressure ratio is so small that a fully dispersed shock wave may arise in the dusty-gas layer. Developments of the flow after the incident shock wave with $p_4/p_5 = 1.5$ penetrates into a dusty-gas region of semi-infinite length are shown in Figs. 21, 22 and 23. The flow structure at $t = 3.12 \times 10^{-4}$ sec is given in Fig. 21. The frozen jump at the shock front is seen to decrease but the formation of the reflected shock wave in the pure gas is very gradual in comparison with the case of a strong shock wave (see Fig. 18).

The variations of flow quantities at $t = 2.81 \times 10^{-3}$ sec are shown in Fig. 22. The solution for the idealized equilibrium gas is also illustrated by the dashed lines for comparison. The present results agree fairly well with it, but the flow is still developing. The flow quantities vary gradually in the reflected wave and a discontinuous jump does not form as yet. The frozen front of the transmitted shock wave has almost decayed.

The flow structure at a later time, $t = 5.30 \times 10^{-3}$ sec, is shown in Fig. 23. It can be seen that the compressive reflected wave has further steepened. An almost stationary contact region has formed, which exhibits discontinuities in density and temperature at the boundary of the particles It should be noted that the transmitted shock wave has dispersed much more since $t = 2.81 \times 10^{-3}$ sec (note that different scales of distance are used in Figs. 22 and 23). The stationary structure of the fully dispersed shock wave, for which the shock pressure ratio is 1.584 corresponding to the present nonstationary case, was solved by means of the Runge-Kutta method and is presented in Fig. 24. A comparison of the shock structures in Figs. 23 and 24 shows that the flow over the transition region in Fig. 23 does not attain the final stationary state. Further dispersion through the interaction between the gas and the particles must follow. Thus, much time is needed for the flow to become stationary even after the frozen shock front has decayed (see Appendix B).

5. TIME-DEPENDENT NONEQUILIBRIUM REFRACTION AT A DUSTY-AIR/AIR CONTACT FRONT

The inverse problem will be considered for the case when a stationary shock wave in a dusty gas is transmitted into a pure gas of semi-infinite length. We take the stationary shock transition shown in Fig. 20 as the initial condition for the incident shock wave. The flow structure at $t = 0.78 \times 10^{-4}$ sec after the shock penetration is shown in Fig. 25. The gas ahead of the particles moves at a higher velocity than it moved in the relaxation region of the incident shock wave, since the gas is not restrained by the particles (Fig. 25d). This increases the discontinuous jump at the shock front transmitted into the pure gas. Concurrently, an expansion of the gas is induced in the downstream region behind the discontinuous shock front. The pressure, density and temperature of the gas decrease from the values for the incident shock wave. The early formation of the reflected rarefaction wave can be seen in Fig. 25. The particles are overtaken by the gas of higher velocity and temperature to be accelerated and heated (Figs. 25c, d).

The flow behaviour at $t = 1.56 \times 10^{-4}$ and 3.12×10^{-4} sec are shown in Figs. 26 and 27, respectively. The discontinuous transmitted shock wave increases in strength. The rarefaction wave reflected into the dusty gas continues to develop. The temperature and velocity of the particles are increased further. It should be noted in Fig. 27c that the temperature of the particles is higher than the gas temperature after the rarefaction wave has passed owing to their thermal inertias. Note also that a contact region begins to form ahead of the boundary of the particles (Fig. 27b).

Further development of the flow is shown in Fig. 28 for $t = 2.81 \times 10^{-3}$ sec. The exact solution for the idealized equilibrium gas is also shown by the dashed lines for comparison. The transmitted wave can be seen to be

quite stationary. The difference in its position between the present result and the idealized solution is due to the delay time required for its formation. It is also seen from Figs. 28b and c that a stationary contact region has formed around the boundary of the particles. This contact region has no discontinuity in the density and temperature of the gas. The reflected rarefaction wave in the dusty gas is still developing. It should be noted that the rarefaction wave is carried by the dusty gas flow to the right against its direction of propagation owing to the high dust velocity. While its position agrees well with that of the idealized solution, the rarefaction wave is considerably extended by comparison with the idealized solution owing to the differences in temperature and velocity between the two phases. The calculations were done up to $t = 5.9\times10^{-3}$ sec. Although at later time the flow structure exhibited almost similar characteristics, the degree of extension of the rarefaction wave diminishes relatively. Since the head and tail of the rarefaction wave must ultimately propagate at the equilibrium speed of sound, the extent of the wave will approach that of the idealized solution after a long time.

The transmission of a fully dispersed shock wave from a dusty gas to a pure gas is solved taking the stationary shock structure shown in Fig. 24 as the initial condition for the calculation. The flow behaviour at $t = 1.87\times10^{-3}$ sec after the shock penetration into the pure gas is shown in Fig. 29. Only small changes in pressure, density and velocity can be seen. The temperature of the gas ahead of the boundary of the particles is raised and a sharp peak in temperature is observed (Fig. 29c). Figure 30 shows the flow structure at $t = 3.74\times10^{-3}$ sec. The flow has changed considerably, but is still far from the idealized equilibrium-gas flow illustrated by the dashed lines. The variation of the pressure does not exhibit any definite structures of the transmitted and reflected waves. The temperature and velocity of the gas ahead of the particles are raised to the values higher than the incident values. However, the variations of flow quantities there are very gradual. Steep changes in density and temperature near the boundary of the particles indicate the formation of a contact region.

The flow structure at a later time, $t = 6.86\times10^{-3}$ sec, is shown in Fig. 31. Although the variation of the flow is still gradual, we can distinguish the formations of the transmitted shock wave and the reflected rarefaction wave. The form of the transmitted shock wave in the pure gas becomes very steep. Nonlinear effects will make this wave discontinuous in time. The temperature and velocity of the particles have approached those of the gas and a structure of the reflected rarefaction wave in the dusty gas can be seen in the figures. The width of the rarefaction wave is much larger than that of the idealized solution as in the case of a strong incident shock wave. The structure of the contact region can also be distinguished. The uniform states of the flow separated by the transmitted shock wave, the contact region and the reflected wave are almost attained. Their positions, however, are much different from those of the idealized equilibrium gas. This means that much time is needed for the relaxation of the two phases to be accomplished when the change of the flow is small.

6. NONEQUILIBRIUM PASSAGE OF A SHOCK WAVE THROUGH A DUSTY-GAS LAYER

The transmission of a shock wave by a dusty gas layer of finite thickness is studied next. Figure 32 shows the flow structure at $t = 2.18\times10^{-3}$ sec

after the shock penetration into the dusty-gas layer of 27.2 cm initial thickness. (The dusty gas has filled initially the region of $0 < X < 10$ in the figures.) Other conditions were the same as those of the semi-infinite case considered in Figs. 16-19. It is seen in Fig. 32 that the shock wave has passed through the layer. The thickness of the layer is so thin that the transmitted shock wave, when it was in the dusty-gas layer, could not attain its stationary value. The reflected shock wave arising when the incident shock wave passed across the contact surface can be seen to propagate in the pure gas to the left in the figures. After the transmitted shock wave passed through the dusty-gas layer, a rarefaction wave is induced to propagate in the layer. This rarefaction wave penetrates into the pure gas upstream. The wave is seen to lie between the reflected shock wave and the boundary of the particles in Fig. 32. Although the rarefaction wave does not overtake the reflected shock wave as yet in the figures, the latter will almost vanish after being overtaken by the former.

The magnitude of the discontinuities in the flow variables at the frozen shock front diminishes while the shock wave propagates in the dusty-gas layeras in Figs. 16-18. After it comes out of the dusty-gas layer, its magnitude recovers with time. It can be seen from Fig. 32 that the values of flow quantities immediately behind the transmitted shock front are very close to those behind the incident shock wave. A weak compression wave, CW, is seen to follow the shock front in Fig. 32a, arising when the reflected rarefaction wave passes across the upstream contact surface of the dusty-gas layer, C (Fig. 34). This compressive wave is transmitted out of the layer and overtakes the preceding shock front δt_2. Their subsequent overtaking cause the shock wave to achieve almost its original incident strength.

The dusty-gas layer has been compressed to be 9.2 cm thick as is seen from Fig. 32b. The pressure and the velocity are almost uniform over the layer. Only the mass concentration and the temperature vary across the layer, but the particles are almost in equilibrium with the gas (see Figs. 32c and d). It can be seen from Figs. 32b and c that the nonuniform state of the gas protrudes downstream of the layer. These nonuniform conditions of the flow around the dusty-gas layer are the remains from the passage of the shock wave through the layer. The nonuniform state will last until the viscous and thermal diffusion of the gas, as well as the particle diffusion, remove it.

Figure 33 shows the flow structure at $t = 4.99 \times 10^{-3}$ sec after the shock penetration into a dusty-gas layer of the 136 cm initial thickness. (The initial position of the dusty gas was over $0 < X \leq 50$ in Fig. 33). A reflected rarefaction wave coming out of the dusty-gas layer is clearly seen to follow the reflected shock wave. The transmitted shock wave is not affected yet by a compression produced when the reflected rarefaction wave passed across the upstream boundary of the particles. The thickness of the dusty-gas layer is fairly large so that the downstream flow structure is close to that of the semi-infinite case (see Fig. 28).

When the thickness of the dusty-gas layer is very large (say 4 meters), we will find the reflected shock wave in the pure gas is like that shown in Fig. 19. The reflected rarefaction wave in the dusty-gas layer and the transmitted shock wave in the pure gas, on the other hand, will be as shown in Fig. 28. Thus the strength of the transmitted shock wave (shock pressure ratio = 4.83) is weaker than that of the incident shock wave (shock pressure

ratio = 5.0) if we neglect the overtaking compression wave that can result from the refraction of the induced rarefaction wave at C_1 (see Fig. 34). The transmitted shock wave will be strengthened when it is overtaken by a shock wave developing from the compression wave, as in Fig. 34. The shock pressure ratio of this final transmitted shock wave can be calculated on the equilibrium-flow approximation and is found to be 5.005 for the present case. Thus, its strength for all intents is almost the same as that of the incident shock wave.

7. CONCLUSIONS

The passage of a shock wave into a dusty-air layer was solved on the basis of an idealized equilibrium gas which ignores the transition zones. Using the full time-dependent equations of motion, it was shown how the shock wave and contact region transitions develop to their equilibrium transitions. The idealized equilibrium-gas analysis provided the criteria for the type of reflected wave which occurs at the contact surface separating a pure gas from a dusty gas. In the present case, a shock wave is reflected when the incident shock wave advances from air into a dusty-air layer and a rarefaction wave is reflected when the shock wave again comes out of the dusty layer into air. Working curves showing the effects of the presence of the dusty-gas layer on the uniform flow states formed after a shock wave passes through the first and second contact surfaces were obtained for a dusty gas with $\gamma = 1.4$ and $\beta = 1$. The strength of the shock wave coming out of a dusty-air layer of large thickness can be found from these curves as a function of the incident shock-pressure ratio. The effects of the subsequent wave interaction by the overtaking compression wave was also analysed for one particular case for illustrative purposes.

The transitions of the flow are studied numerically by means of a modified random-choice method with an operator-splitting technique. Calculations were done for the propagation of a shock wave through a layer with a semi-infinite or finite thickness of dusty air containing 10 μm glass particles. When the shock wave penetrates into the dusty gas, its frozen front decreases as a result of the absorption of energy by the particles. Consequently, the pressure of the gas at some distance behind the shock front increases beyond its initial value owing to the deceleration of the flow caused by the particles. Similar transition effects occur for all physical quantities. A shock wave is reflected from the first contact region into the pure air and a rarefaction wave from the second contact region into the dusty gas. When the shock wave comes out of the dusty-gas layer, the gas is released from the restraint of having particles to accelerate and the shock wave recovers much of its strength. An expansion of the gas occurs downstream as a result of its acceleration and a rarefaction wave forms and is reflected back into the dusty air. The contact regions have finite transition thicknesses. For a dusty-air layer of finite thickness, the reflected rarefaction wave interacts with the first contact region and reflects as a compression wave, which is transmitted at the second contact region and then overtakes the emergent shock wave and causes it to recover more of its original strength. For the particular case of an incident shock strength of pressure ratio of 5.000 the final transmitted wave strength is for all intents the same (5.005). Only the variations of mass concentrations and temperatures of the mixture remain in the dusty-air layer as remnants of the shock-wave passage. For a weak incident shock wave, the transmitted

shock wave in the dusty gas can be fully dispersed. Here the formation of the reflected shock and rarefaction waves at the contact transmission fronts are found to take a long time.

Experimental verification of this analysis will be done in the near future at UTIAS. Of course, different layers and gases can be used and analysed. However, the present study will provide important insight into the forthcoming experimental studies and into the practical field cases of blast waves passing through dusty-air layers.

REFERENCES

1. Soo, S. L. "Fluid Dynamics of Multiphase Systems", Blaisdell, Waltham, 1967.

2. Rudinger, G. "Relaxation in Gas-Particle Flow", in P. P.Wegener, "Nonequilibrium Flows", Vol. 1, Part 1, Marcel Dekker, New York, 1969, pp. 119-161.

3. Wallis, G. B. "One-Dimensional Two-Phase Flow", McGraw-Hill, New York, 1969.

4. Marble, F. E. "Dynamics of Dusty Gases", Annual Review of Fluid Mechanics, Vol. 2, 1970, pp. 397-446.

5. Boothroyd, R. G. "Flowing Gas-Solid Suspensions", Chapman and Hall, London, 1971.

6. Rudinger, G. "Fundamentals of Gas-Particle Flow", Elsevier, Amsterdam, 1980.

7. Crowe, C. T.
Nicholls, J. A.
Morrison, R. B. "Drag Coefficients of Inert and Burning Particles Accelerating in Gas Streams", 9th Int. Symp. Combustion, Academic Press, 1963, pp. 395-406.

8. Selberg, B. P.
Nicholls, J. A. "Drag Coefficient of Small Spherical Particles", AIAA Journal, Vol. 6, 1968, pp. 401-408.

9. Rudinger, G. "Effective Drag Coefficient for Gas-Particle Flow in Shock Tubes", Trans. ASME, Journal of Basic Engng., Vol. 92, 1970, pp. 165-172.

10. Mirtich, M. J.
Herman, M. "Feasibility of Accelerating Micron-Size Particles in Shock Tube Flows for Hypervelocity Degradation of Reflective Surfaces", NASA Tech. Note TDN-3187, 1966.

11. Nettleton, M. A.
Stirling,R. "The Ignition of Clouds of Particles in Shock Heated Oxygen", Proc. Roy. Soc. A300, 1967, pp. 62-77.

12. Outa, E.
Tajima, K.
Morii, H. "Experiments and Analyses on Shock Waves Propagating Through a Gas-Particle Mixture", Bulletin of JSME, Vol. 19, 1976, pp. 384-394.

13. Lowenstein, A. I.
von Rosenberg, C. W., Jr. "Shock Tube Studies of Coal Devolatilization", Shock Tube and Shock Wave Research, Proc. 11th Int. Symp. on Shock Tubes and Waves, Seattle, 1977.

14. Oman, R. A.
Konopka, W.
Calia, V. S. "A Technique for Controlled Gas/Particle Radiation Experiments", Grumman Res. Dept. Memo, RM-686J, 1979.

15. Marconi, F.
Rudman, S.
Calia, V. "One Dimensional Unsteady Two-Phase Flows with Shock Waves", AIAA 13th Fluid and Plasma Dynamics Conf., 1980, AIAA-80-1448.

16. Miura, H.
Glass, I. I.
"On a Dusty-Gas Shock Tube", UTIAS Report No. 250, 1981.

17. Bitondo, D.
Glass, I . I.
Patterson, G. N.
"One-Dimensional Theory of Absorption and Amplification of a Plane Shock Wave by a Gaseous Layer", UTIA Report No. 5, 1950.

18. Bitondo, D.
"Experiments on the Amplification of a Plane Shock Wave", UTIA Report No. 7, 1950.

19. Ford, C. A.
Glass, I. I.
"An Experimental Study of One-Dimensional Shock-Wave Refraction", J. Aeronaut. Sci., Vol. 23, 1956, pp. 189-191.

20. Glass, I . I.
Hall, J. G.
Handbook of Supersonic Aerodynamics, Section 18, Shock Tubes, Government Printing Office, Washington, D.C., 1959.

21. Gilbert, M.
Davis, L.
Altman, D.
"Velocity Lag of Particle in Linearly Accelerated Combustion Gases", Jet Propulsion, Vol. 25, 1955, p. 26.

22. Knudsen, J. G.
Katz, D. L.
"Fluid Mechanics and Heat Transfer", McGraw-Hill, New York, 1958.

23. Chapman, S.
Cowling, T. G.
"The Mathematical Theory of Non-Uniform Gases", Cambridge Univ. Press, 1961.

24. Glimm, J.
"Solutions in the Large for Nonlinear Hyperbolic Systems of Equations", Comm. on Pure & Appl. Math., Vol. 18, 1965, pp. 697-715.

25. Chorin, A. J.
"Random Choice Solution of Hyperbolic Systems", J. Computational Physics, Vol. 22, 1976, pp.517-533.

26. Sod, G. A.
"A Numerical Study of a Converging Cylindrical Shock", J. Fluid Mech., Vol. 83, 1977, pp. 785-794.

27. Saito, T.
Glass, I. I.
"Applications of Random-Choice Method to Problems in Shock and Detonation-Wave Dynamics", UTIAS Report No. 240, 1979.

PLATE 1(a) REFRACTION OF A PLANE SHOCK WAVE IN AIR THROUGH A LAYER OF HELIUM.

Composite photograph of two (x,t)-plane schlieren records showing the double refraction of a plane shock wave at a helium layer and the resulting subsequent overtaking of two shock waves moving in the same direction.

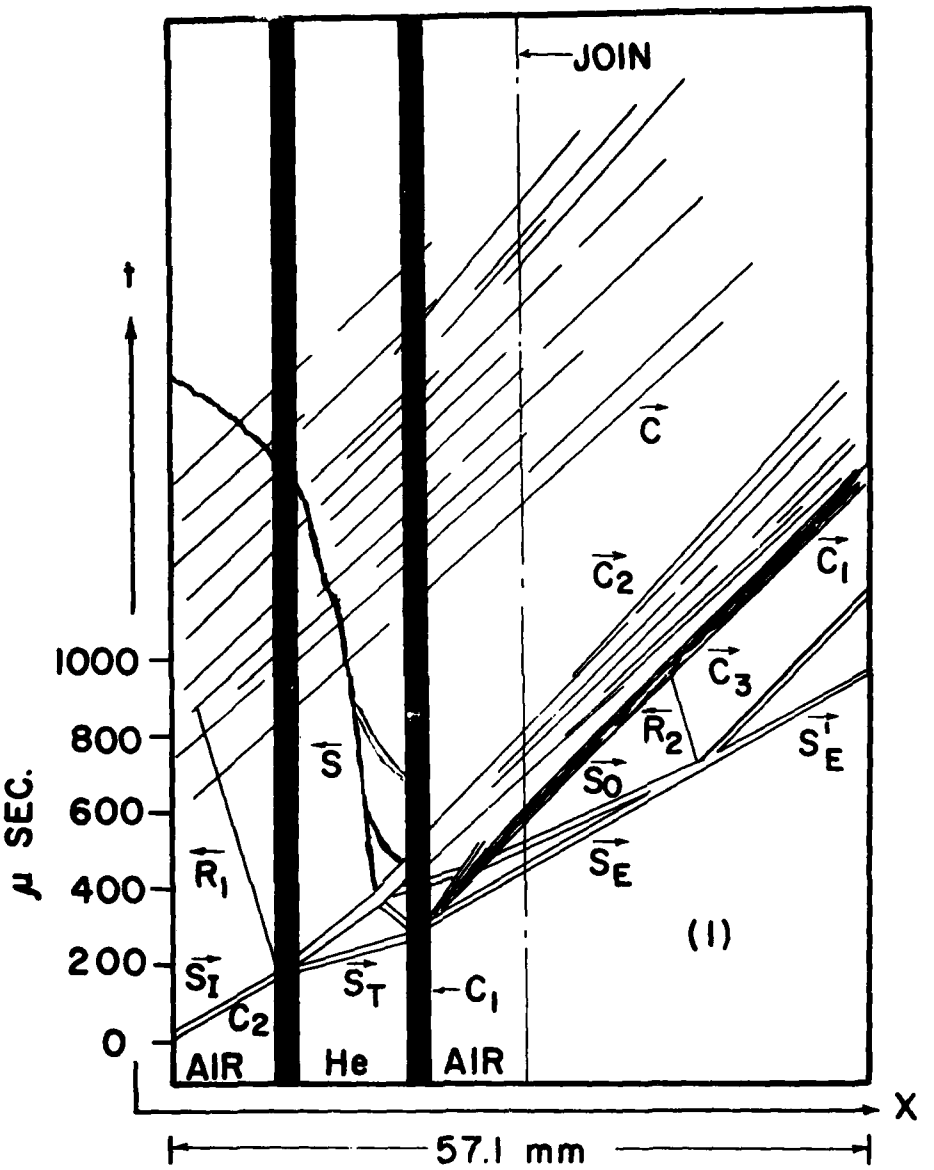

PLATE 1(b) REFRACTION OF A PLANE SHOCK WAVE IN AIR THROUGH A LAYER OF HELIUM.

Explanatory line diagram of (a). The gases are at rest and at atmospheric pressure initially. The incident shock wave S_I, in air, refracts into helium at the microfilm contact surface C_2, causing a transmitted shock wave S_T, and a reflected rarefaction wave R_1. The transmitted shock wave S_T refracts into air at the microfilm contact surface C_1, generating an emerging shock wave S_E, and a reflected shock wave S, which refracts at C_2, producing a reflected shock wave S_O; which overtakes S_E. This gives rise to the final shock wave S_E', a perfect contact surface C_3, and a very weak reflected rarefaction wave R_2. The initial refraction at C_2 causes shock S_I to attenuate in pressure ratio in the helium layer. The second refraction at C_1 amplifies the pressure ratio of S_E in air. However, owing to the nonlinear nature of the refractions S_E is weaker than S_I. The overtaking of S_O and S_E now amplify S_E' so that it is nearly the same strength as S_I. Note the rapid diffusion of the helium-air contact surfaces at C_1 and C_2 and the very stable contact surface C_3 in air, Mach numbers of S_I = 1.70, S_E = 1.65 and S_E' = 1.69, pressure ratio across R_2 = 0.97.

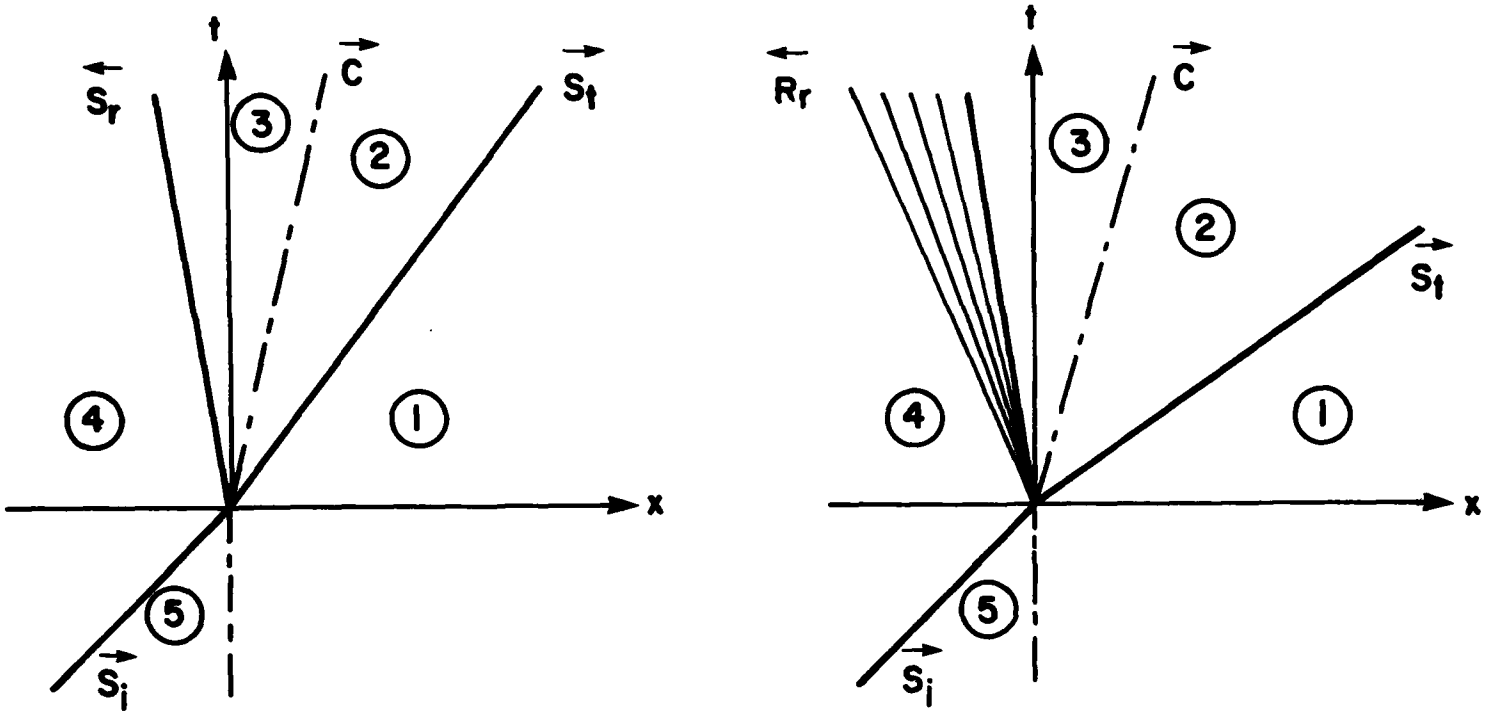

(A) REFLECTED SHOCK WAVE

(B) REFLECTED RAREFACTION WAVE

FIG. 1 SCHEMATIC DIAGRAM OF TRANSMISSION AND REFLECTION OF A SHOCK WAVE AT A DUSTY-GAS CONTACT SURFACE.

$\vec{S}_i$ = INCIDENT SHOCK WAVE; $\vec{S}_t$ = TRANSMITTED SHOCK WAVE; $\vec{C}$ = CONTACT SURFACE; $\vec{S}_r$ = REFLECTED SHOCK WAVE; $\vec{R}_r$ = REFLECTED RAREFACTION WAVE.

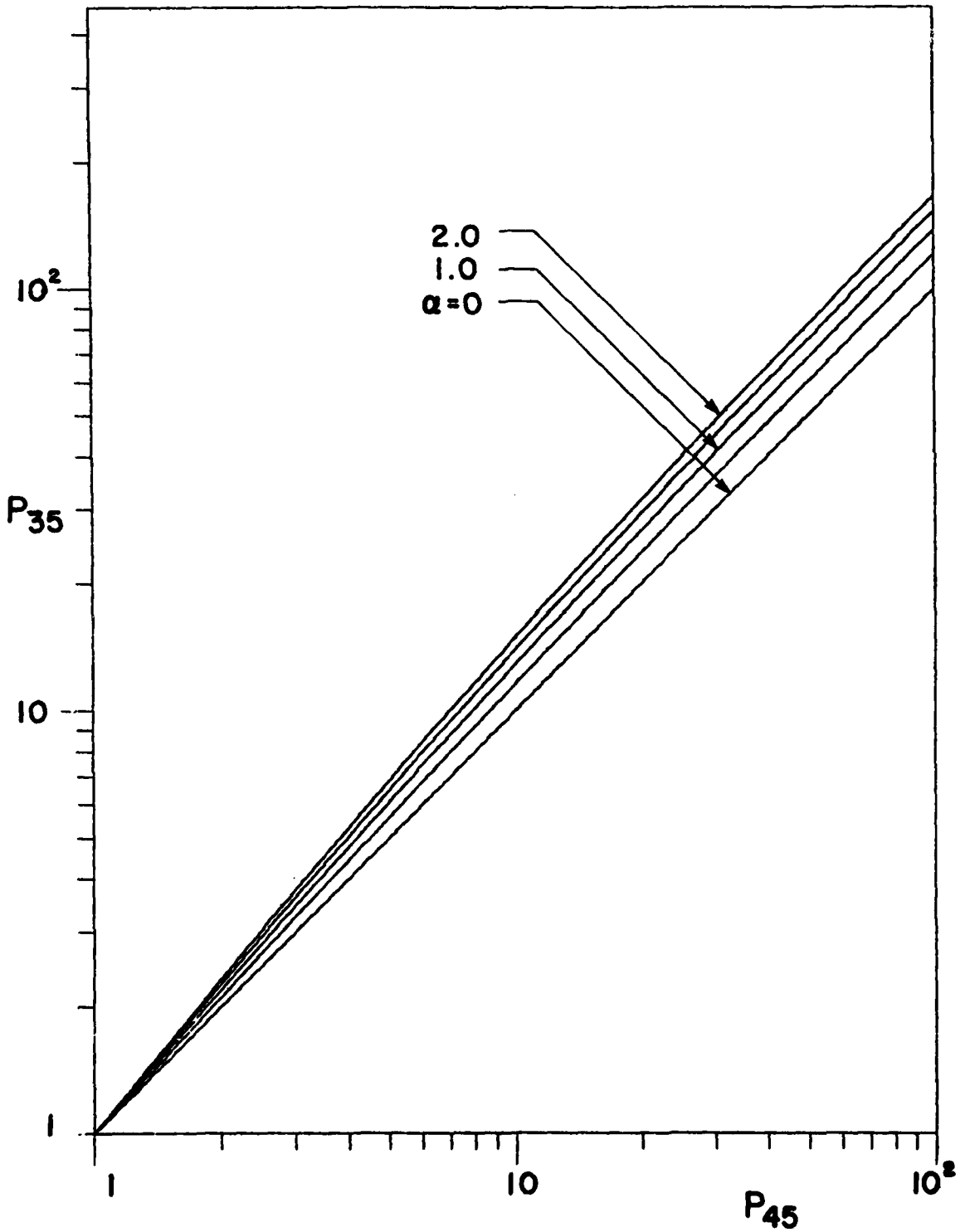

FIG. 2 VARIATION OF FLOW PRESSURE RATIO p_3/p_5 (= p_2/p_1) WITH INCIDENT SHOCK PRESSURE RATIO p_4/p_5.

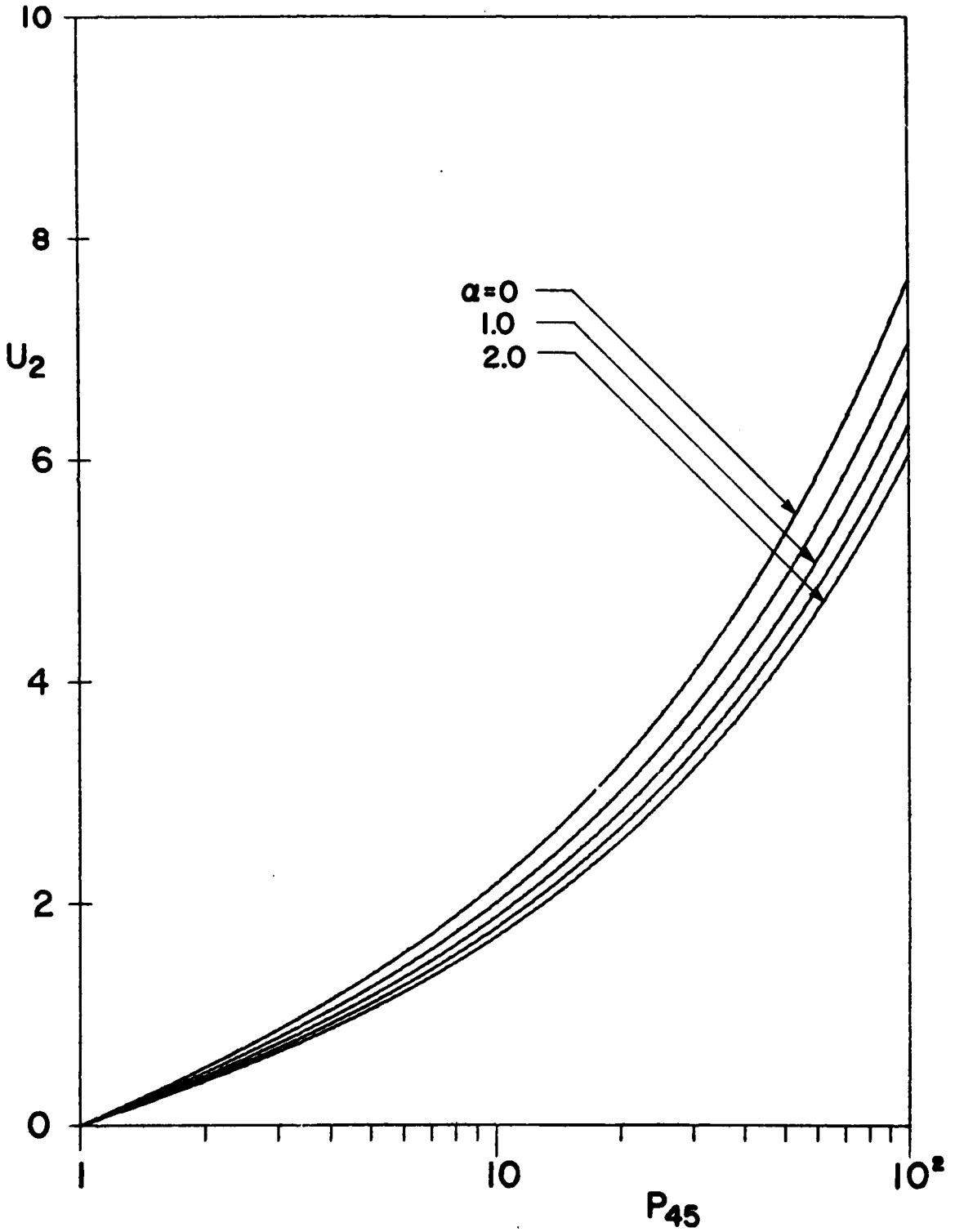

FIG. 3 VARIATION OF FLOW VELOCITY u_2/a_5 WITH INCIDENT SHOCK PRESSURE RATIO p_4/p_5.

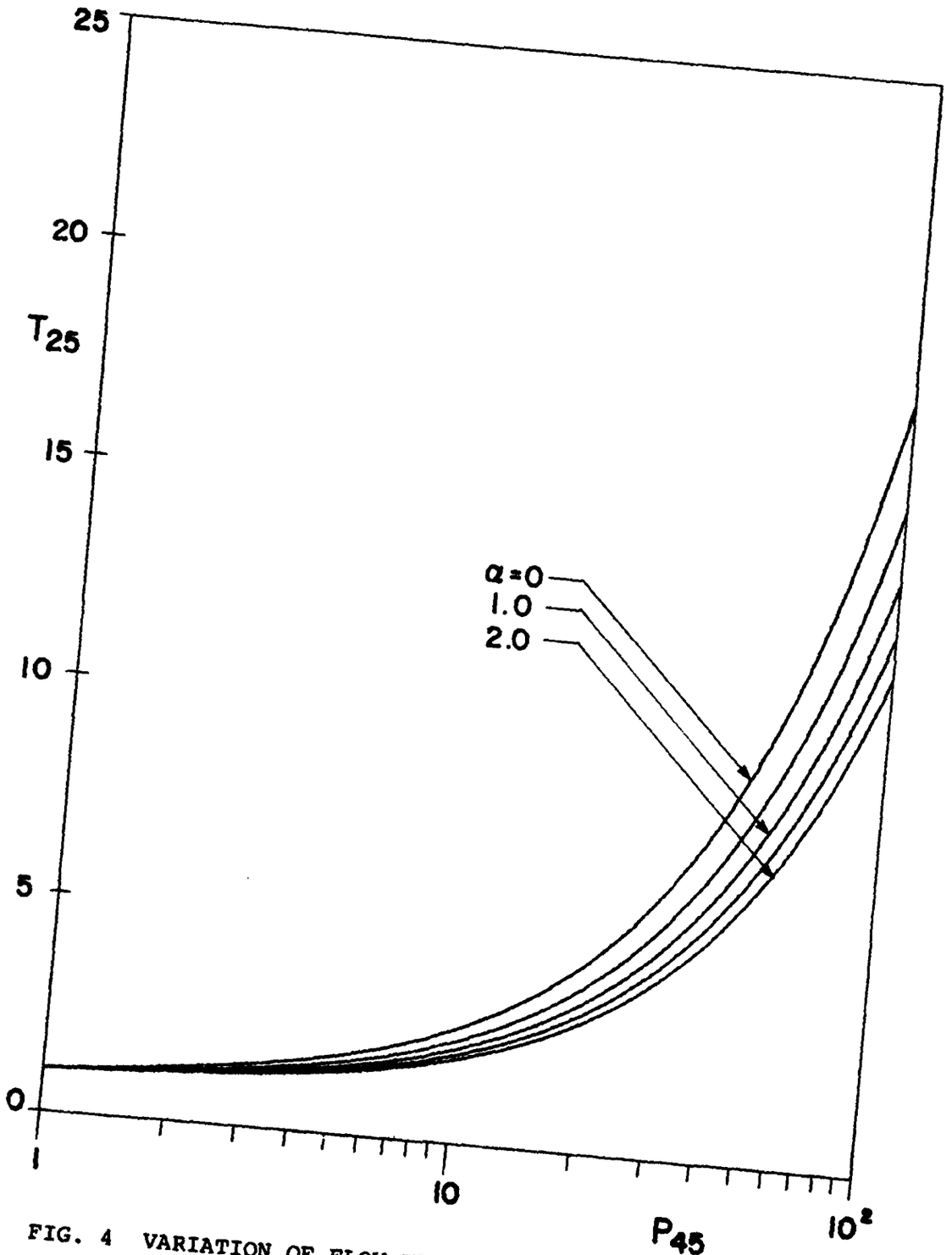

FIG. 4 VARIATION OF FLOW TEMPERATURE RATIO T_2/T_5 WITH INCIDENT SHOCK PRESSURE RATIO P_4/P_5.

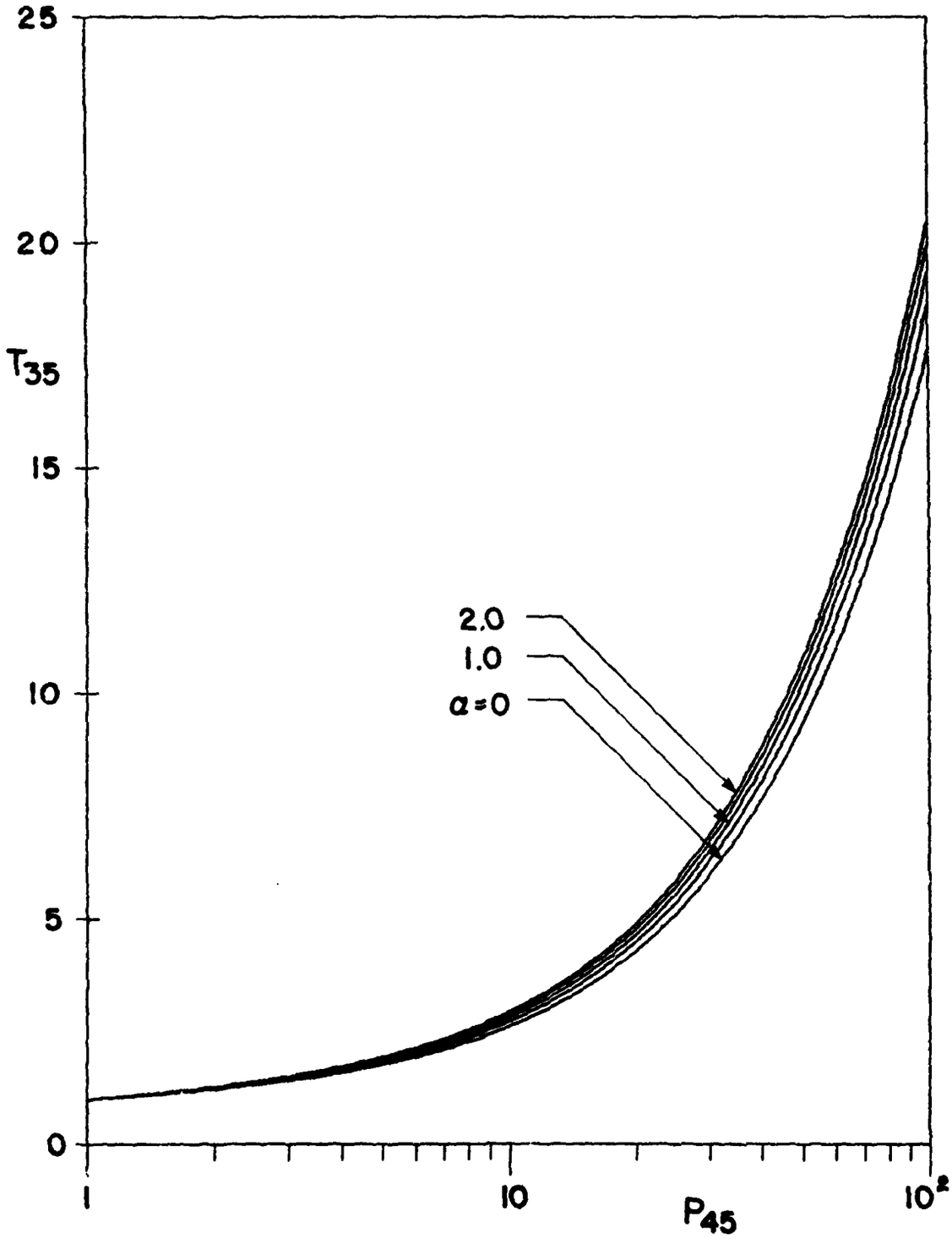

FIG. 5 VARIATION OF FLOW TEMPERATURE RATIO T_3/T_5 WITH INCIDENT SHOCK PRESSURE RATIO p_4/p_5.

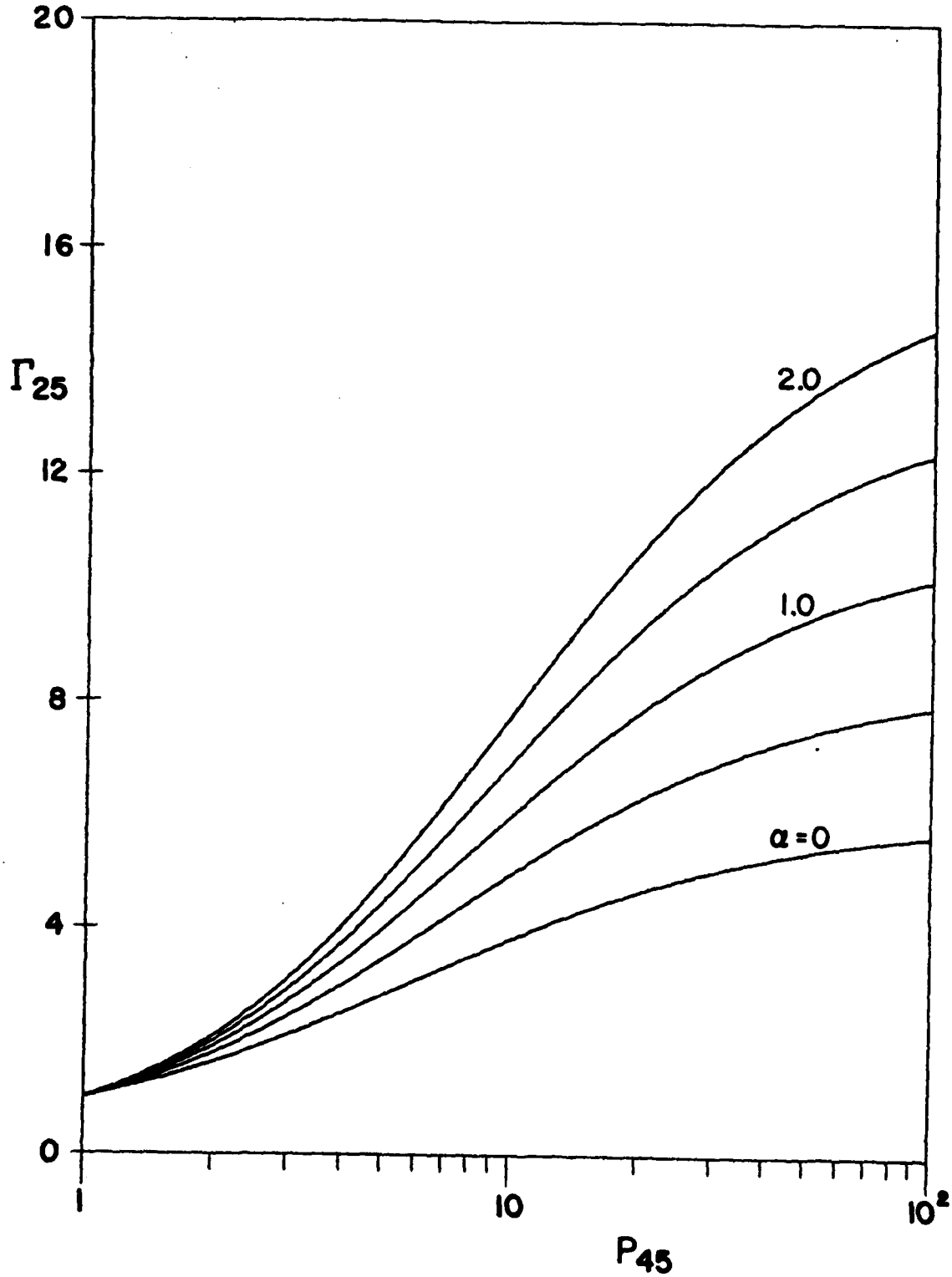

FIG. 6. VARIATION OF FLOW DENSITY RATIO ρ_2/ρ_5 $(= \sigma_2/\sigma_1)$ WITH INCIDENT SHOCK PRESSURE RATIO p_4/p_5.

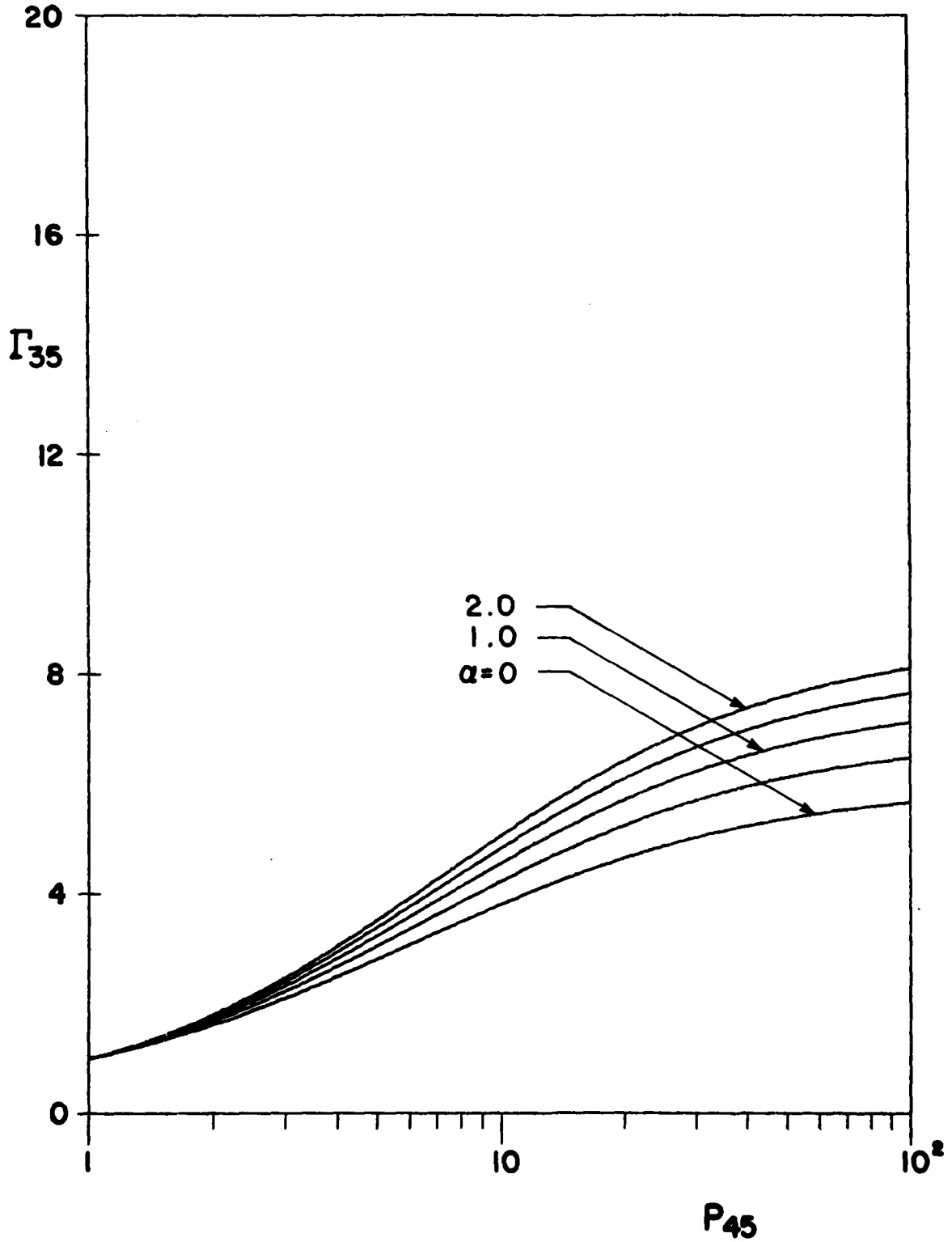

FIG. 7 VARIATION OF FLOW DENSITY RATIO ρ_3/ρ_5 WITH INCIDENT SHOCK PRESSURE RATIO p_4/p_5.

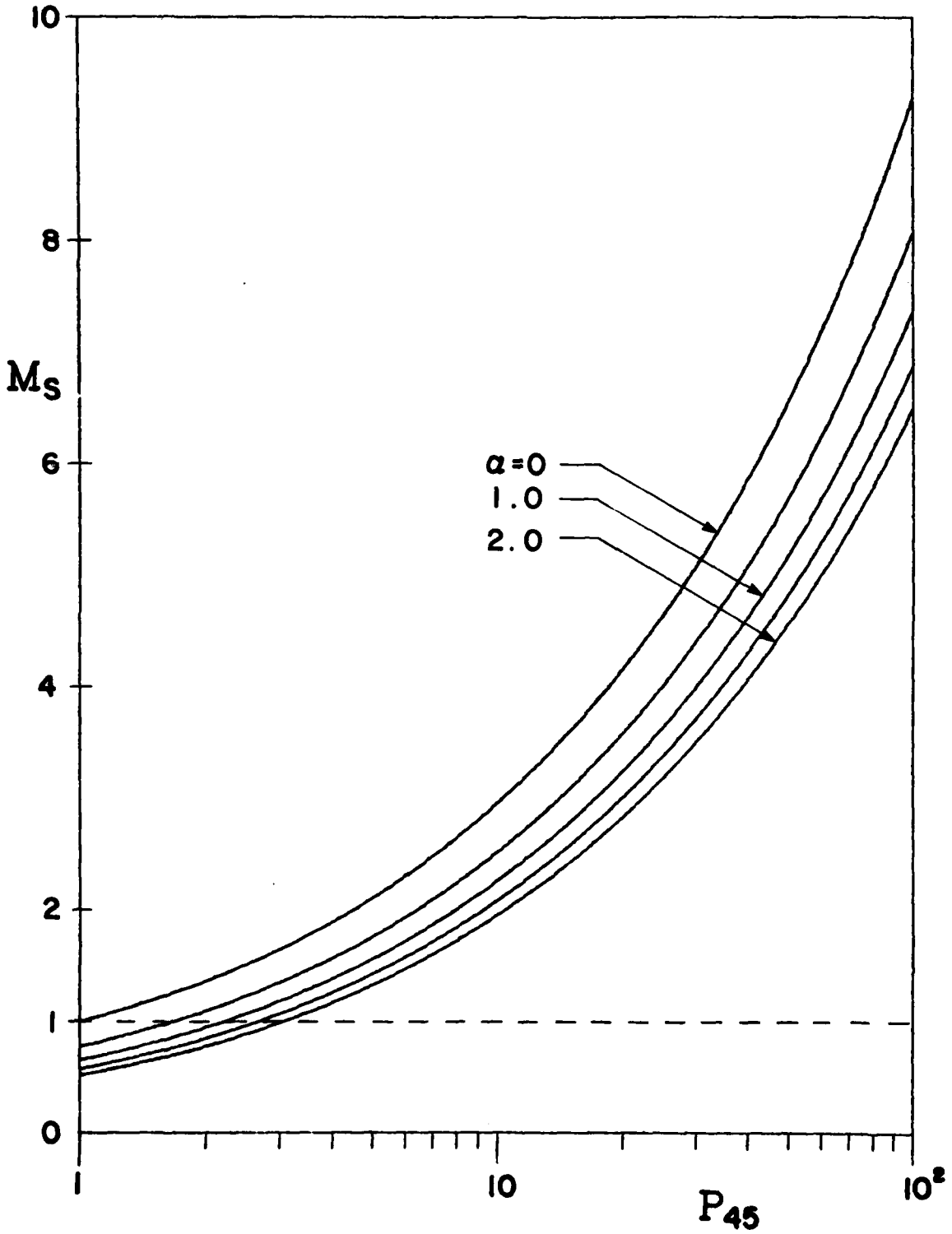

FIG. 8 VARIATION OF TRANSMITTED SHOCK MACH NUMBER $M_S = u_s/a_5$ WITH INCIDENT SHOCK PRESSURE RATIO p_4/p_5.

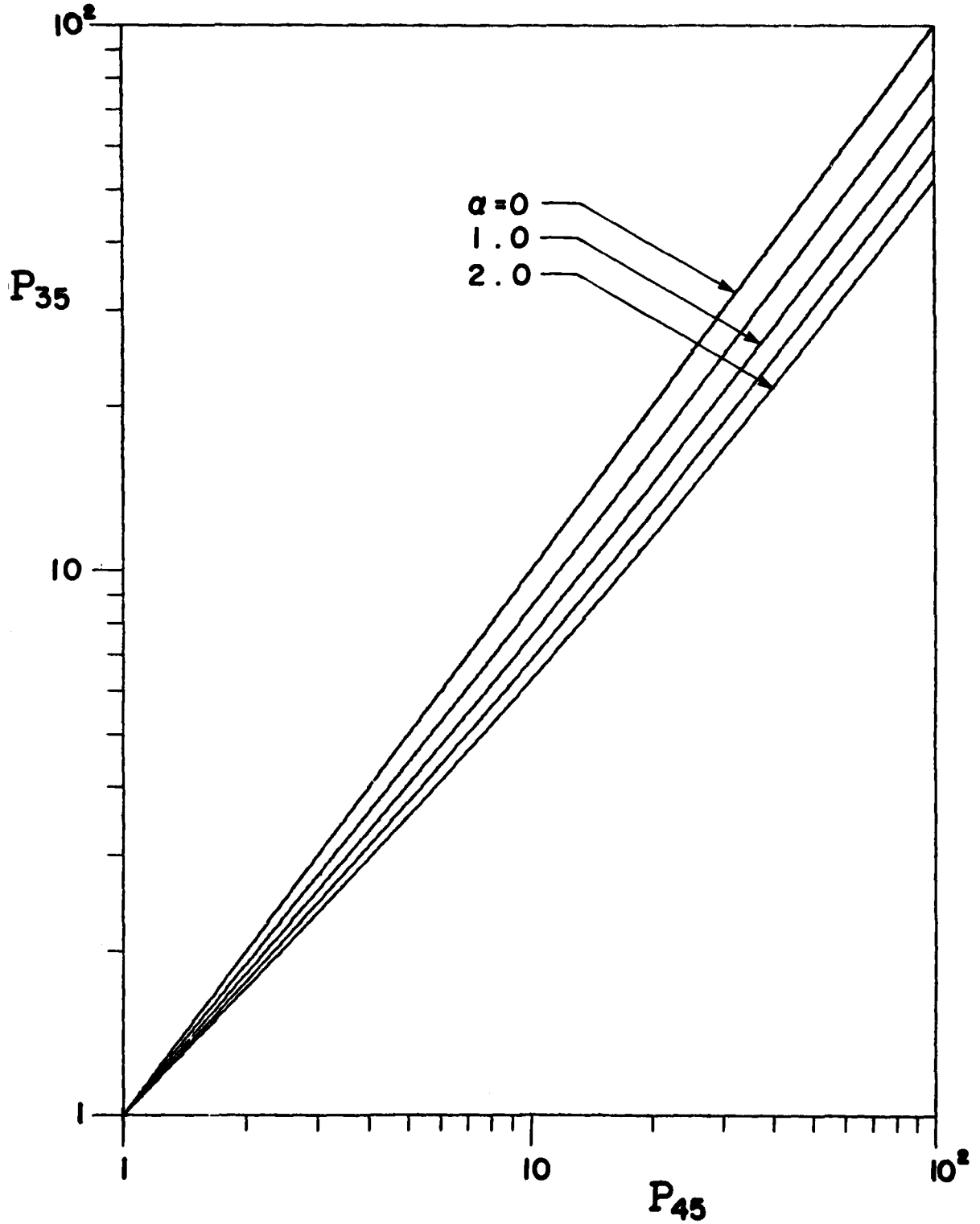

FIG. 9 VARIATION OF FLOW PRESSURE RATIO p_3/p_5 ($= p_2/p_1$) WITH INCIDENT SHOCK PRESSURE RATIO p_4/p_5.

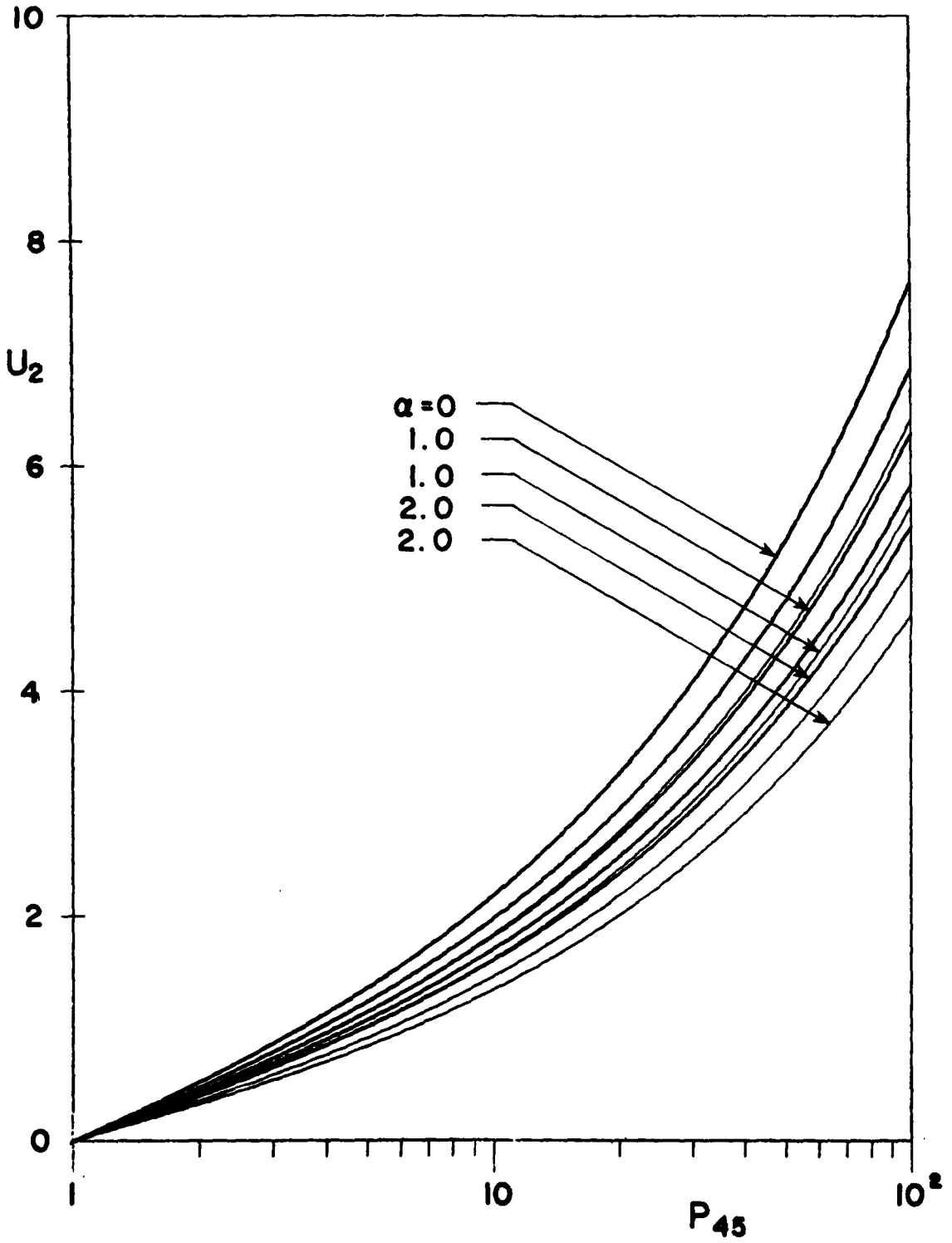

FIG. 10 VARIATION OF FLOW VELOCITY u_2/a_1 WITH INCIDENT SHOCK PRESSURE RATIO p_4/p_5.

——— u_2/a_1, ——— u_4/a_1.

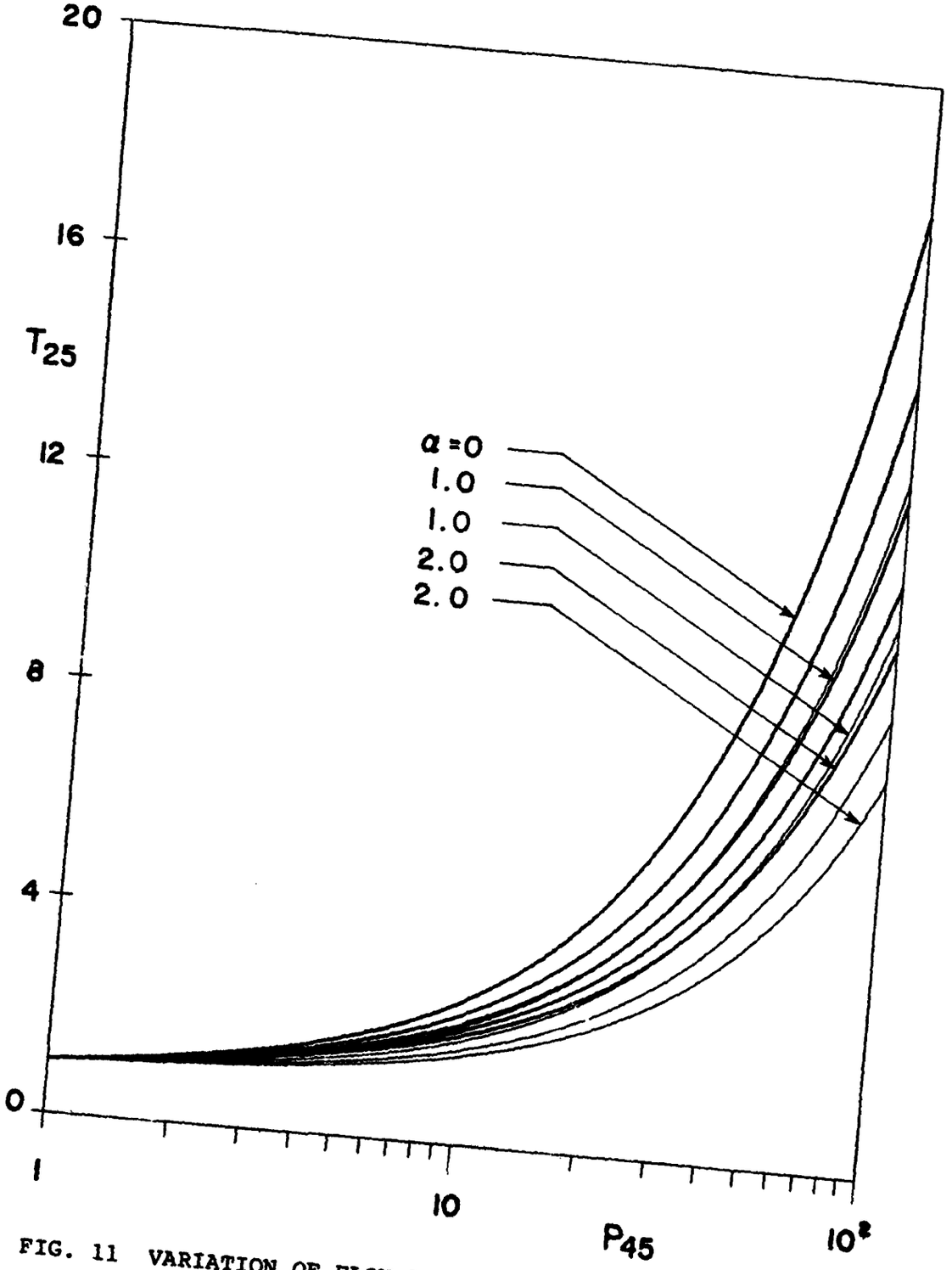

FIG. 11 VARIATION OF FLOW TEMPERATURE RATIO T_2/T_5 WITH INCIDENT SHOCK PRESSURE RATIO p_4/p_5.
——— T_2/T_5, ——— T_4/T_5.

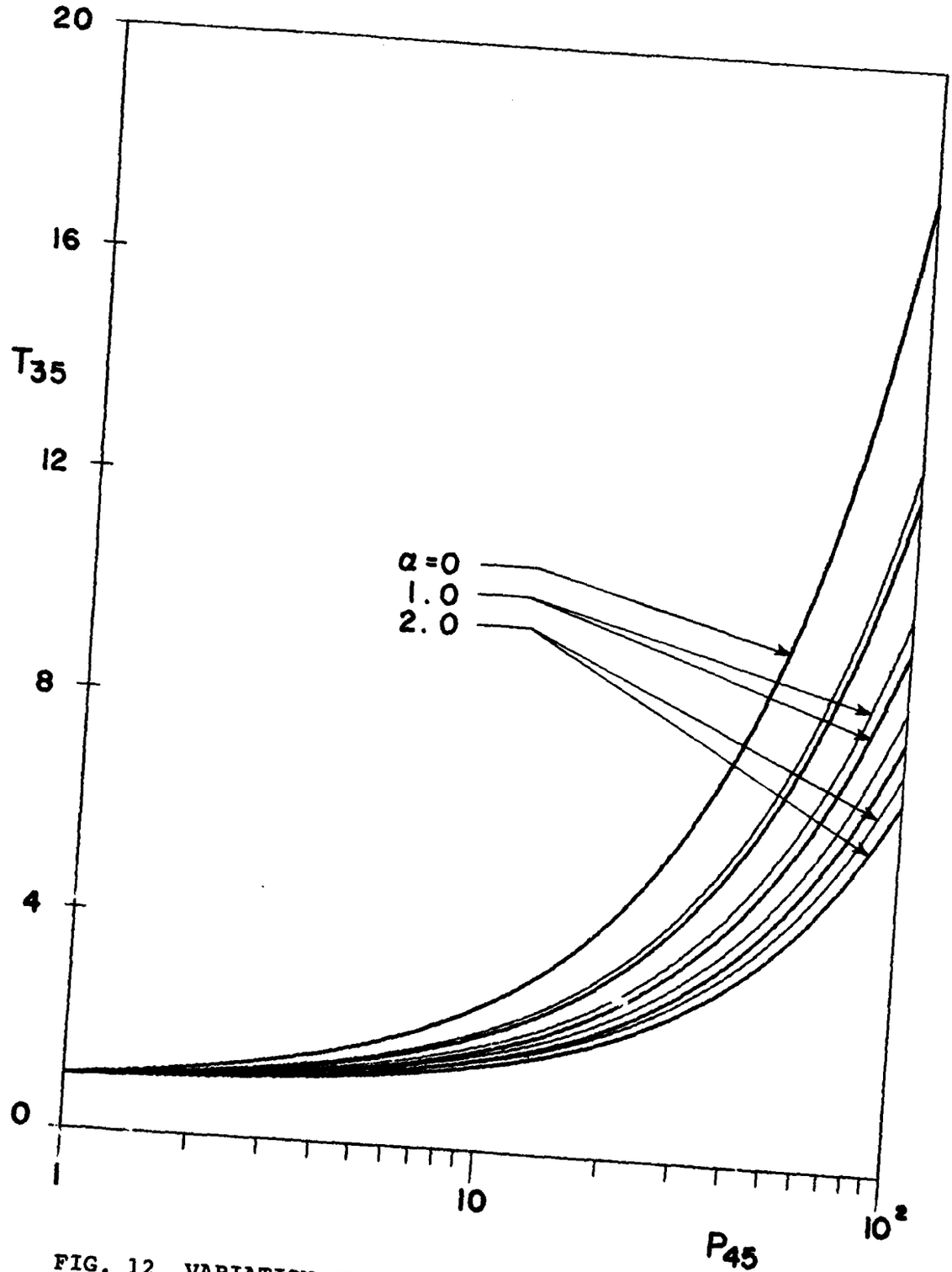

FIG. 12 VARIATION OF FLOW TEMPERATURE RATIO T_3/T_5 WITH INCIDENT SHOCK PRESSURE RATIO P_4/P_5.
——— T_3/T_5, ——— T_4/T_5.

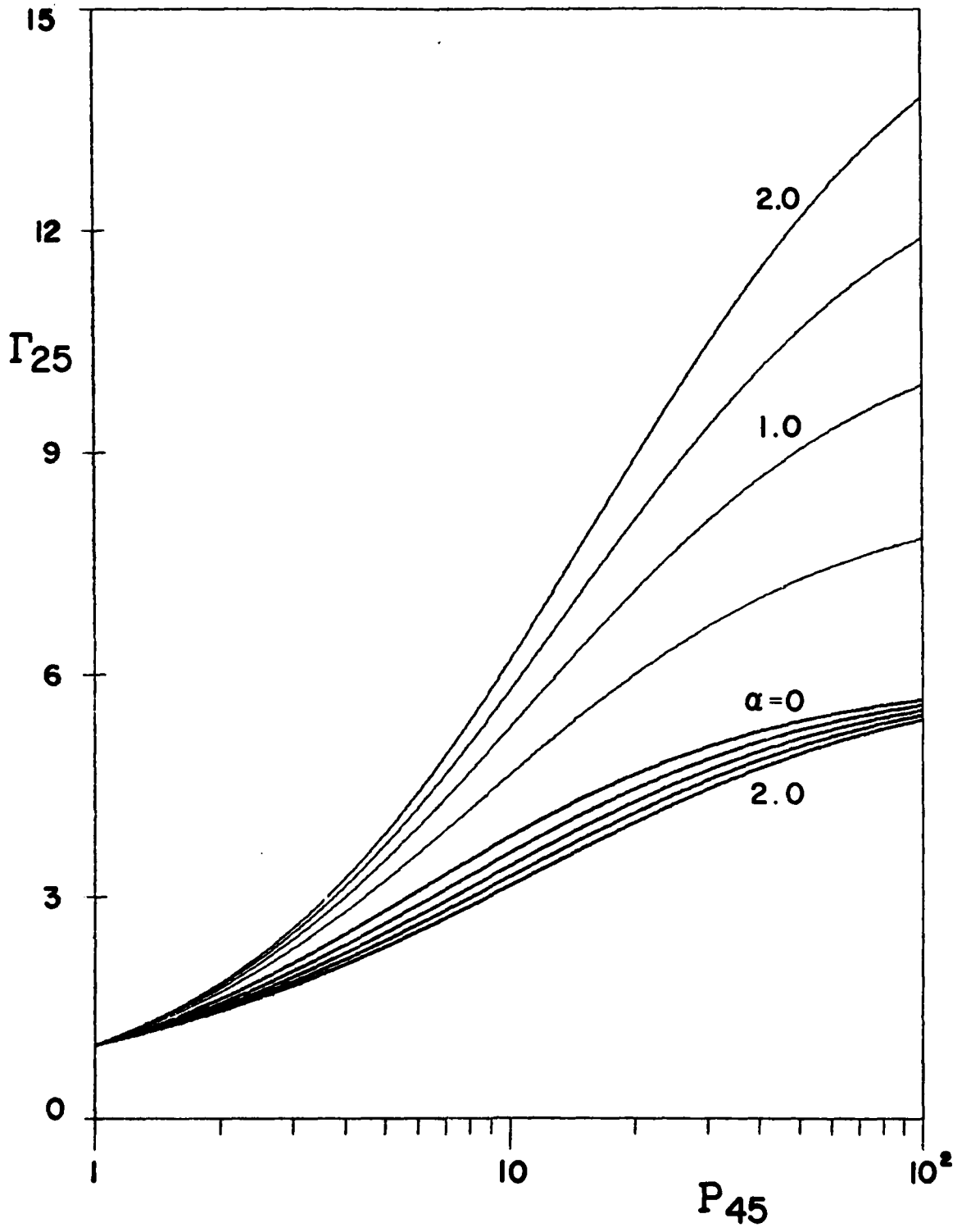

FIG. 13 VARIATION OF FLOW DENSITY RATIO ρ_2/ρ_5 WITH INCIDENT SHOCK PRESSURE RATIO p_4/p_5.

——— ρ_2/ρ_5, ——— ρ_4/ρ_5.

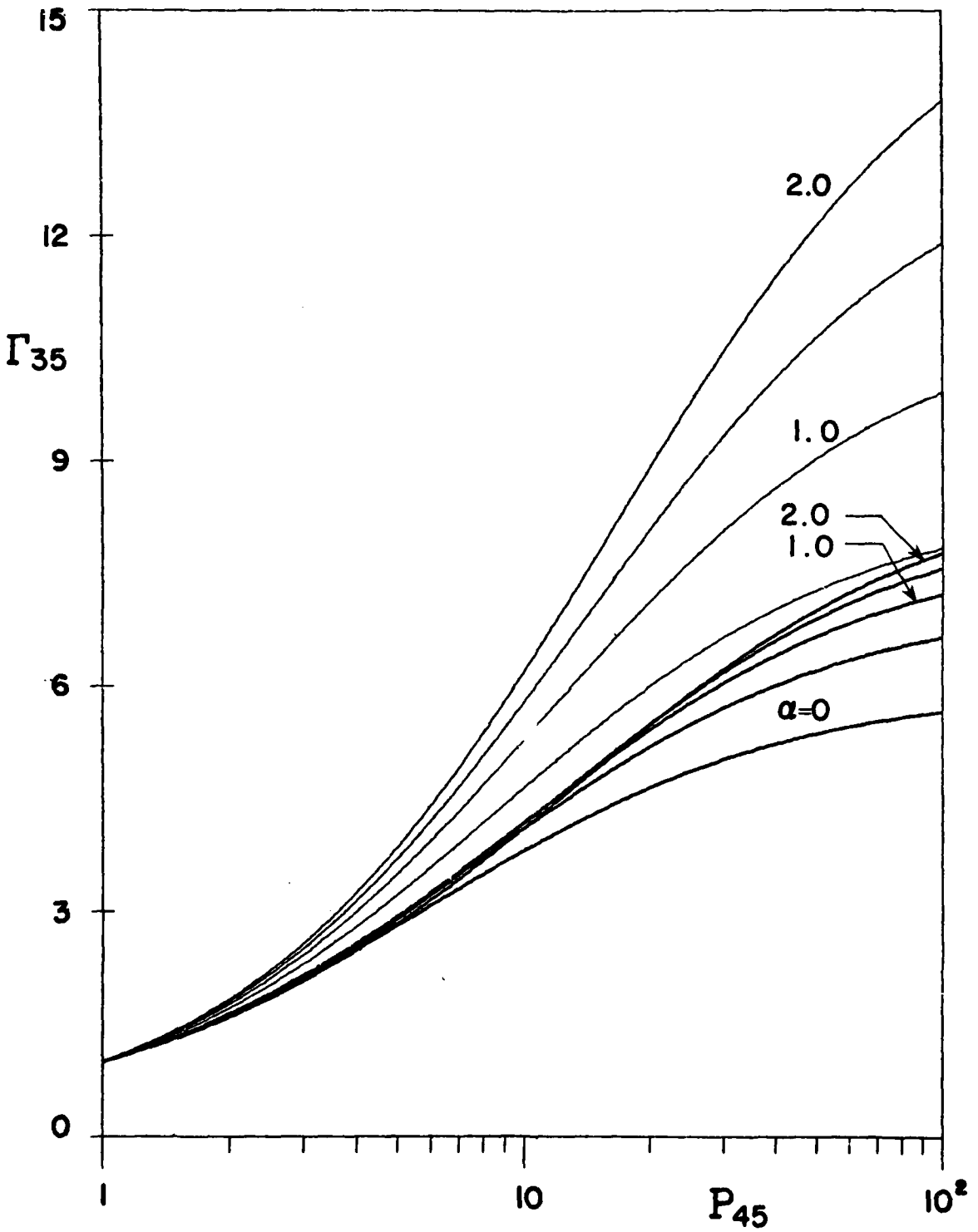

FIG. 14 VARIATION OF FLOW DENSITY RATIO ρ_3/ρ_5 (= σ_3/σ_5) WITH INCIDENT SHOCK PRESSURE RATIO p_4/p_5.

——— ρ_3/ρ_5, ——— ρ_4/ρ_5.

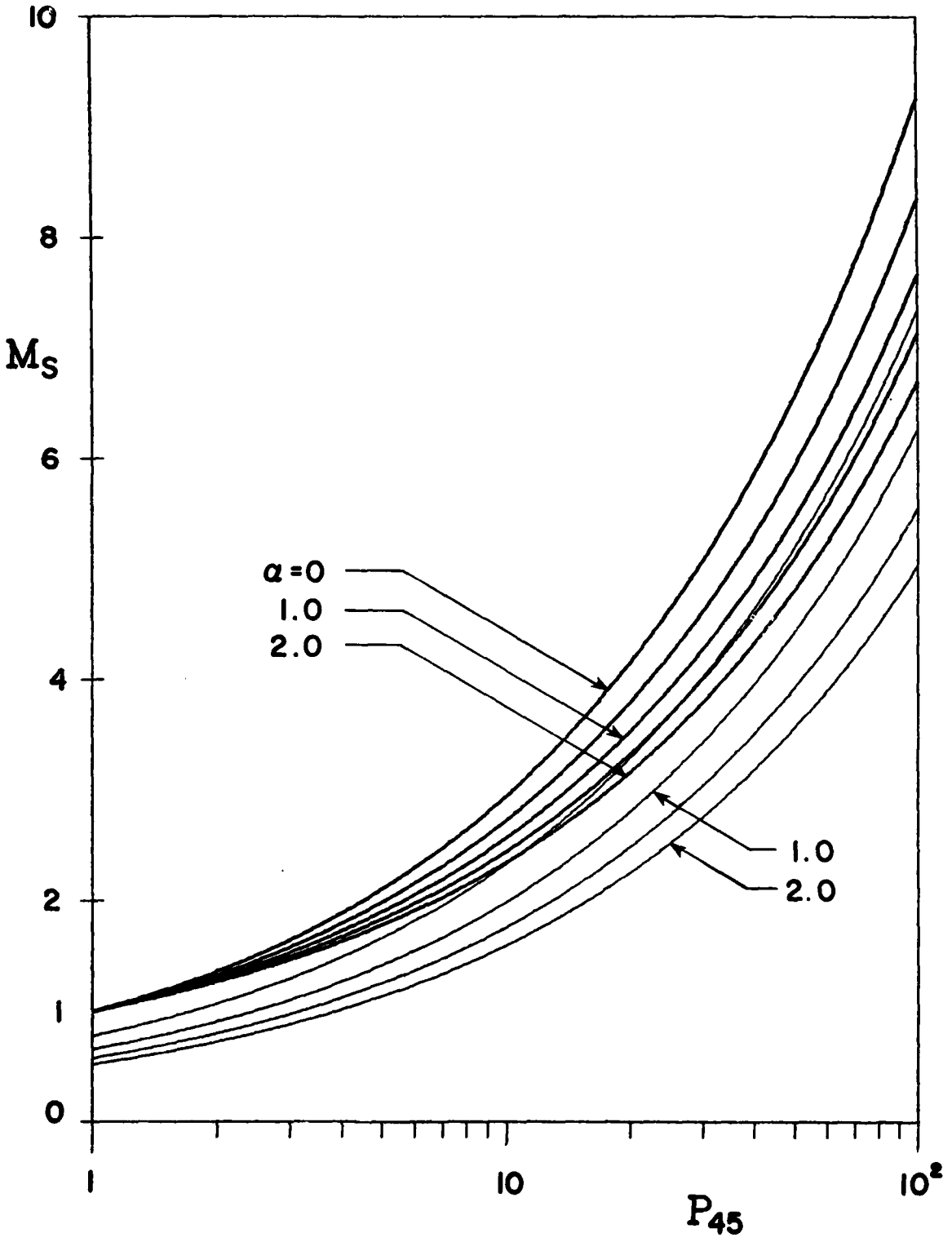

FIG. 15 VARIATION OF TRANSMITTED SHOCK MACH NUMBER $M_s = u_s/a_1$ WITH INCIDENT SHOCK PRESSURE RATIO p_4/p_5.

——— TRANSMITTED SHOCK WAVE, ——— INCIDENT SHOCK WAVE.

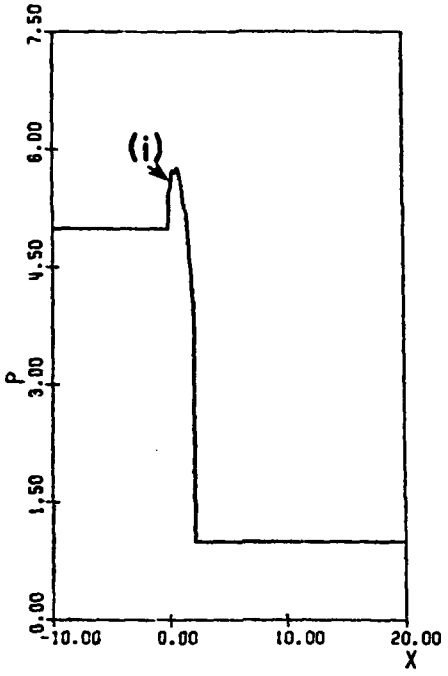

(a) Pressure

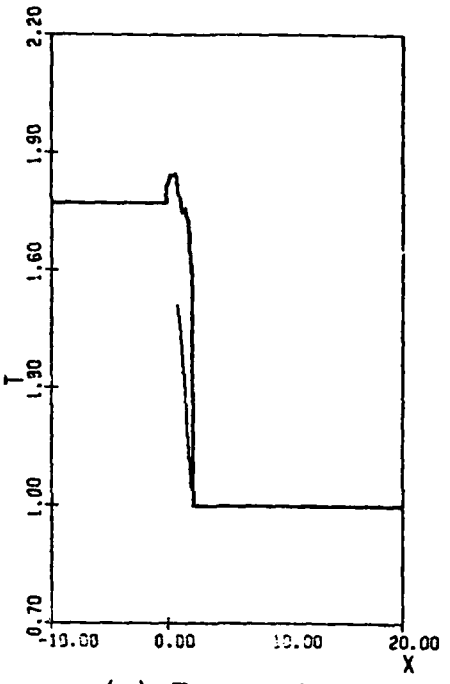

(c) Temperature

(b) Mass Concentration

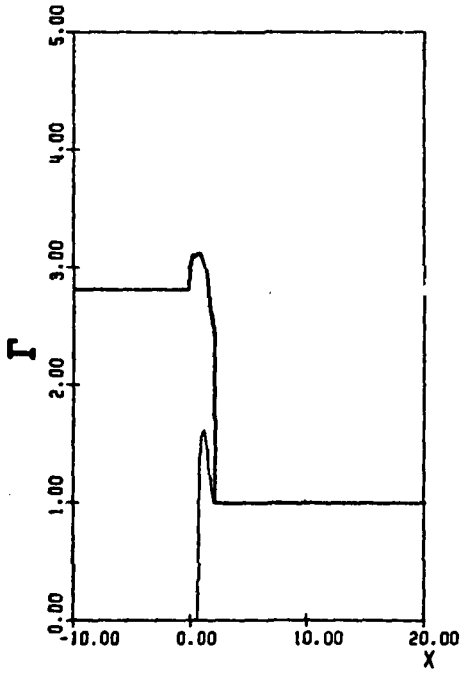

(d) Velocity

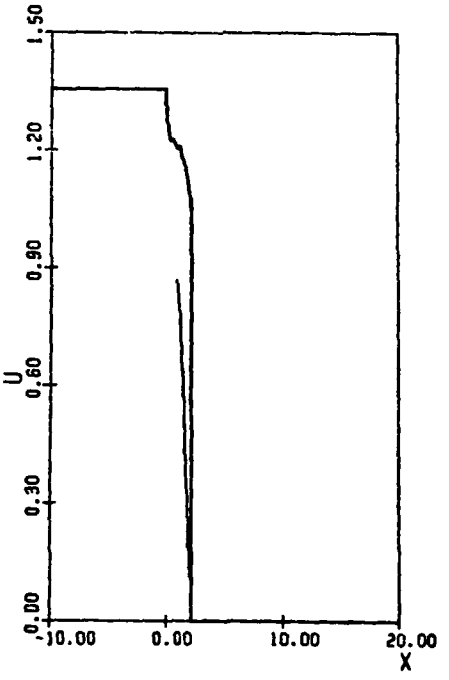

FIG. 16 FLOW QUANTITIES AT $t = 0.78 \times 10^{-4}$ SEC ($p_4/p_5 = 5$).
——— GAS, ——— PARTICLES.
(i) THE BEGINNING OF FORMATION OF A REFLECTED SHOCK WAVE.

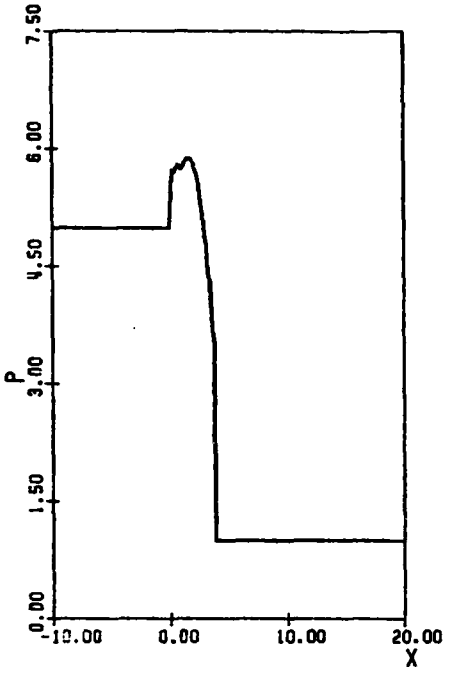

(a) Pressure

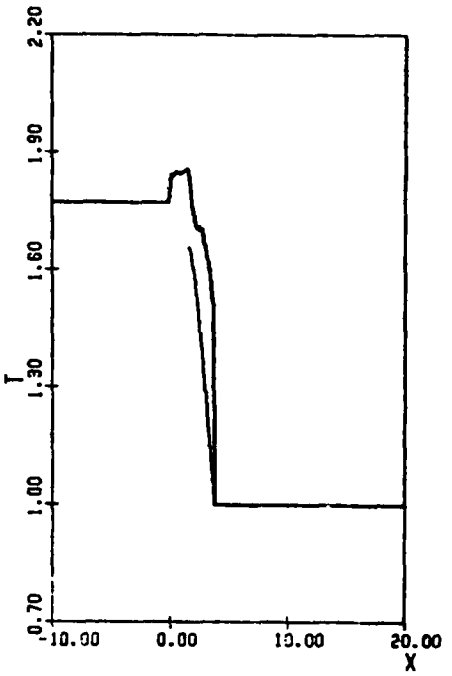

(c) Temperature

(b) Mass Concentration

(d) Velocity

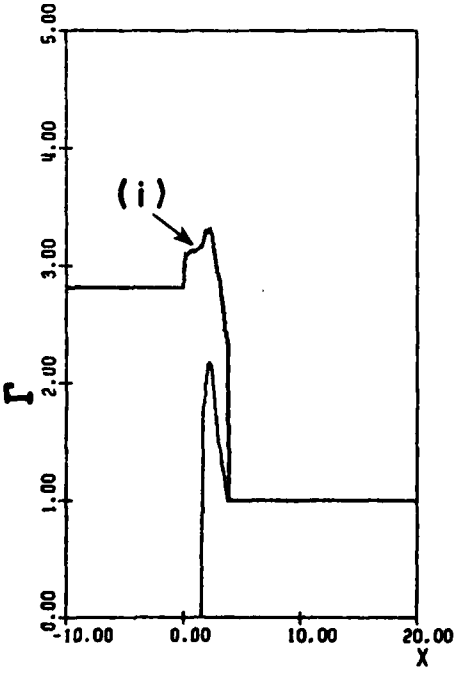

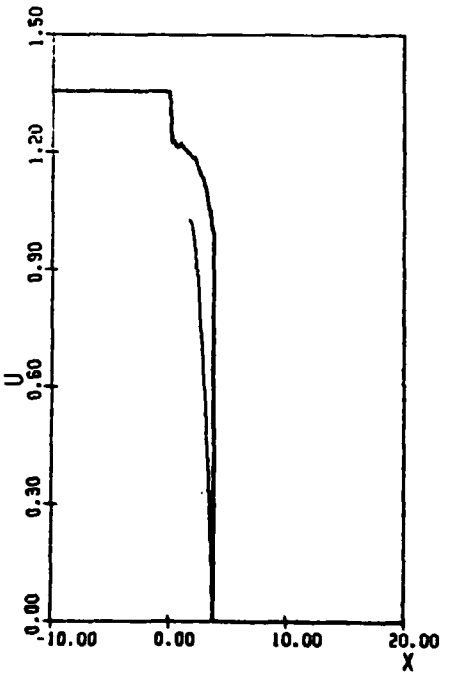

FIG. 17 FLOW QUANTITIES AT $t = 1.56 \times 10^{-4}$ SEC ($p_4/p_5 = 5$).
——— GAS, ——— PARTICLES.
(i) THE BEGINNING OF FORMATION OF A CONTACT REGION.

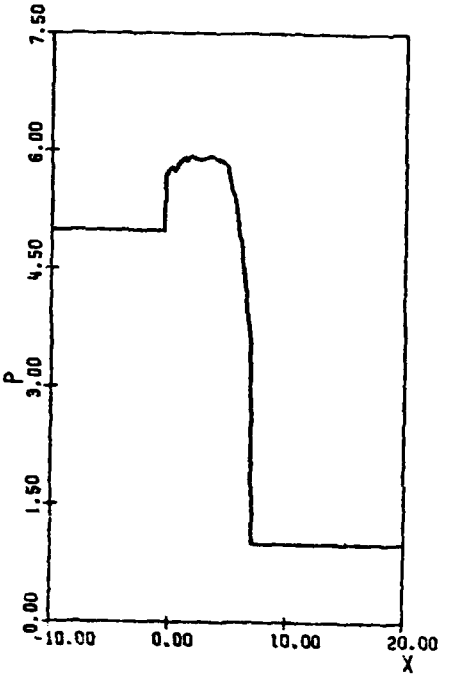

(a) Pressure

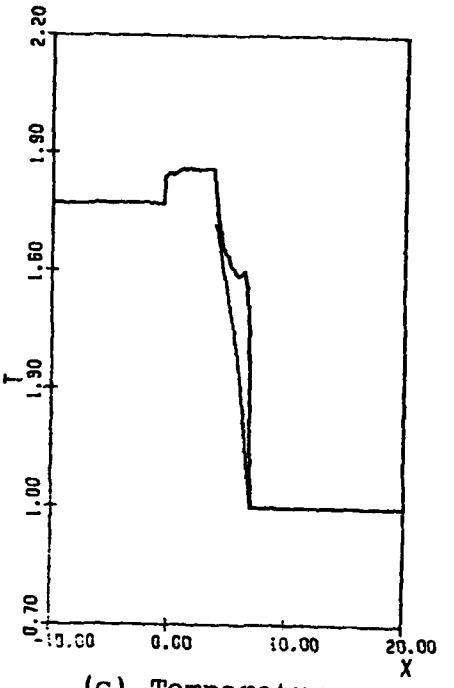

(c) Temperature

(b) Mass Concentration

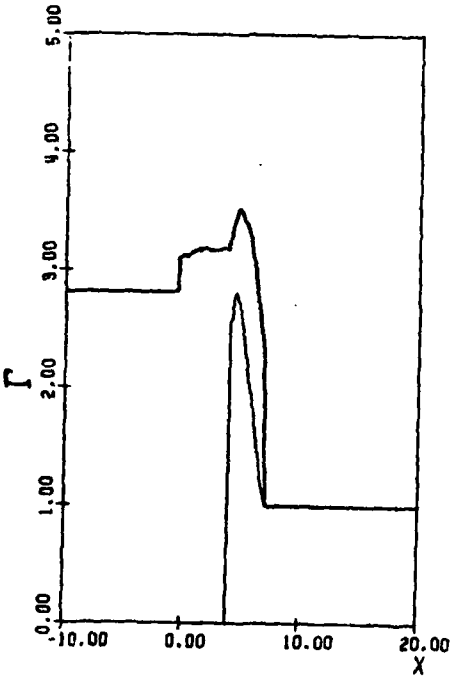

(d) Velocity

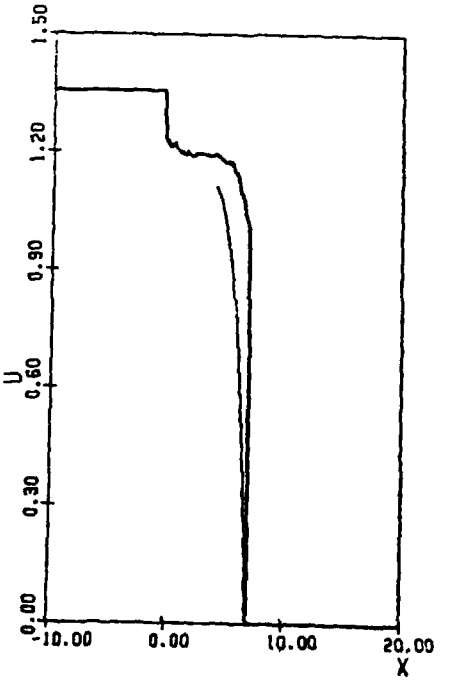

FIG. 18 FLOW QUANTITIES AT $t = 3.12 \times 10^{-4}$ SEC ($p_4/p_5 = 5$)
——— GAS, ——— PARTICLES.

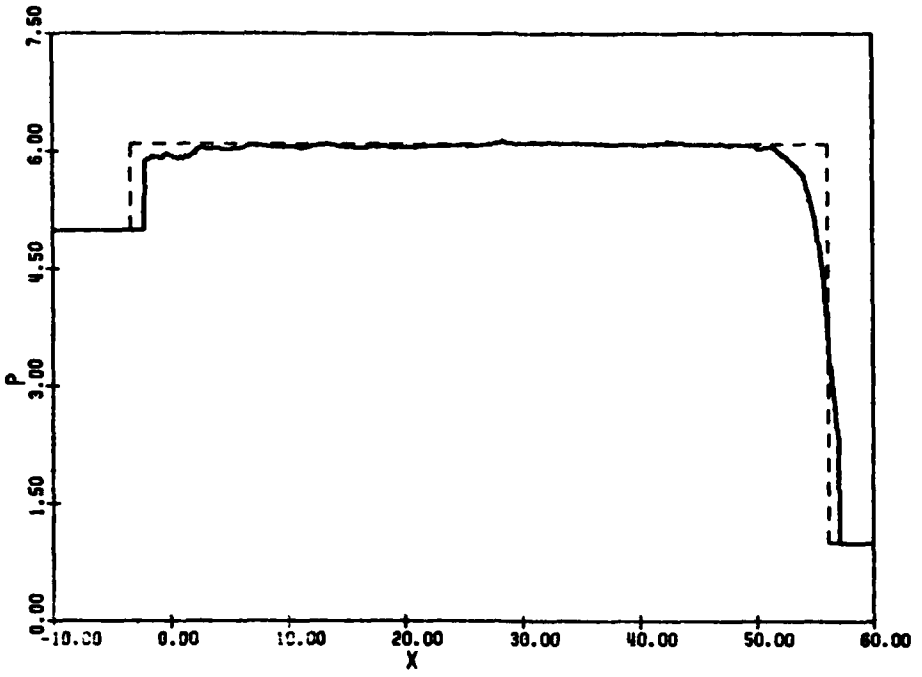

(a) Pressure

(b) Mass Concentration

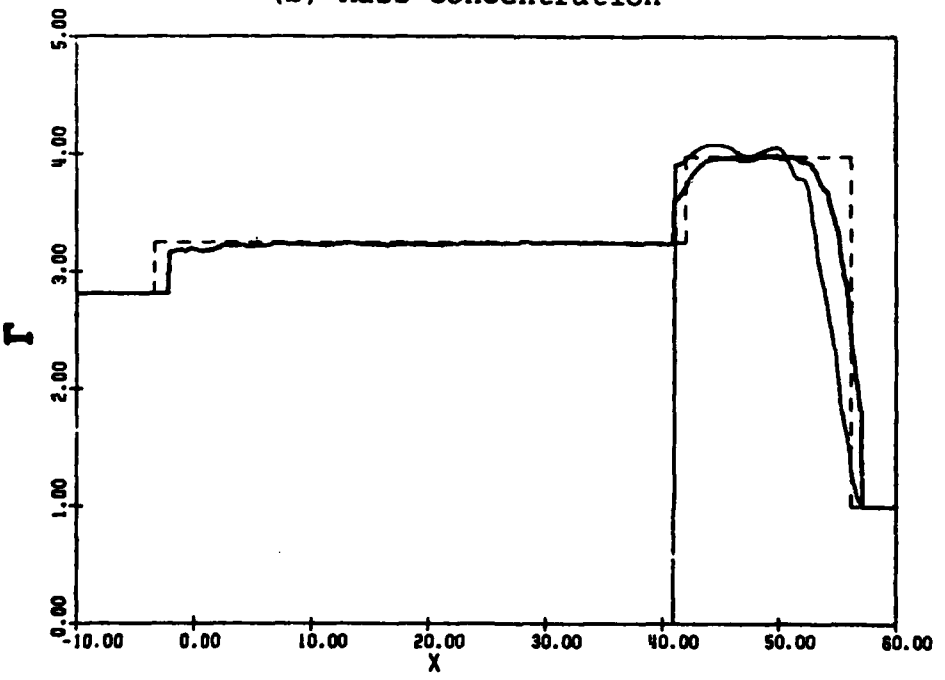

FIG. 19 FLOW QUANTITIES AT $t = 2.81 \times 10^{-3}$ SEC ($p_4/p_5 = 5$)
——— GAS, ——— PARTICLES, ------ EQUILIBRIUM FLOW.

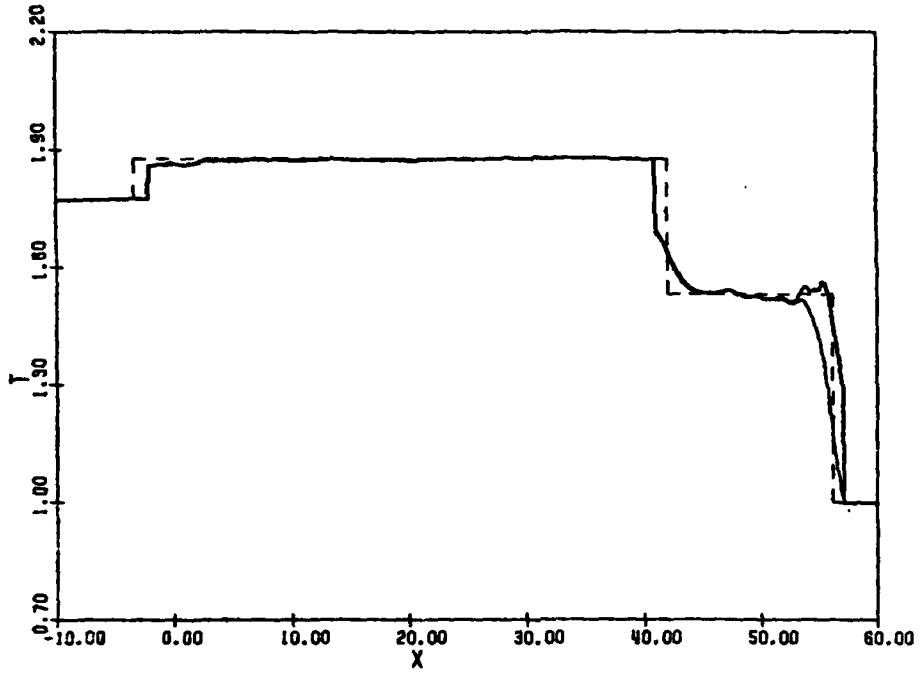

(c) Temperature

(d) Velocity

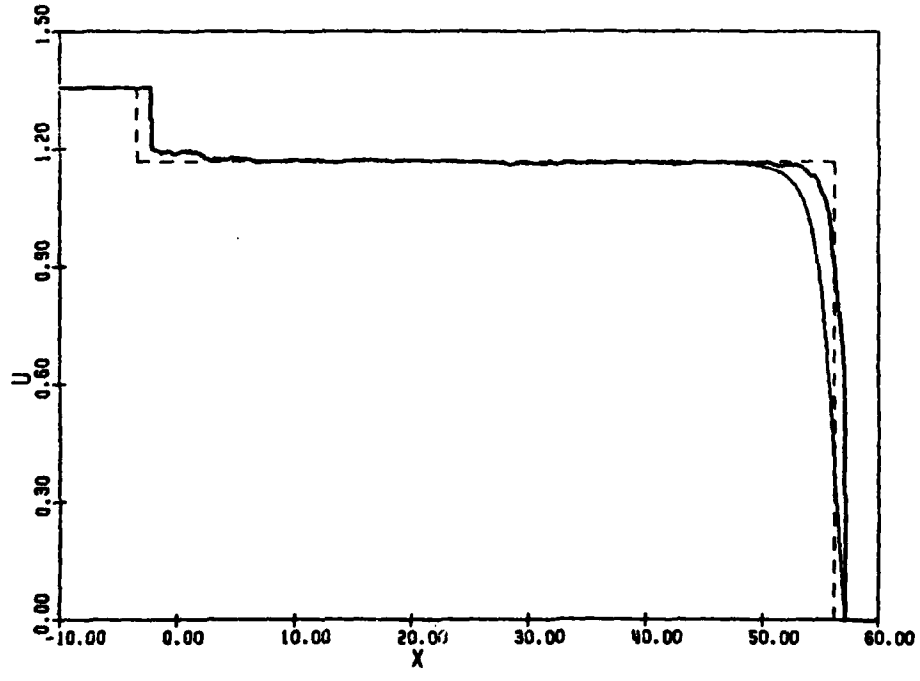

FIG. 19 - CONTINUED.
FLOW QUANTITIES AT $t = 2.81 \times 10^{-3}$ SEC ($p_4/p_5 = 5$)
——— GAS, ——— PARTICLES, ------ EQUILIBRIUM FLOW.

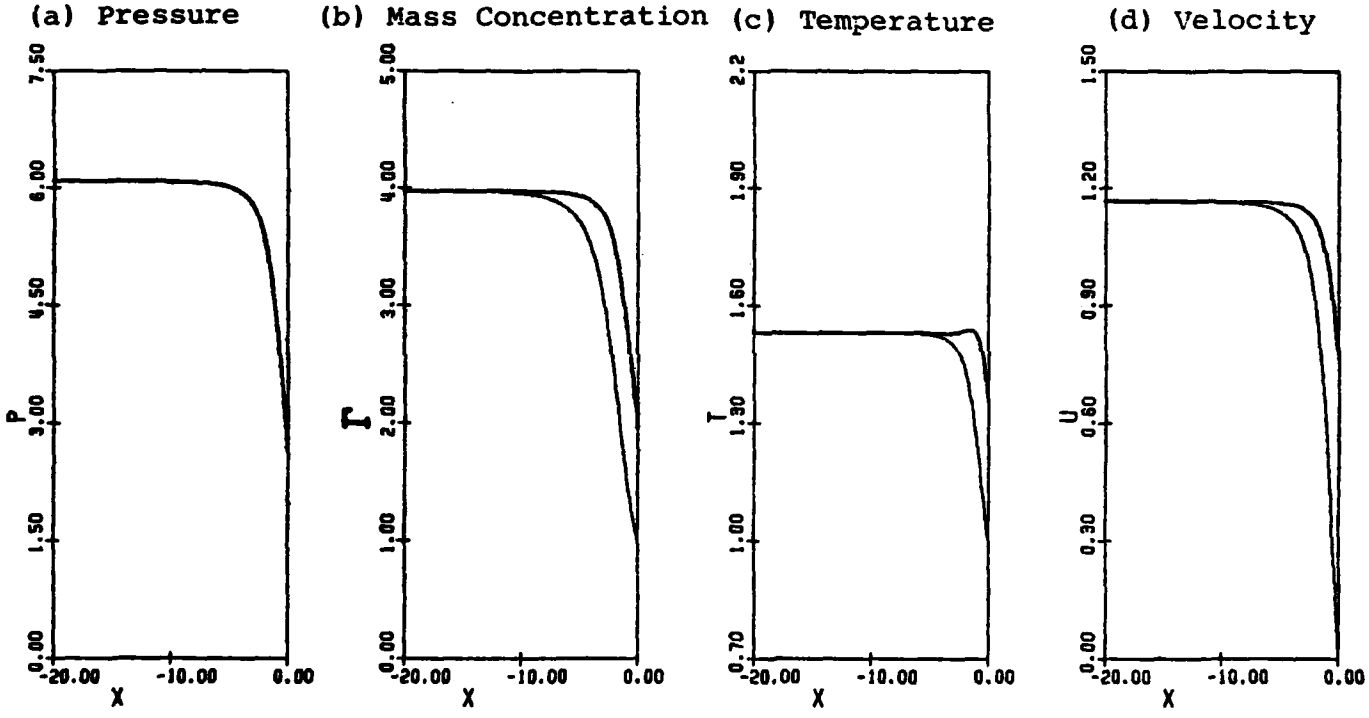

FIG. 20 STATIONARY STRUCTURE OF A SHOCK WAVE IN A DUSTY GAS (SHOCK PRESSURE RATIO = 6.09).

——— GAS, ——— PARTICLES.

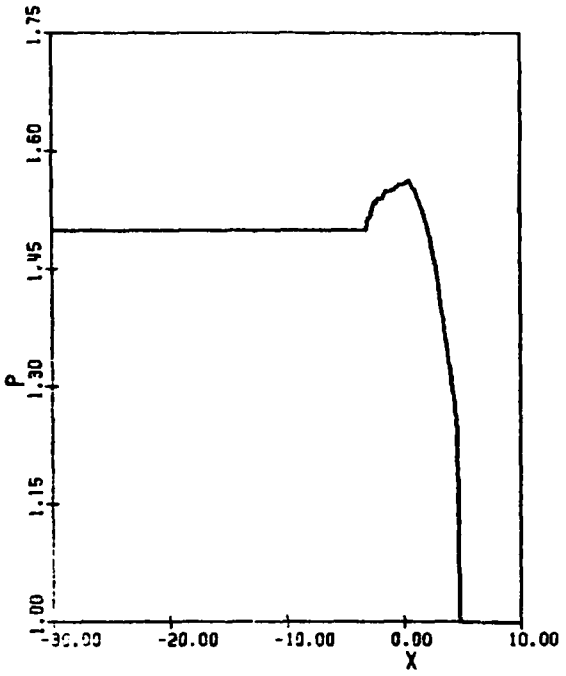

(a) Pressure

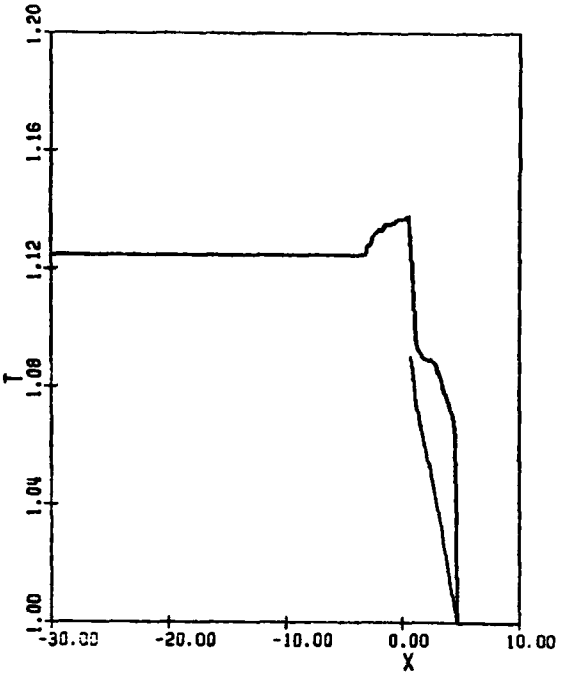

(b) Mass Concentration

(c) Temperature

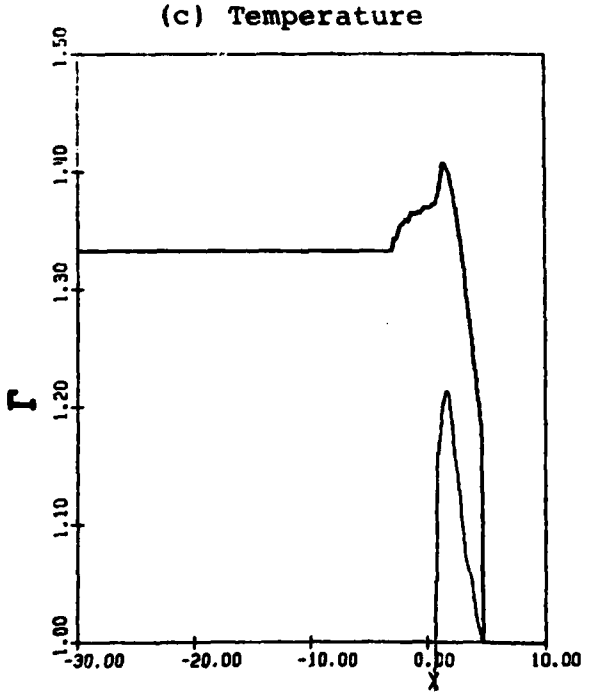

(d) Velocity

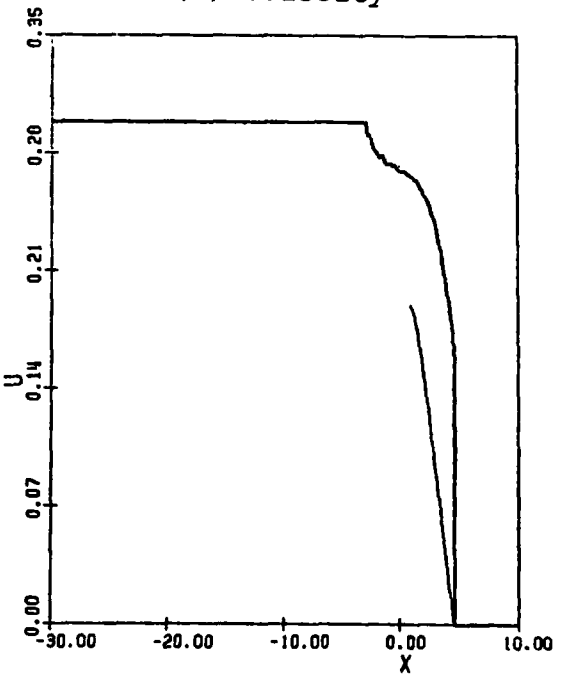

FIG. 21 FLOW QUANTITIES AT $t = 3.12 \times 10^{-4}$ SEC ($p_4/p_5 = 1.5$).
——— GAS, ——— PARTICLES.

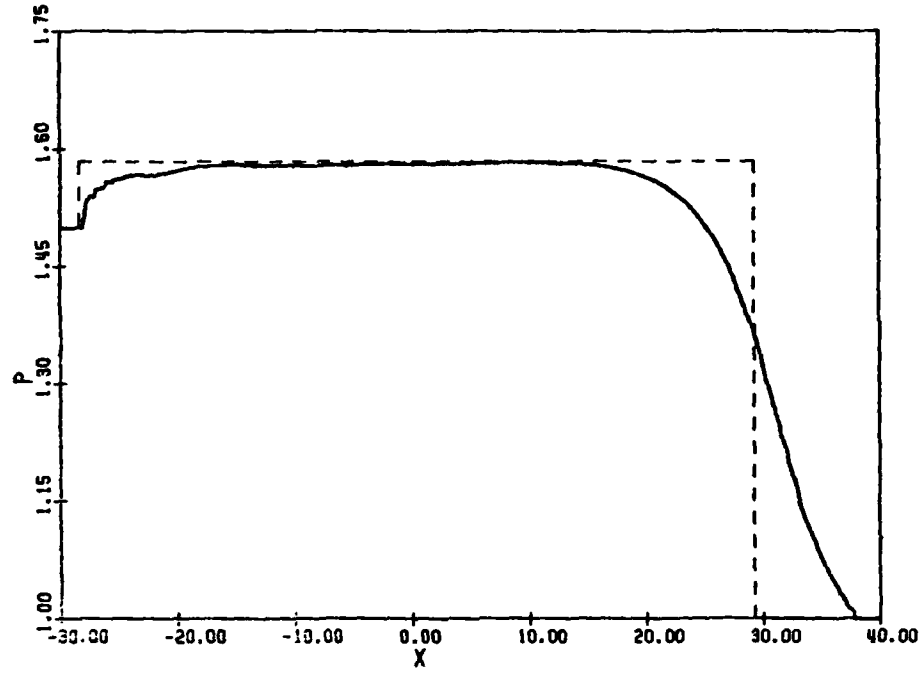

(a) Pressure

(b) Mass Concentration

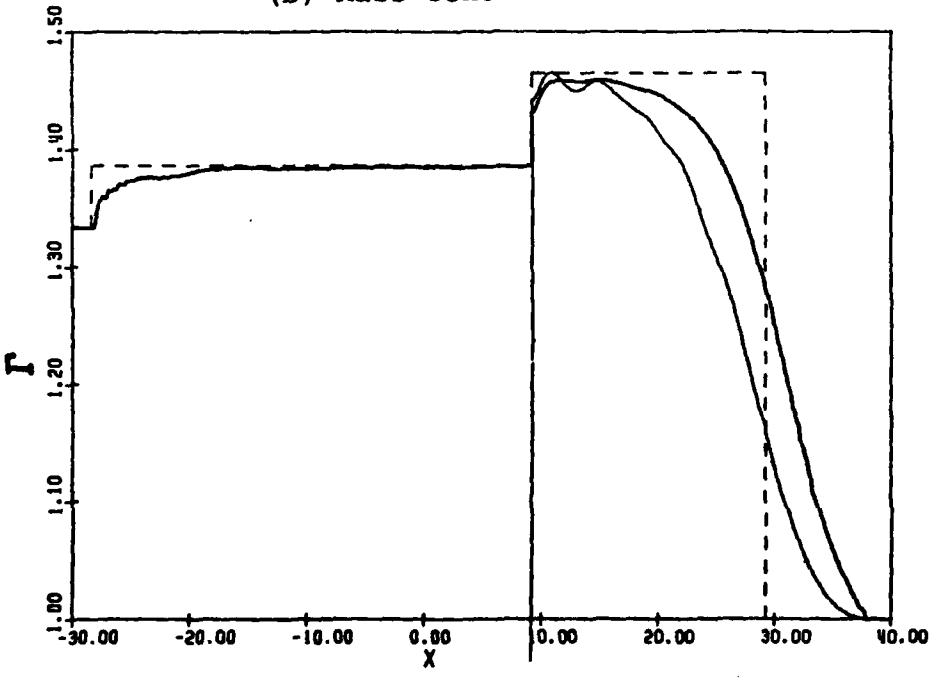

FIG. 22 FLOW QUANTITIES AT t = 2.81×10^{-3} SEC (p_4/p_5 = 1.5).
——— GAS, ——— PARTICLES, ------ EQUILIBRIUM FLOW.

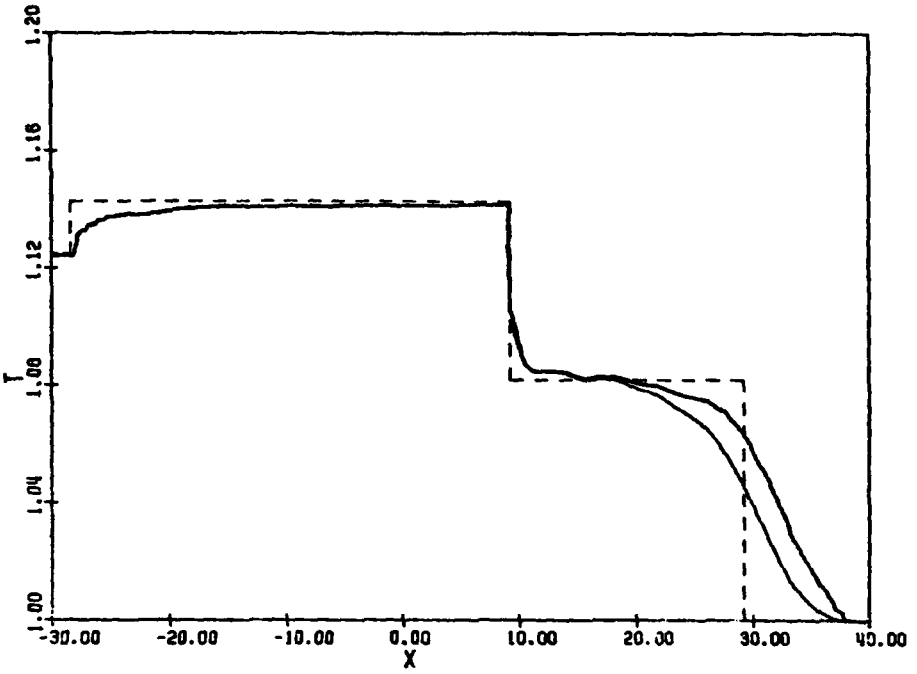

(c) Temperature

(d) Velocity

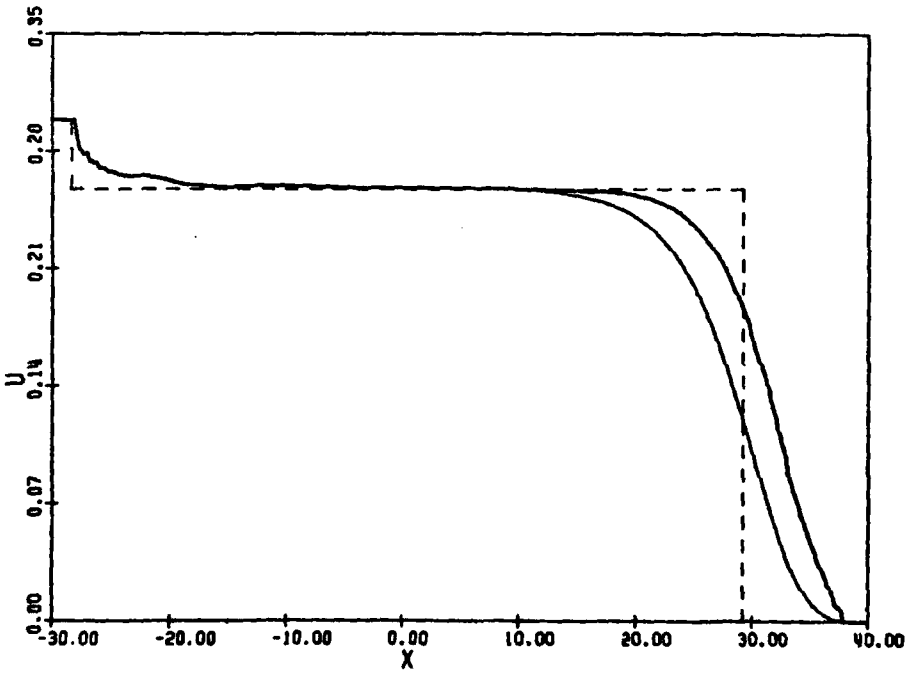

FIG. 22 - CONTINUED.
FLOW QUANTITIES AT $t = 2.81 \times 10^{-3}$ SEC ($p_4/p_5 = 1.5$).
——— GAS, ——— PARTICLES, ------ EQUILIBRIUM FLOW.

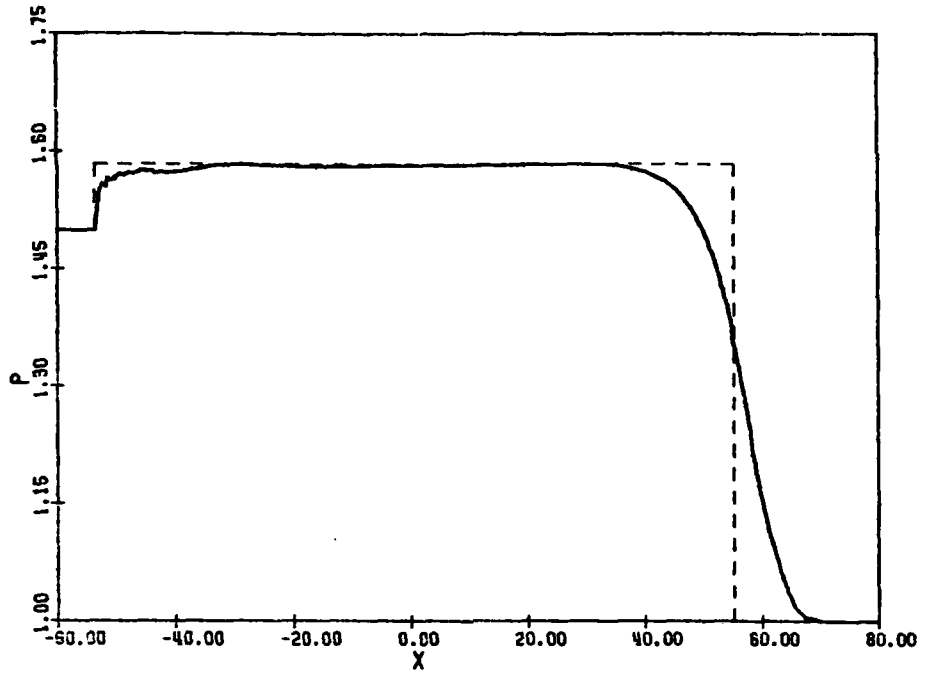

(a) Pressure

(b) Mass Concentration

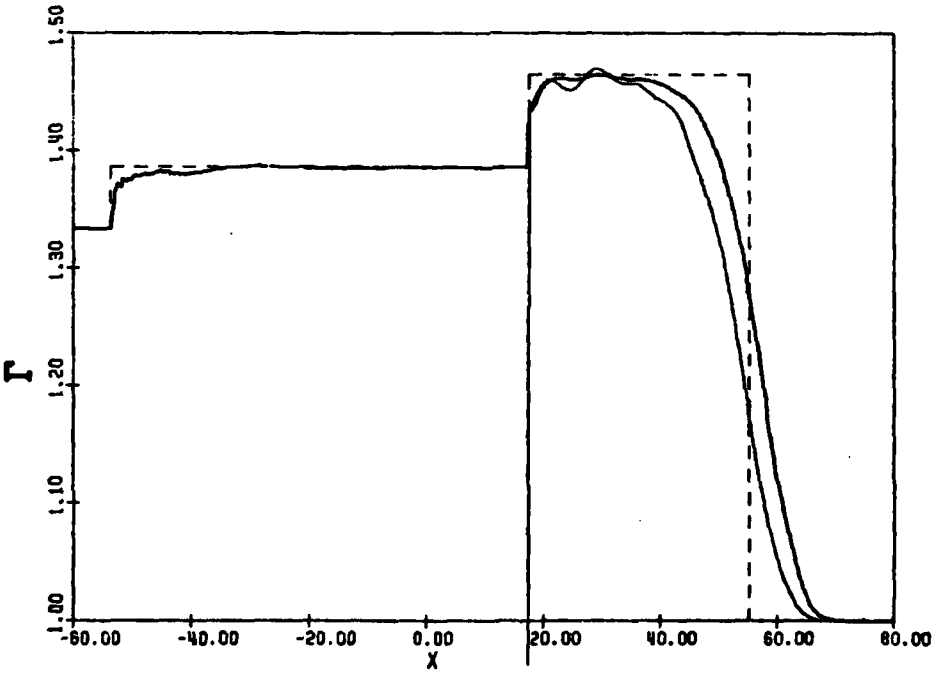

FIG. 23 FLOW QUANTITIES AT $t = 5.30 \times 10^{-3}$ SEC ($p_4/p_5 = 1.5$).
——— GAS, ——— PARTICLES, ------ EQUILIBRIUM FLOW.

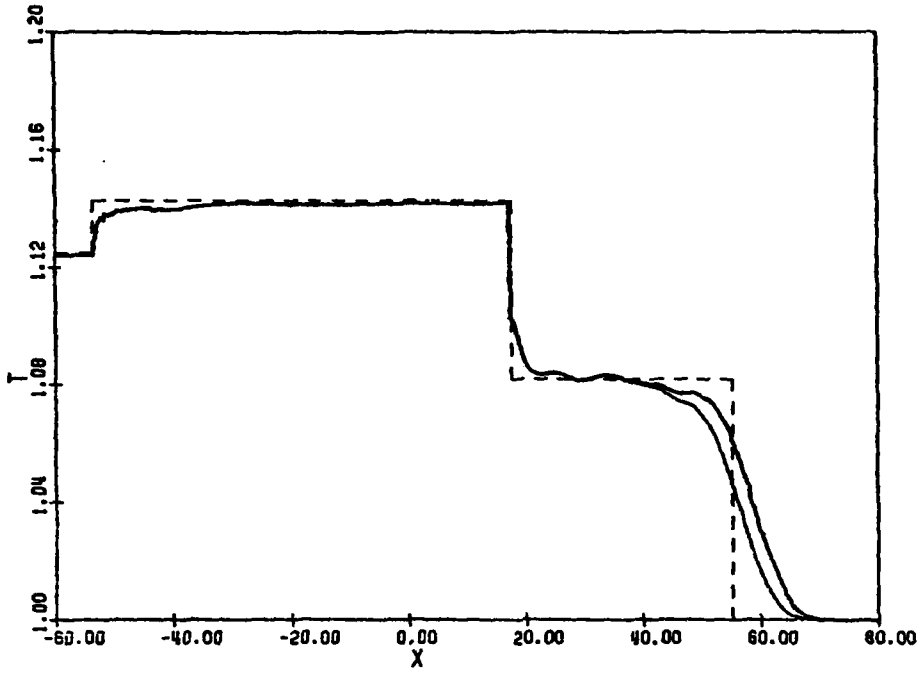

(c) Temperature

(d) Velocity

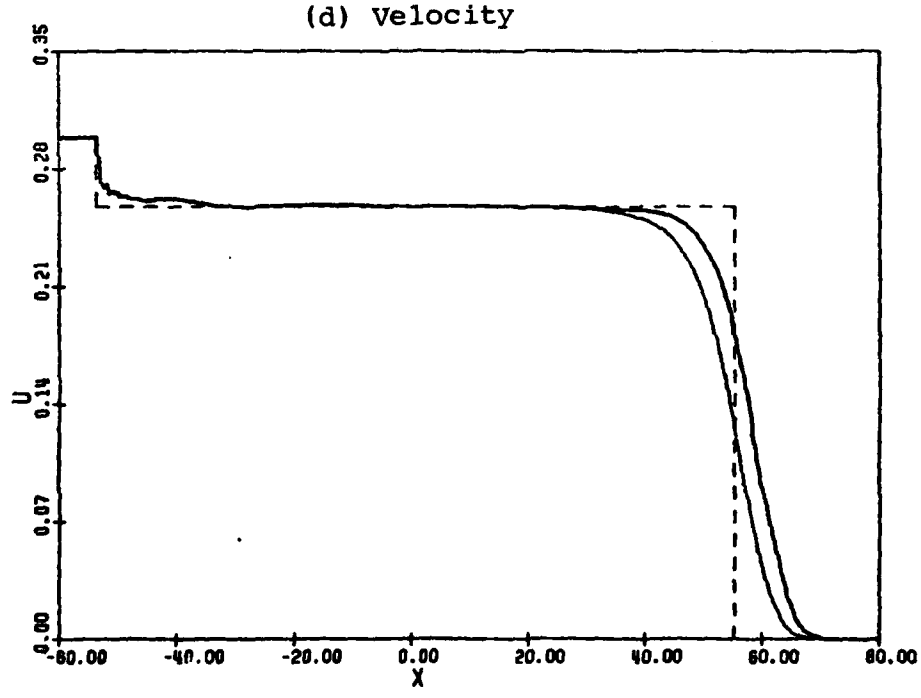

FIG. 23 - CONTINUED.
FLOW QUANTITIES AT $t = 5.30 \times 10^{-3}$ SEC ($p_4/p_5 = 1.5$).
——— GAS, ——— PARTICLES, ------ EQUILIBRIUM FLOW.

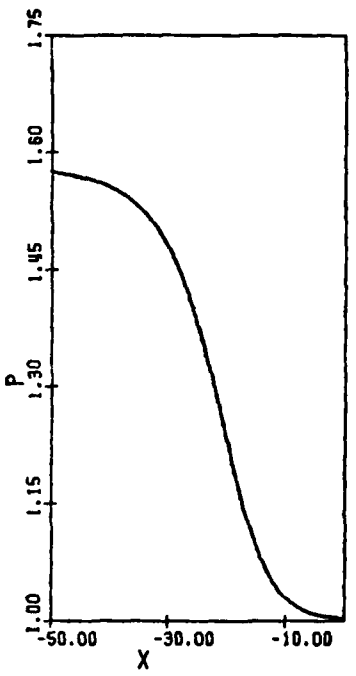

(a) Pressure

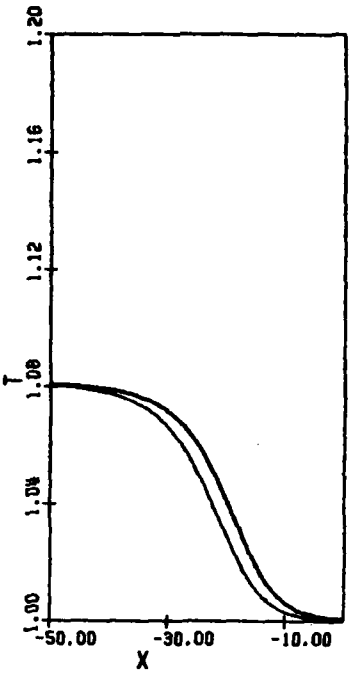

(c) Temperature

(b) Mass Concentration

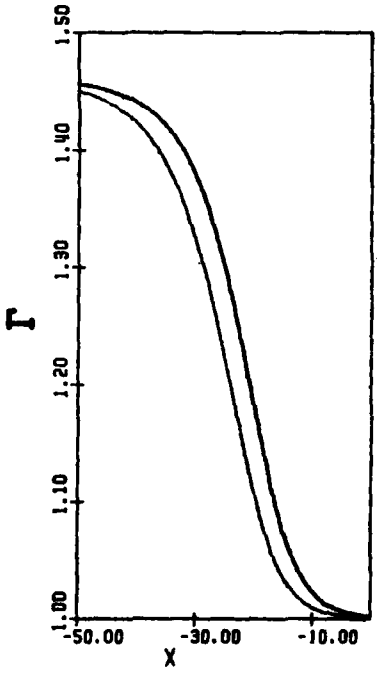

(d) Velocity

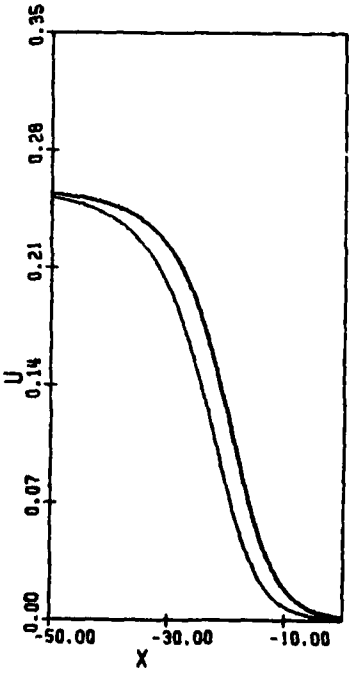

FIG. 24 STATIONARY STRUCTURE OF A FULLY DISPERSED SHOCK WAVE (SHOCK PRESSURE RATIO = 1.584).

——— GAS, ——— PARTICLES.

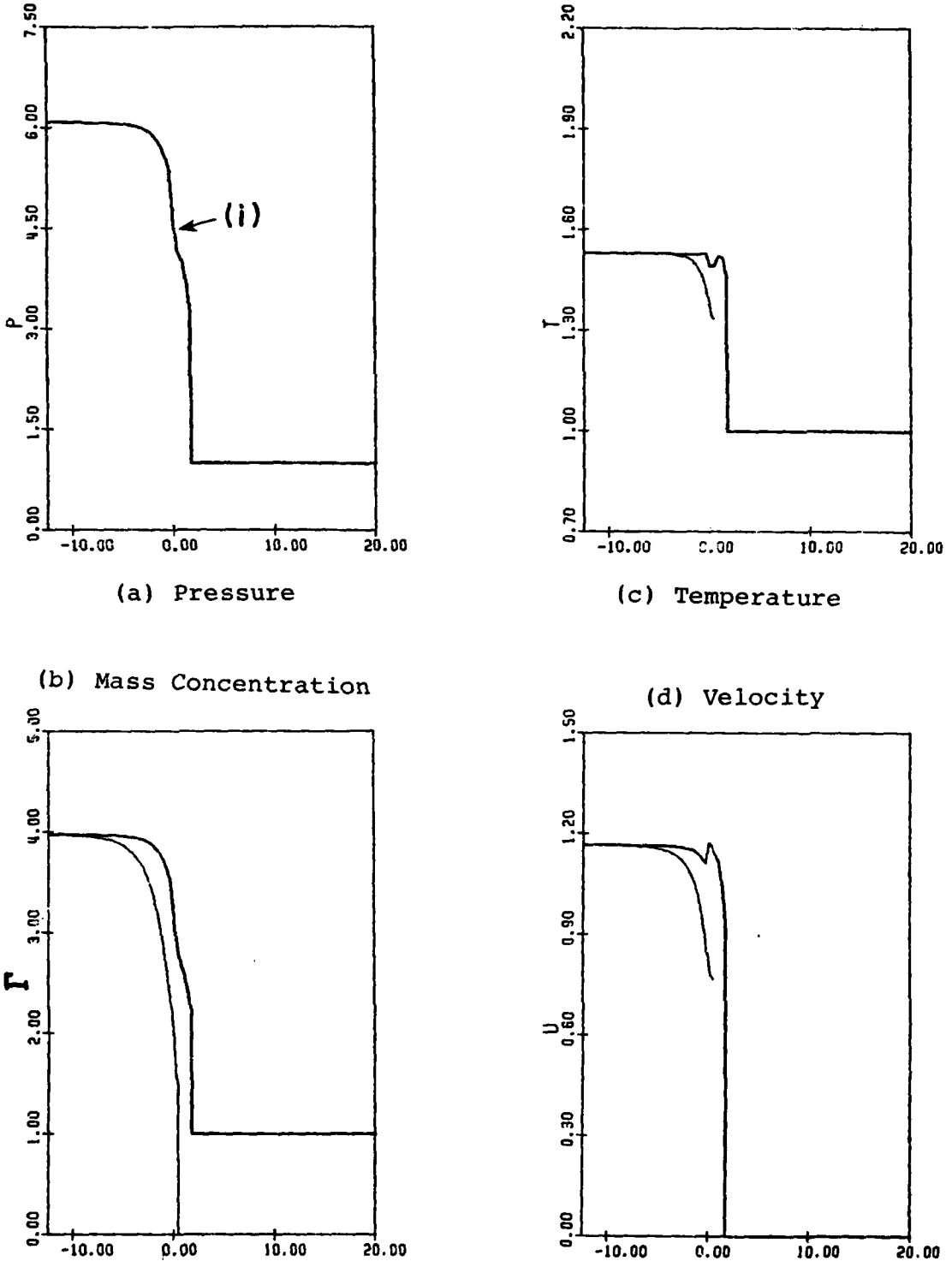

FIG. 25 FLOW QUANTITIES AT $t = 0.78 \times 10^{-4}$ SEC ($p_4/p_5 = 6.09$).

——— GAS, ——— PARTICLES.

(i) THE BEGINNING OF FORMATION OF A REFLECTED RAREFACTION WAVE.

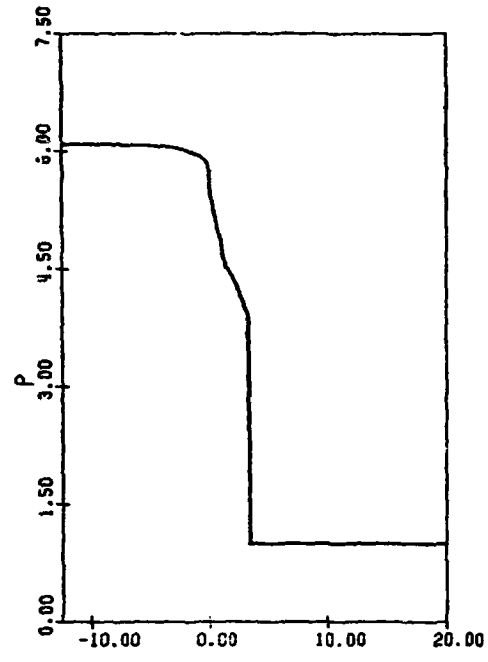

(a) Pressure

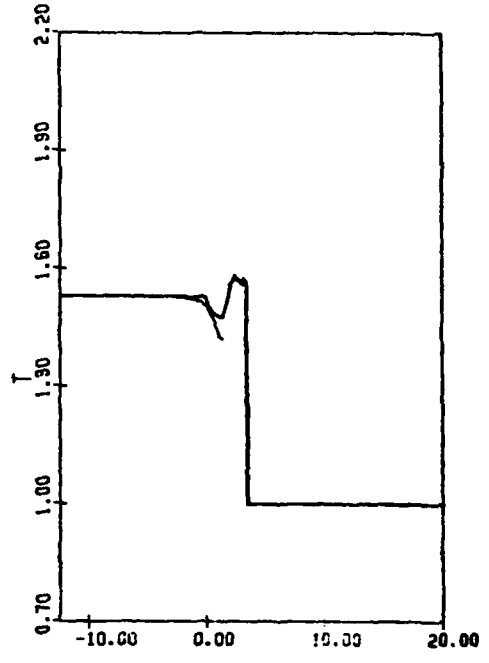

(c) Temperature

(b) Mass Concentration

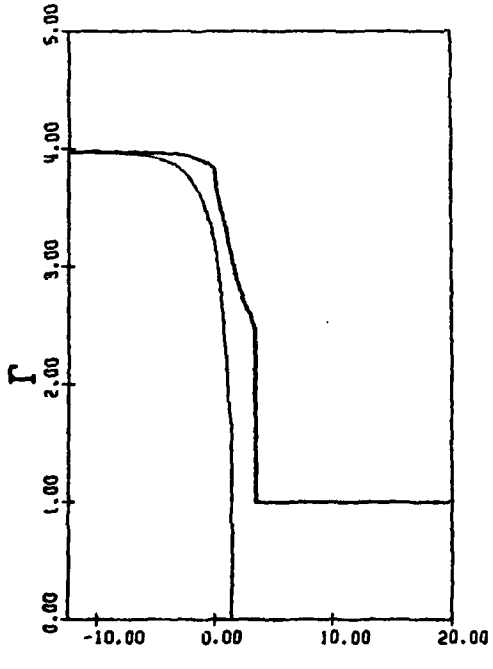

(d) Velocity

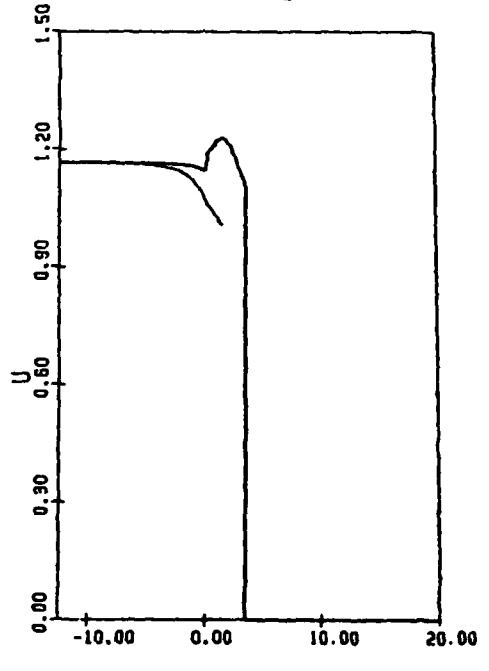

FIG. 26 FLOW QUANTITIES AT $t = 1.56 \times 10^{-4}$ SEC ($p_4/p_5 = 6.09$).
——— GAS, ——— PARTICLES.

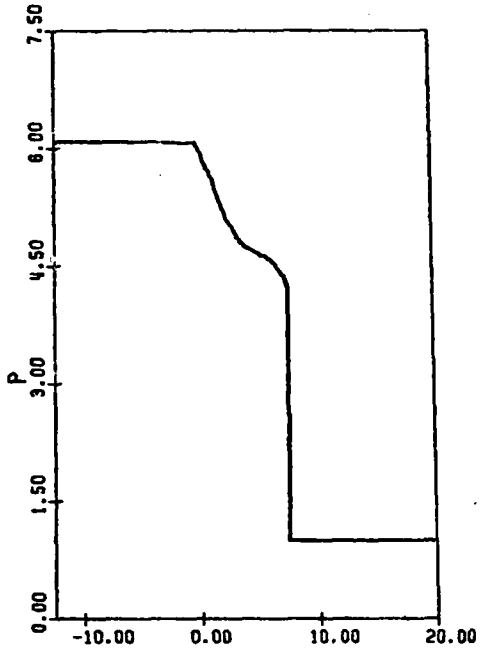

(a) Pressure

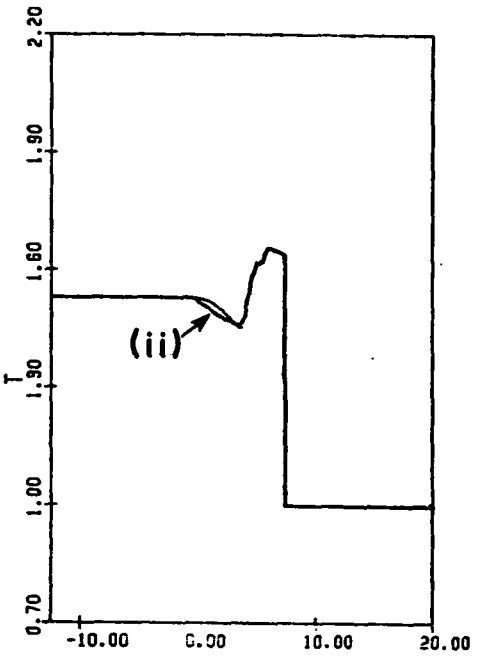

(c) Temperature

(b) Mass Concentration

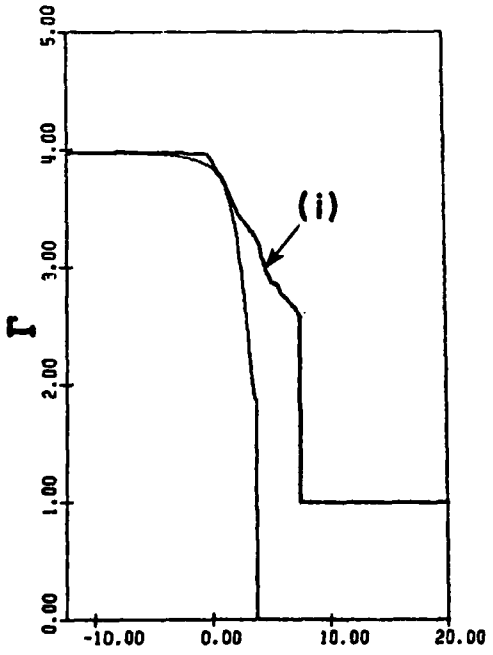

(d) Velocity

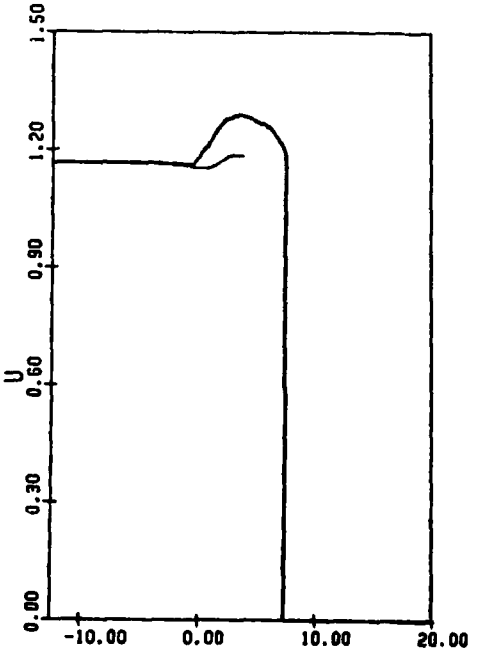

FIG. 27 FLOW QUANTITIES AT $t = 3.12 \times 10^{-4}$ SEC ($p_4/p_5 = 6.09$).
——— GAS, - - - - - PARTICLES.
(i) THE BEGINNING OF FORMATION OF A CONTACT REGION.
(ii) REFLECTED RAREFACTION WAVE.

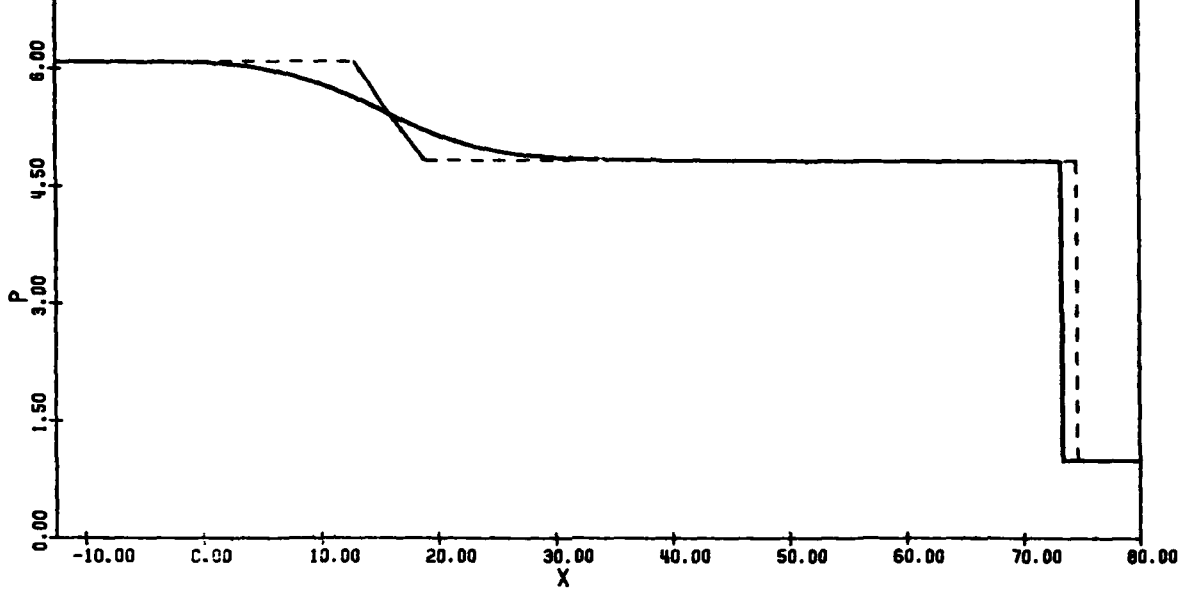

(a) Pressure

(b) Mass Concentration

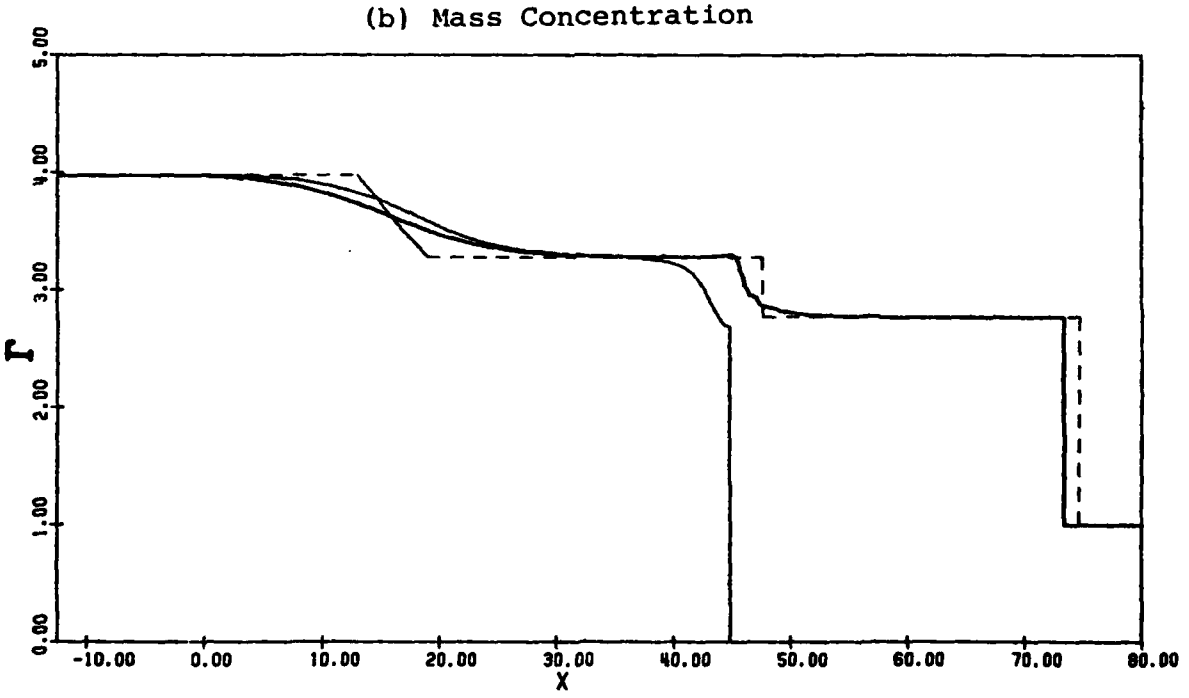

FIG. 28 FLOW QUANTITIES AT $t = 2.81 \times 10^{-3}$ SEC ($p_4/p_5 = 6.09$).
——— GAS, ——— PARTICLES, ------ EQUILIBRIUM FLOW.

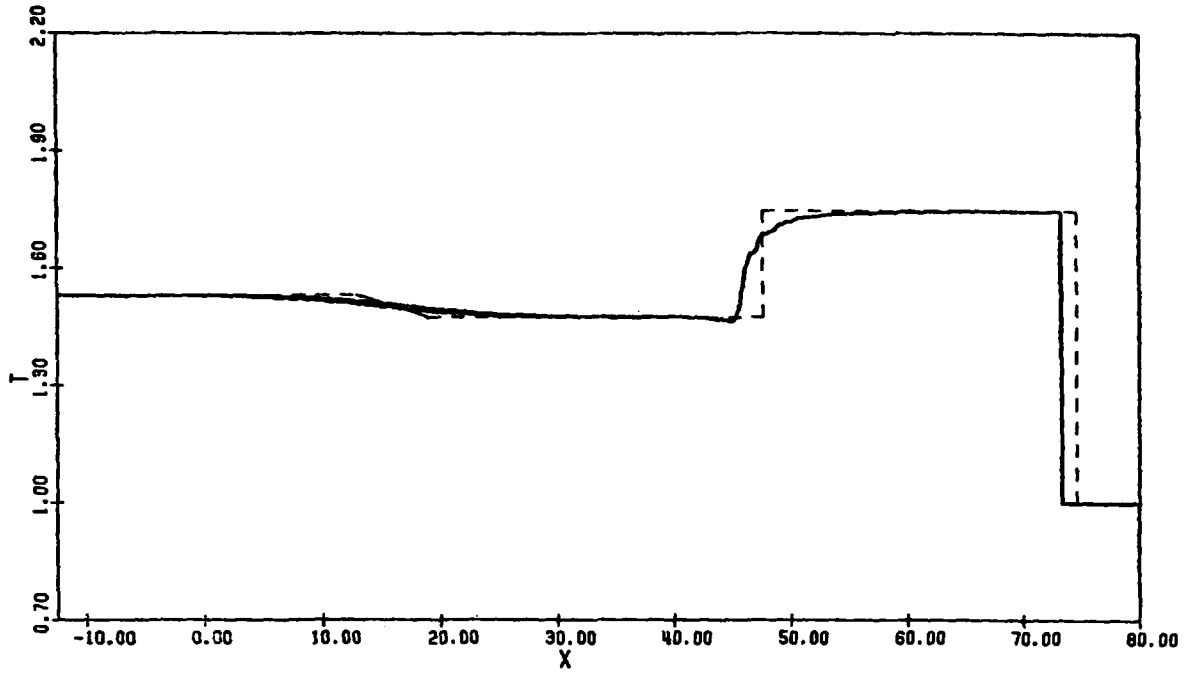

(c) Temperature

(d) Velocity

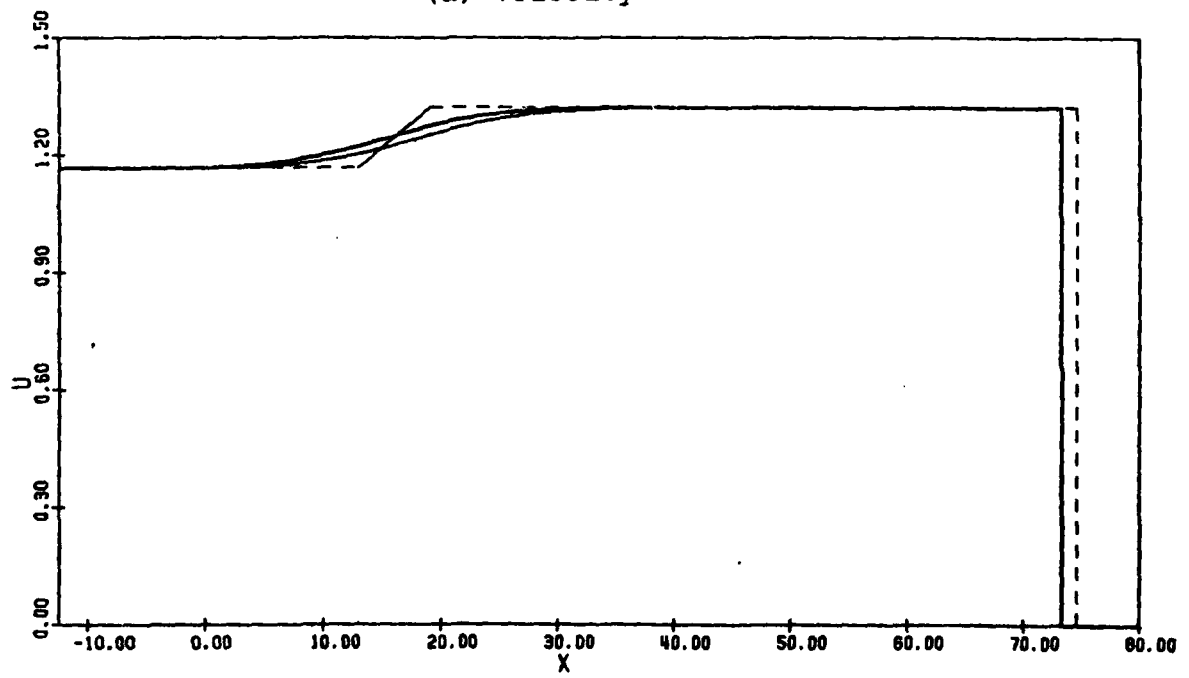

FIG. 28 - CONTINUED.
FLOW QUANTITIES AT $t = 2.81 \times 10^{-3}$ SEC ($p_4/p_5 = 6.09$).
——— GAS, ——— PARTICLES, ------ EQUILIBRIUM FLOW.

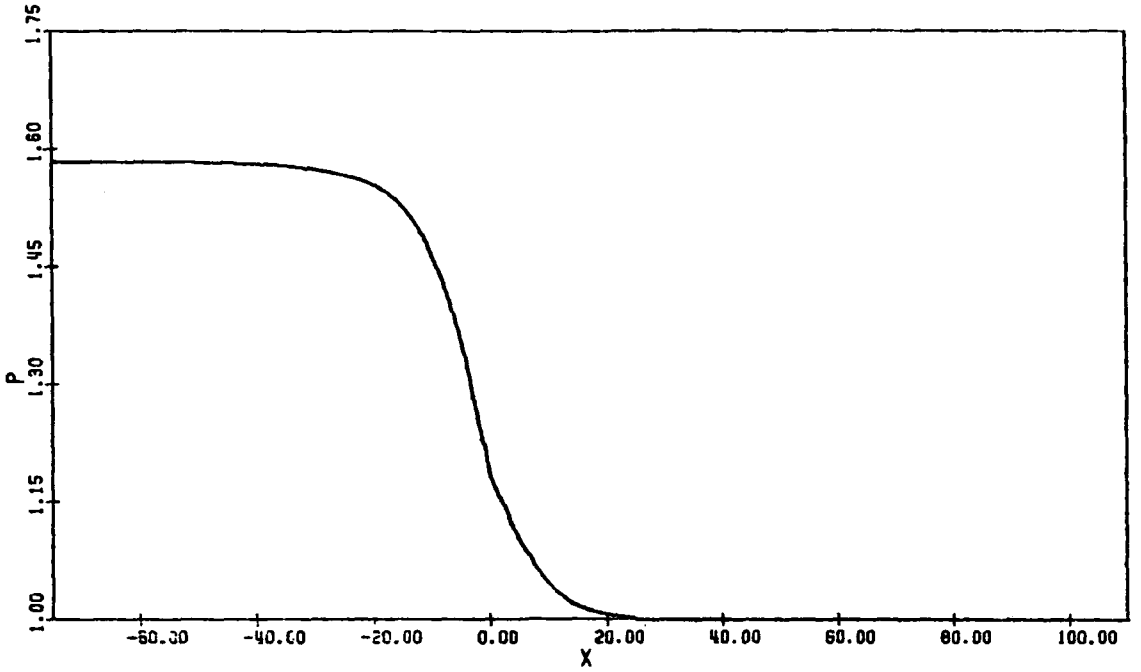

(a) Pressure

(b) Mass Concentration

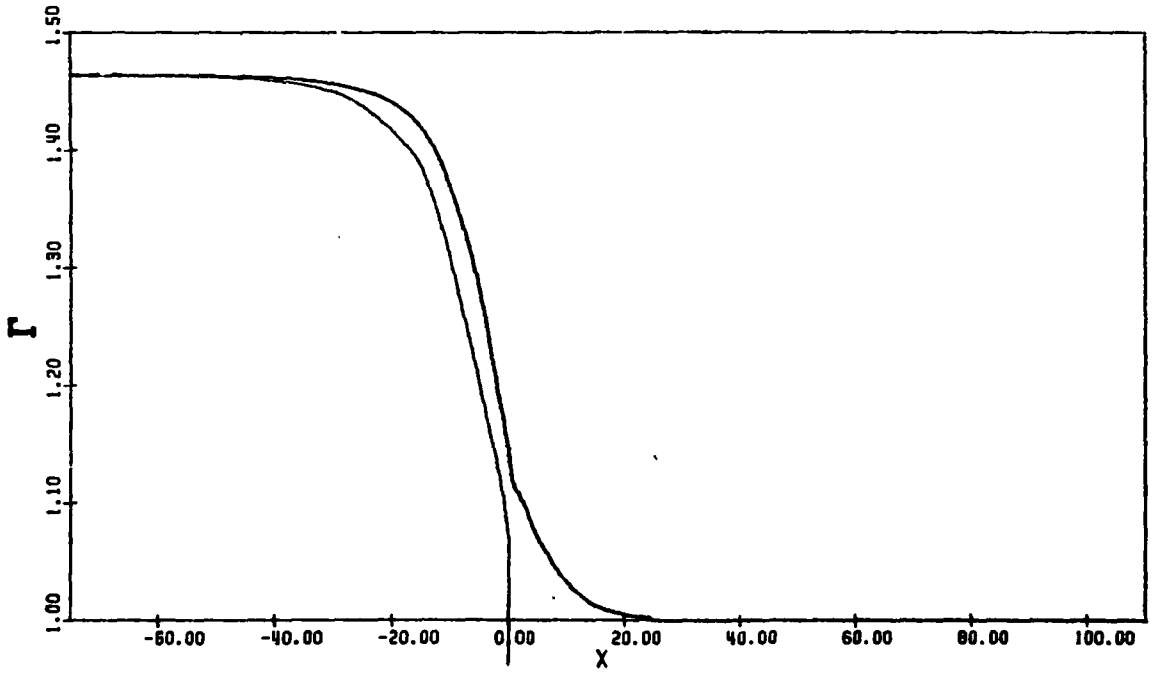

FIG. 29 FLOW QUANTITIES AT $t = 1.87 \times 10^{-3}$ SEC ($p_4/p_5 = 1.584$).
——— GAS, ——— PARTICLES.

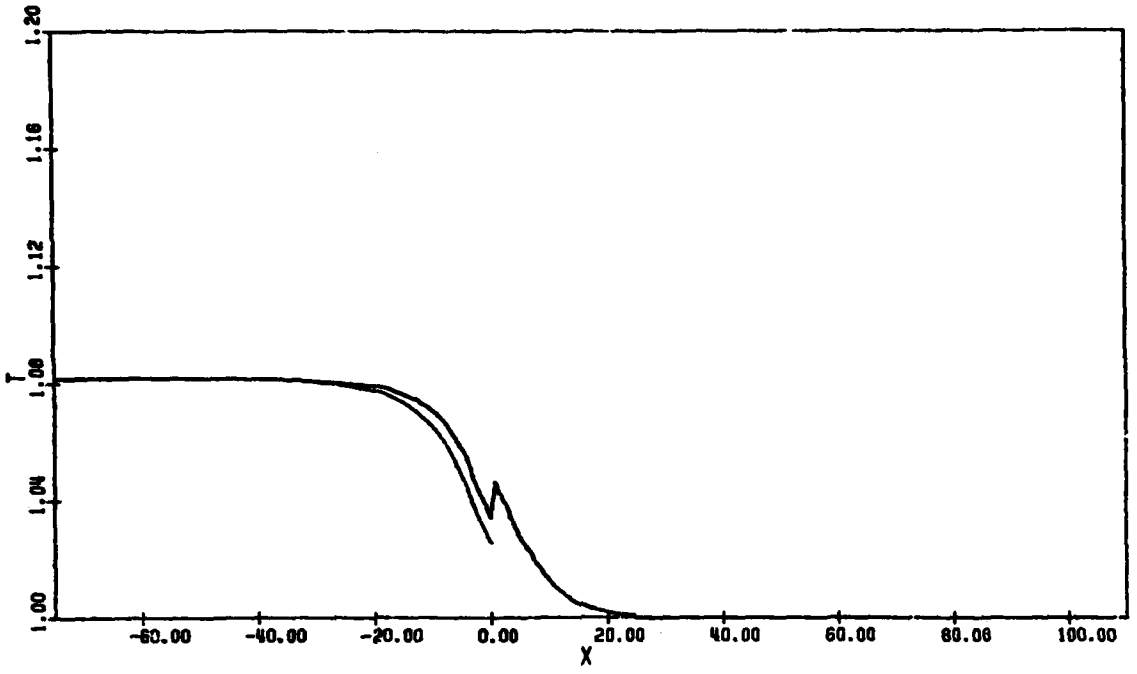

(c) Temperature

(d) Velocity

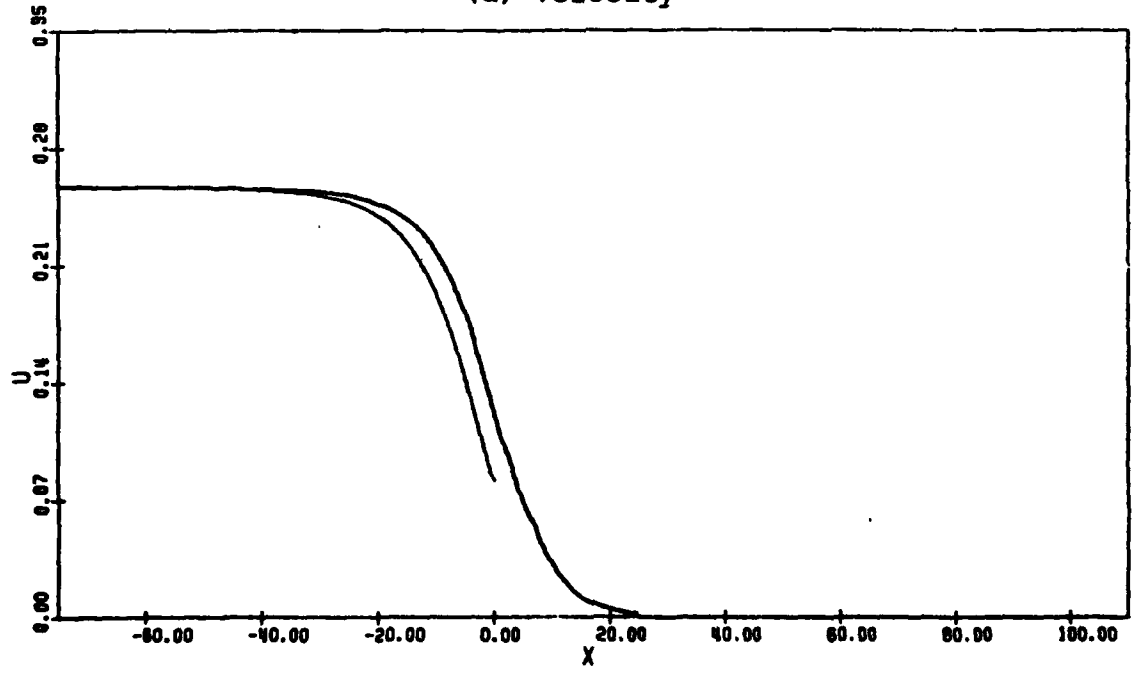

FIG. 29 - CONTINUED.
FLOW QUANTITIES AT $t = 1.87 \times 10^{-3}$ SEC ($p_4/p_5 = 1.584$).
——— GAS, ——— PARTICLES.

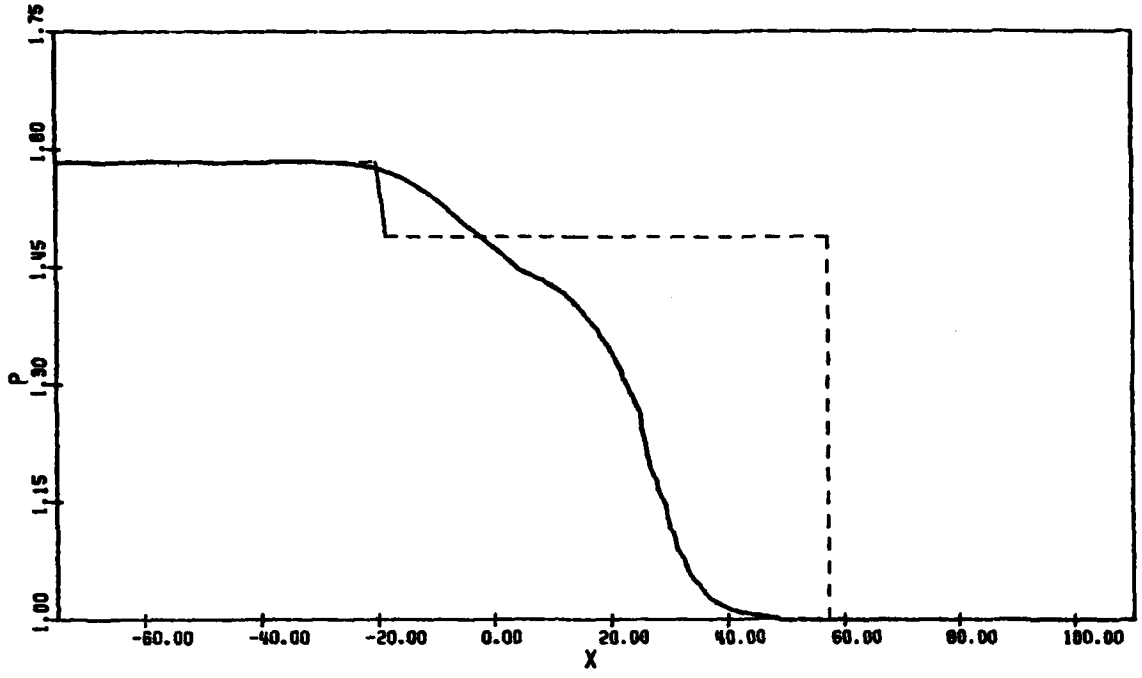

(a) Pressure

(b) Mass Concentration

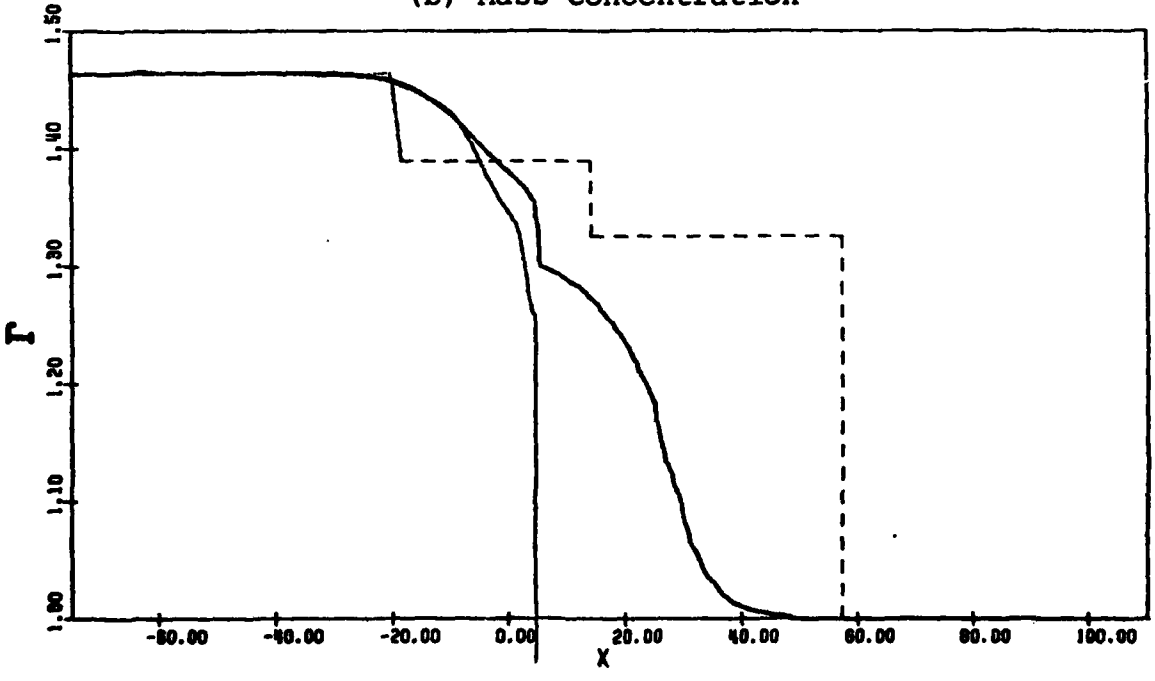

FIG. 30 FLOW QUANTITIES AT $t = 3.74 \times 10^{-3}$ SEC ($p_4/p_5 = 1.584$).
——— GAS, ——— PARTICLES, ------ EQUILIBRIUM FLOW.

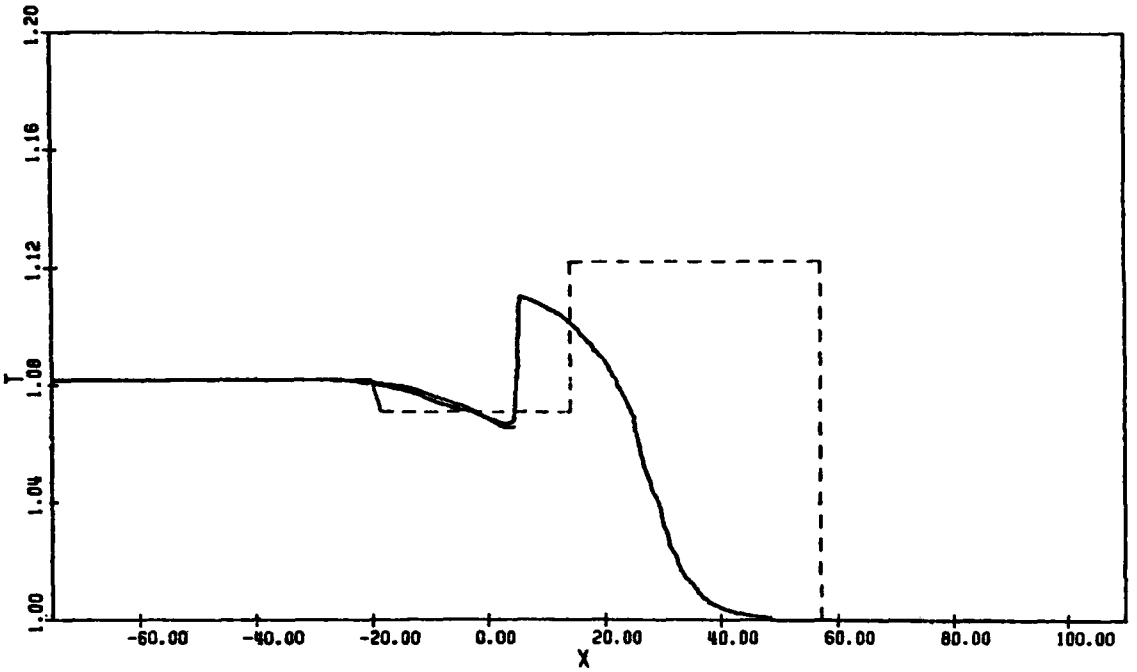

(c) Temperature

(d) Velocity

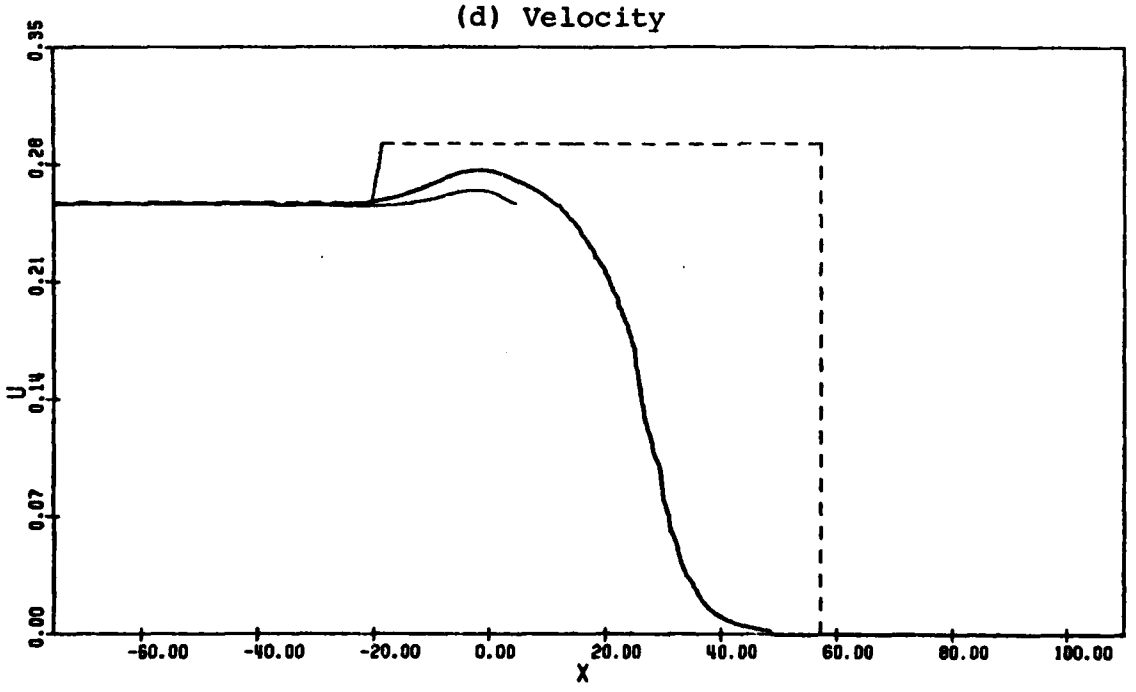

FIG. 30 - CONTINUED.
FLOW QUANTITIES AT $t = 3.74 \times 10^{-3}$ SEC ($p_4/p_5 = 1.584$).
——— GAS, ——— PARTICLES, ------ EQUILIBRIUM FLOW.

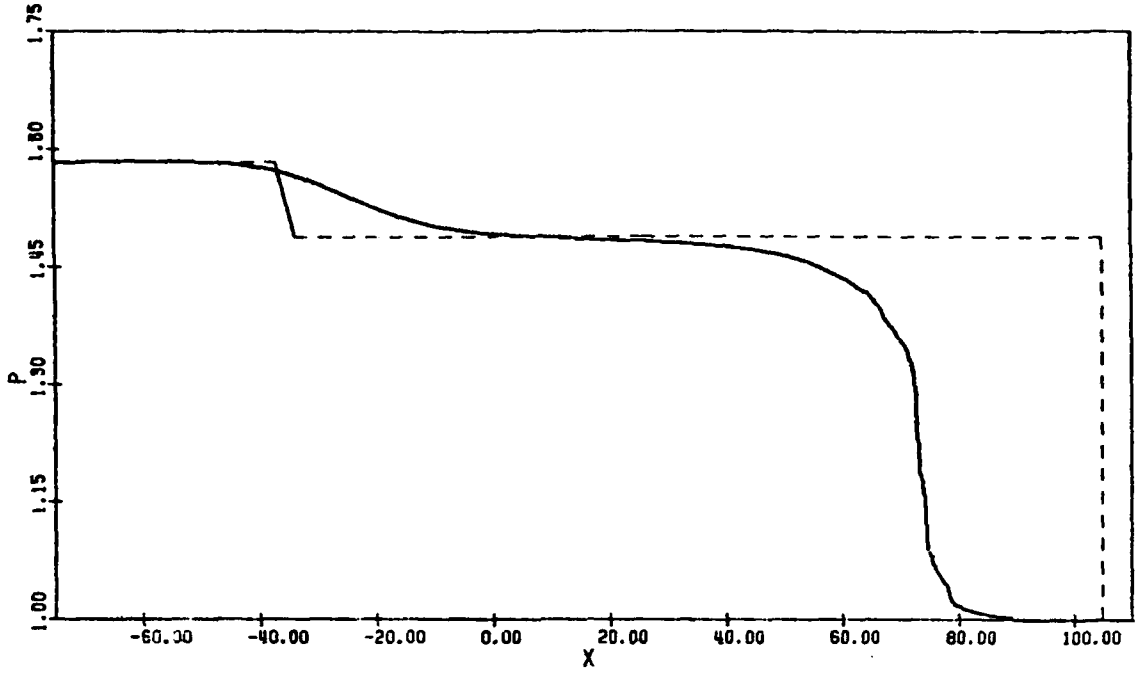

(a) Pressure

(b) Mass Concentration

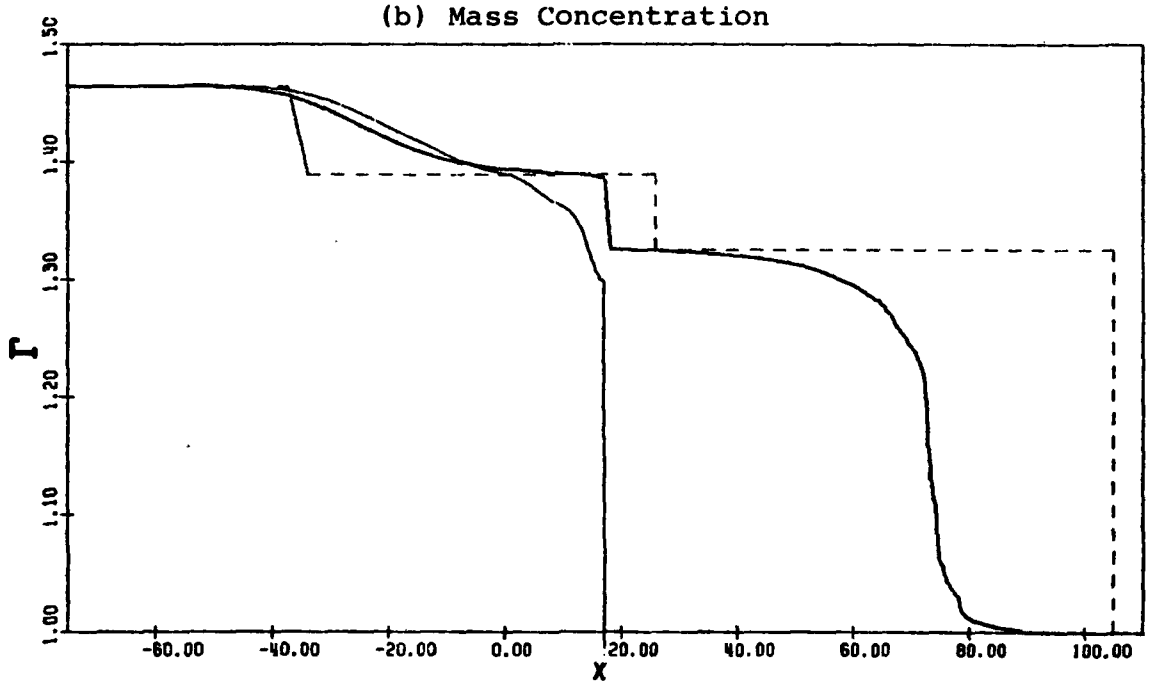

FIG. 31 FLOW QUANTITIES AT $t = 6.86 \times 10^{-3}$ SEC ($p_4/p_5 = 1.584$).
——— GAS, ——— PARTICLES, ------ EQUILIBRIUM FLOW.

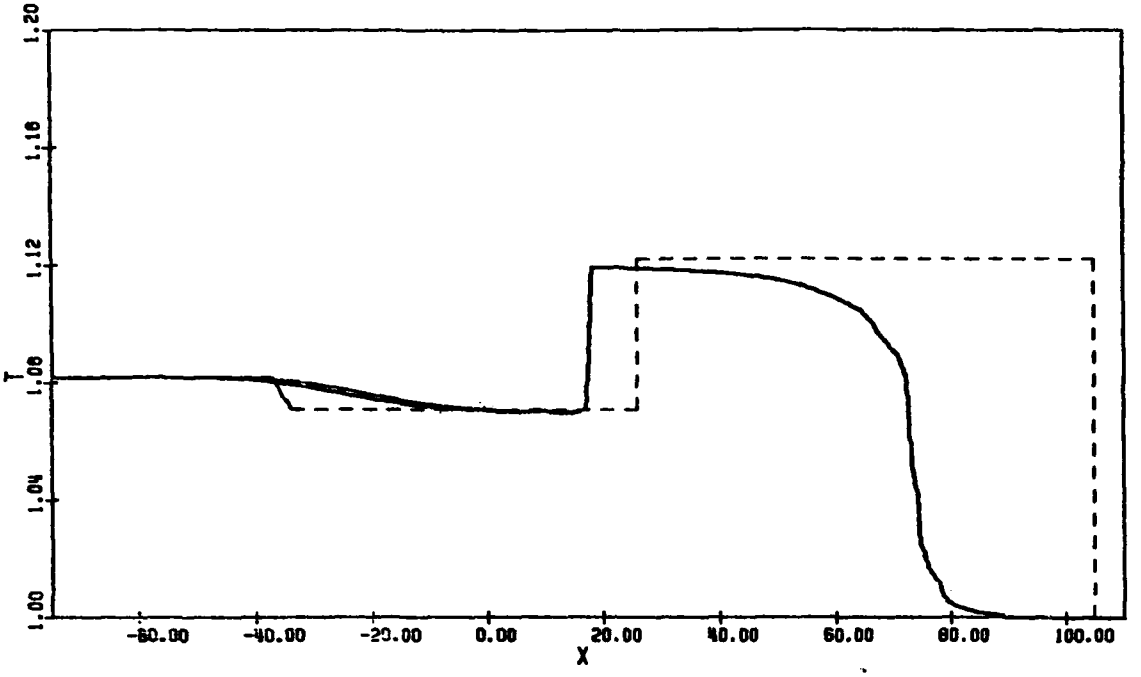

(c) Temperature

(d) Velocity

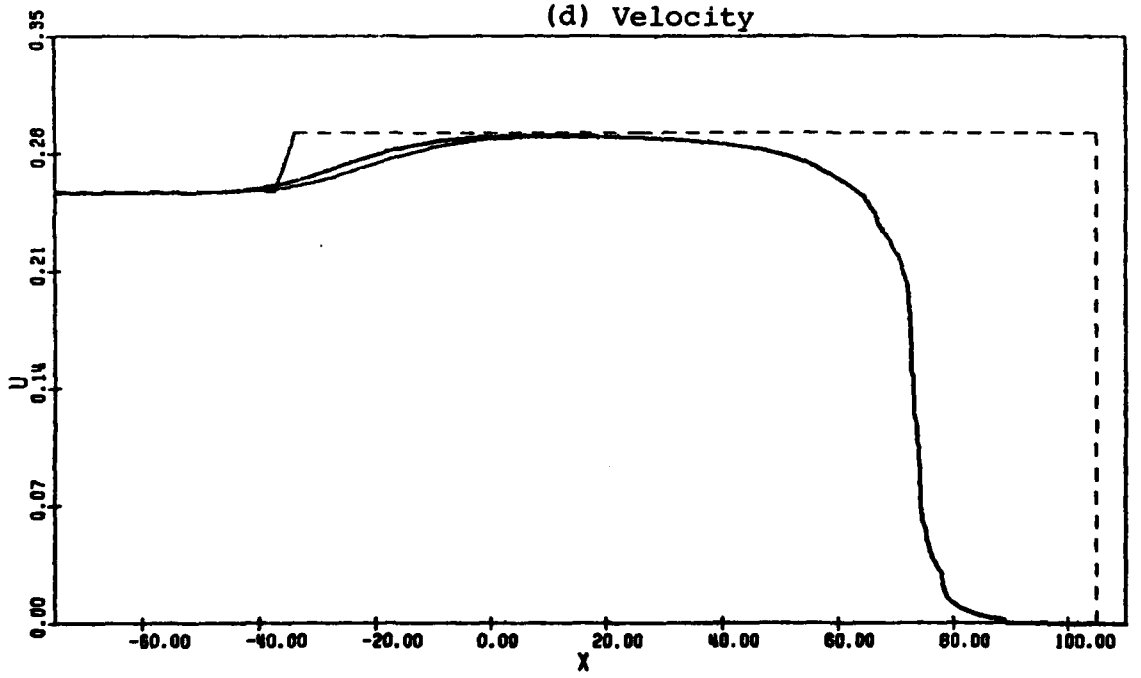

FIG. 31 - CONTINUED.
FLOW QUANTITIES AT $t = 6.86 \times 10^{-3}$ SEC ($p_4/p_5 = 1.584$).
——— GAS, ——— PARTICLES, ------ EQUILIBRIUM FLOW.

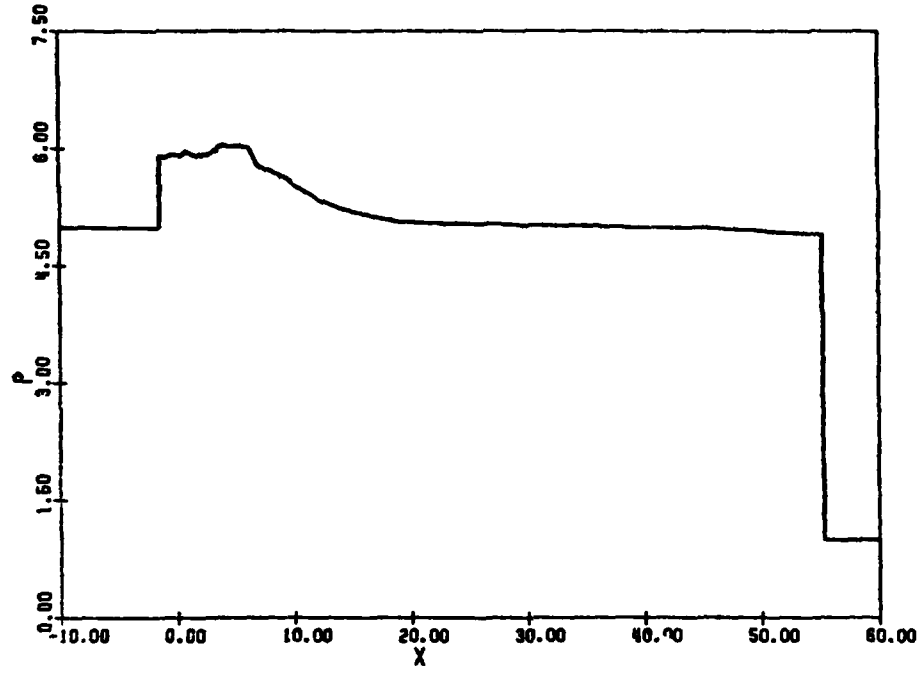

(a) Pressure

(b) Mass Concentration

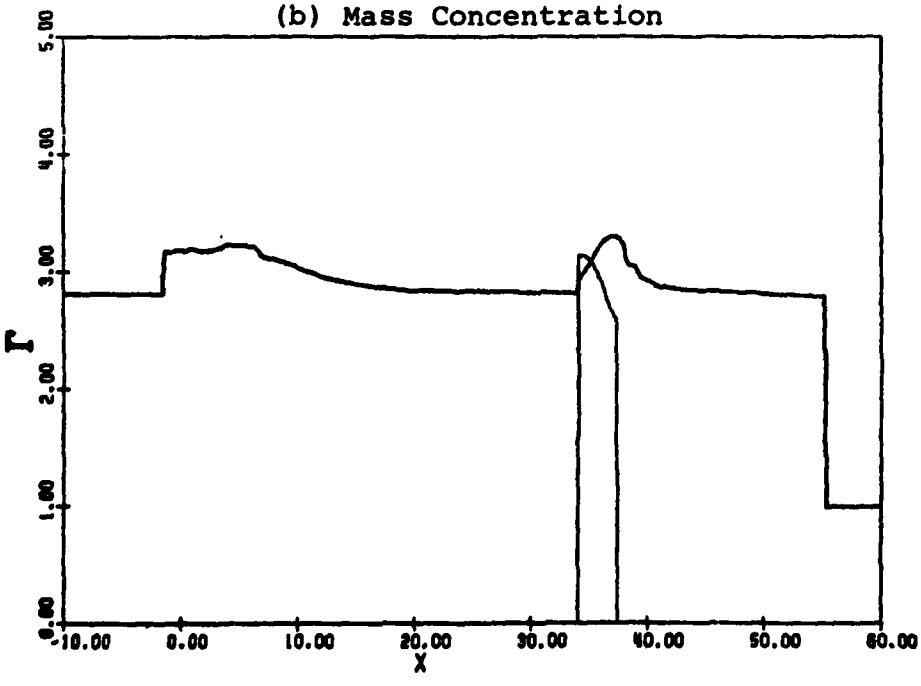

FIG. 32 FLOW QUANTITIES AT $t = 2.18 \times 10^{-3}$ SEC ($p_4/p_5 = 5$, INITIAL LAYER-THICKNESS = 27.2 cm).

——— GAS, ——— PARTICLES.

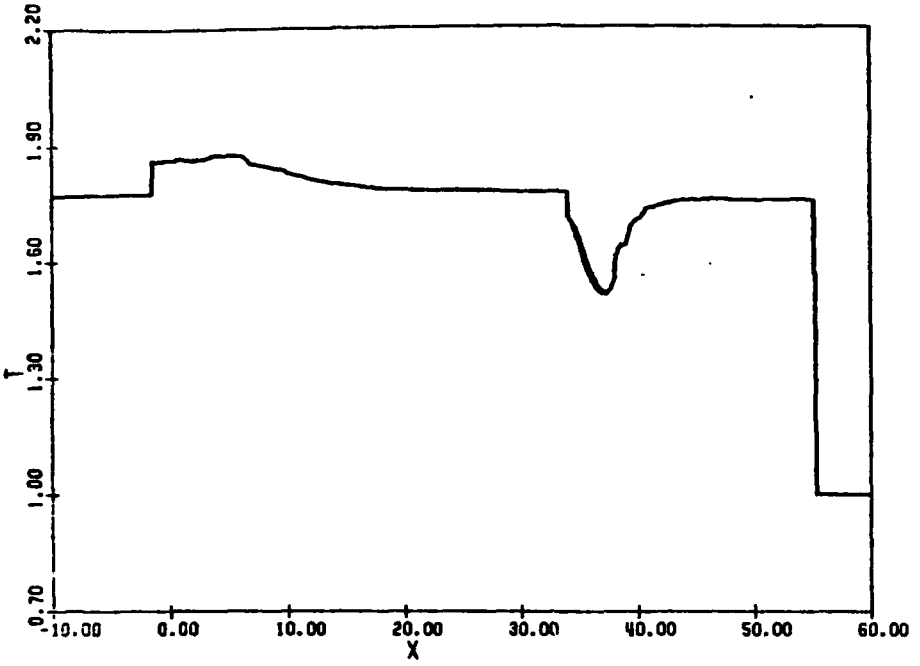

(c) Temperature

(d) Velocity

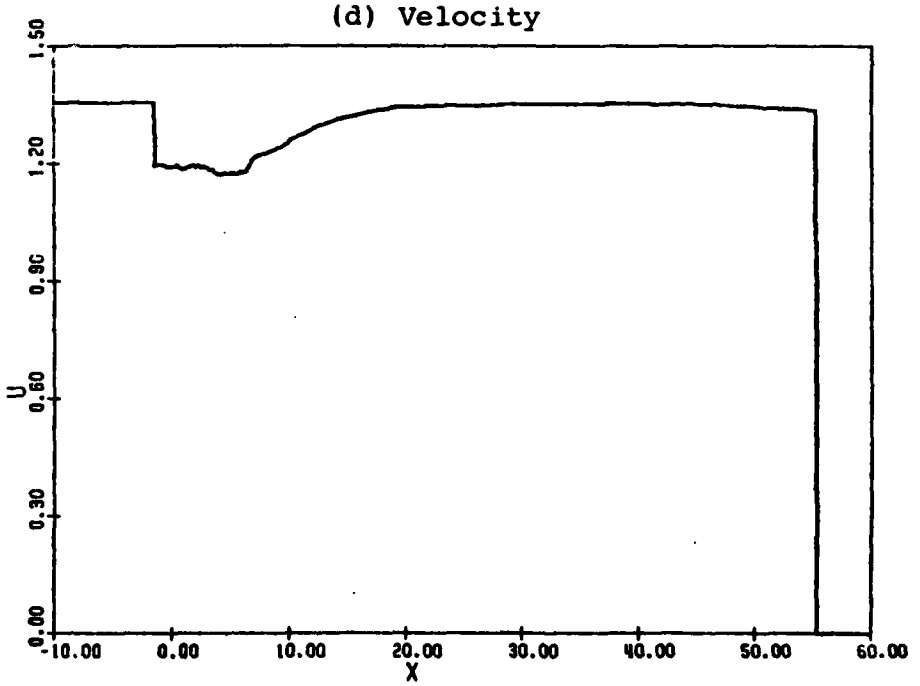

FIG. 32 - CONTINUED.
FLOW QUANTITIES AT $t = 2.18 \times 10^{-3}$ SEC ($p_4/p_5 = 5$, INITIAL LAYER-THICKNESS = 27.2 cm).

——— GAS, ——— PARTICLES.

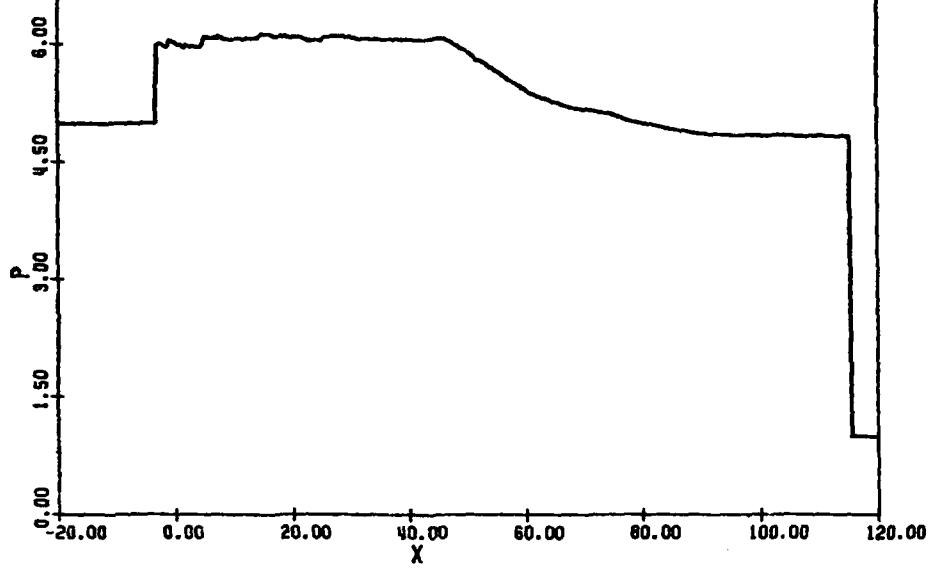

(a) Pressure

(b) Mass Concentration

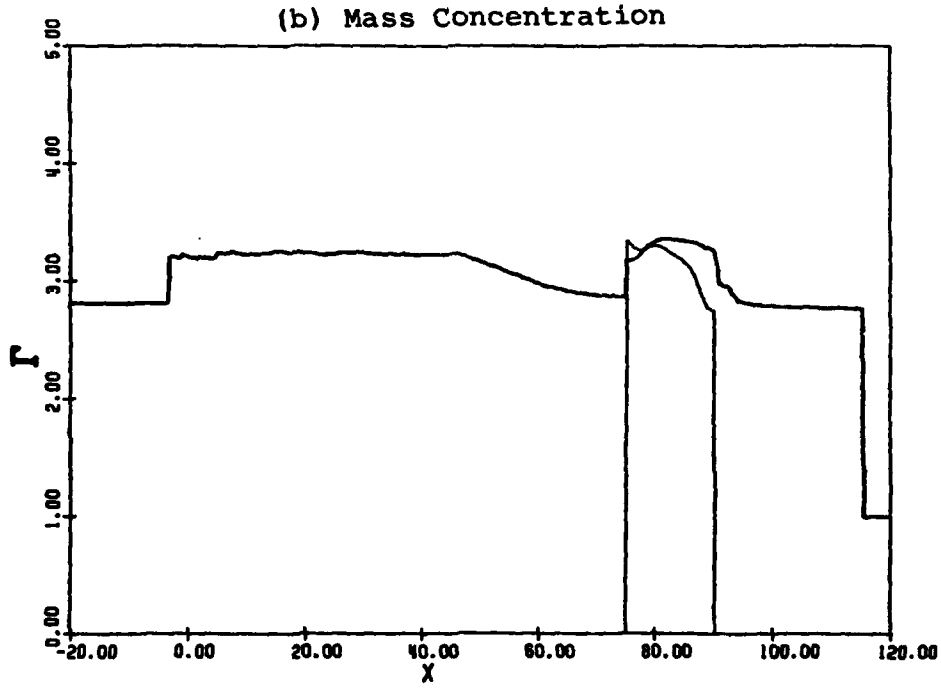

FIG. 33 FLOW QUANTITIES AT $t = 4.99 \times 10^{-3}$ SEC ($p_4/p_5 = 5$, INITIAL LAYER-THICKNESS = 136 cm).

——— GAS, ——— PARTICLES.

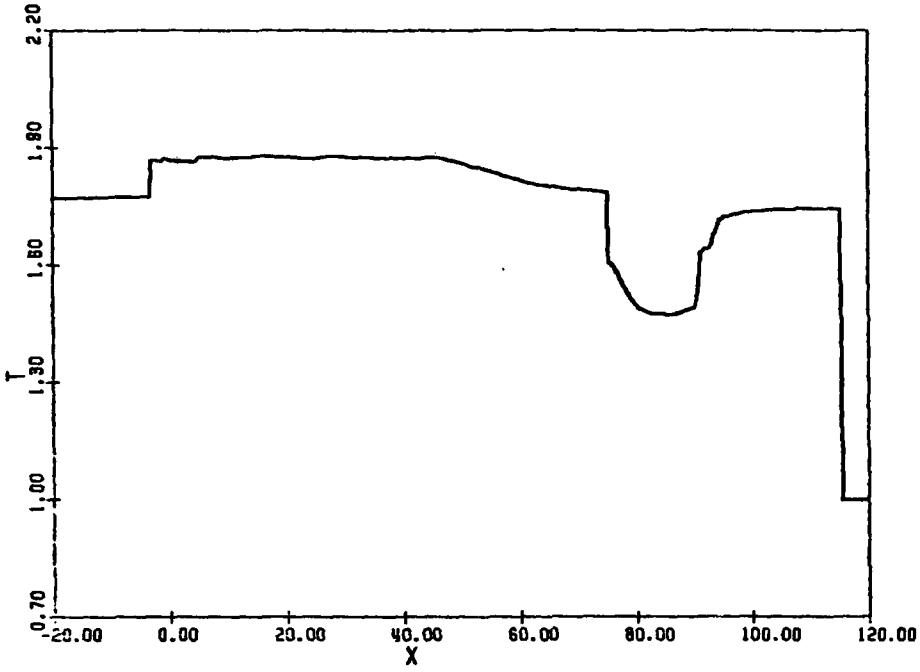

(c) Temperature

(d) Velocity

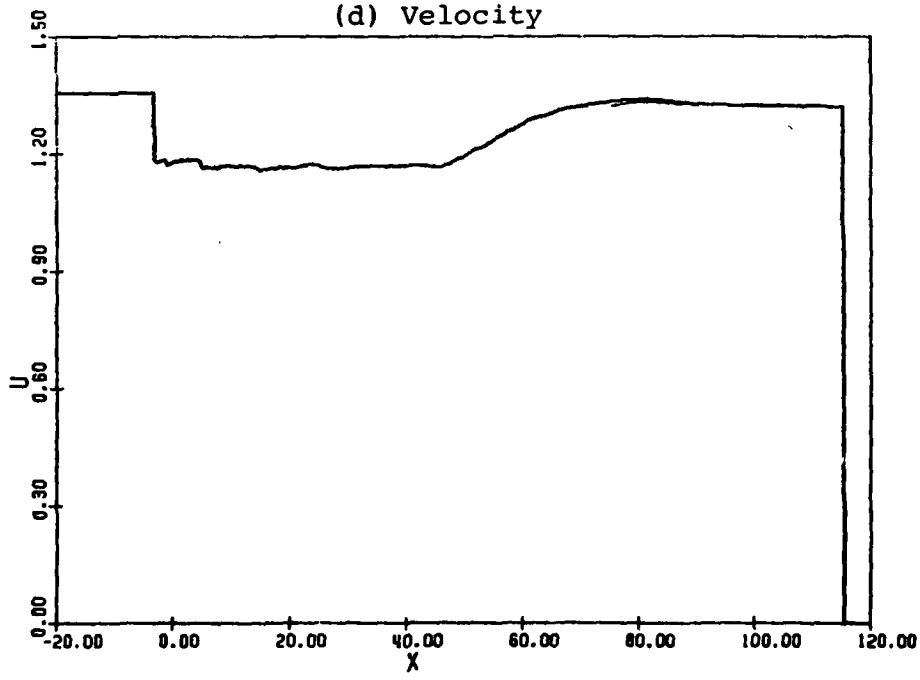

FIG. 33 - CONTINUED
FLOW QUANTITIES AT t = 4.99×10^{-3} SEC (p_4/p_5 = 5, INITIAL LAYER-THICKNESS = 136 cm).

——— GAS, ——— PARTICLES.

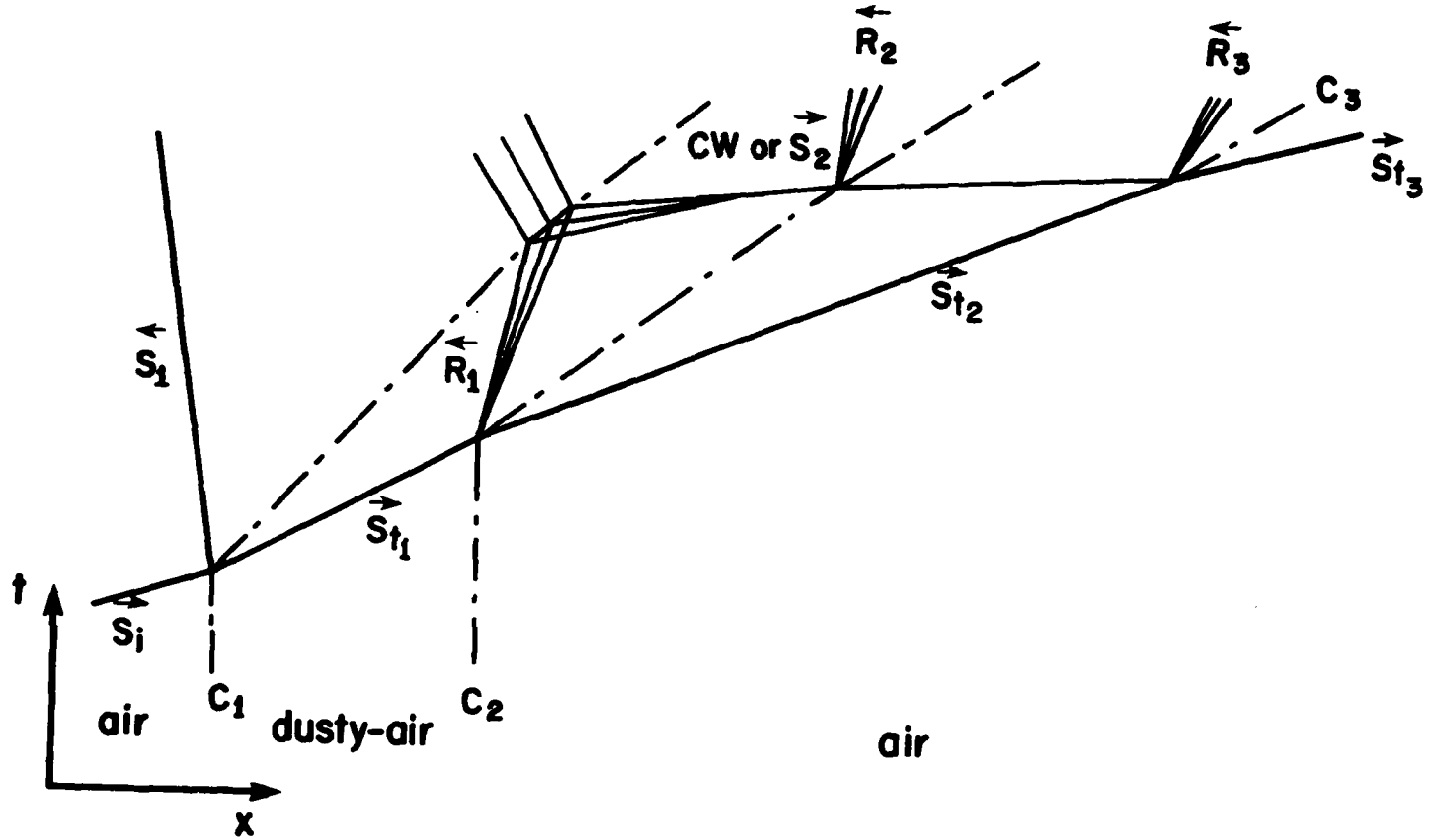

FIG. 34 SCHEMATIC x-t DIAGRAM OF THE PASSAGE OF A SHOCK WAVE THROUGH A DUSTY-AIR LAYER.

S_i: INCIDENT SHOCK WAVE, S_t: TRANSMITTED SHOCK WAVE, C: CONTACT FRONT, S: INDUCED SHOCK WAVE, R: INDUCED RAREFACTION WAVE, CW: COMPRESSION WAVE.

APPENDIX A

RANKINE-HUGONIOT AND ISENTROPIC RELATIONS

We can find the pressure $p_3 = p_2$ in the region between the transmitted shock wave and the reflected wave for a given incident shock pressure ratio p_4/p_5 by solving the algebraic equations (7) or (9). The other flow quantities behind the transmitted shock wave can be obtained then from the Rankine-Hugoniot relations as follows:

$$\frac{\rho_2}{\rho_1} = \frac{1 + (\gamma_1+1)/(\gamma_1-1) \times (p_2/p_1)}{(\gamma_1+1)/(\gamma_1-1) + p_2/p_1} \tag{A1}$$

$$\frac{T_2}{T_1} = \frac{p_2}{p_1} \cdot \frac{(\gamma_1+1)/(\gamma_1-1) + p_2/p_1}{1 + (\gamma_1+1)/(\gamma_1-1) \times (p_2/p_1)} \tag{A2}$$

$$\frac{u_2}{a_1} = \frac{1}{\gamma_1}\left(\frac{p_2}{p_1} - 1\right)\sqrt{\frac{2\gamma_1}{\gamma_1+1}\Big/\left(\frac{p_2}{p_1} + \frac{\gamma_1-1}{\gamma_1+1}\right)} \tag{A3}$$

$$\frac{u_s}{a_1} = \sqrt{\frac{\gamma_1-1}{2\gamma_1} + \frac{\gamma_1+1}{2\gamma_1} \cdot \frac{p_2}{p_1}} \tag{A4}$$

When a shock wave is reflected at the contact surface, the flow quantities behind the reflected shock wave are calculated in a similar way. If the reflected wave is a rarefaction wave, the isentropic relations across the rarefaction wave are given by

$$\frac{T_3}{T_4} = \left(\frac{p_3}{p_4}\right)^{\frac{\gamma_4-1}{\gamma_4}} \tag{A5}$$

$$\frac{\rho_3}{\rho_4} = \left(\frac{p_3}{p_4}\right)^{\frac{1}{\gamma_4}} \tag{A6}$$

Using these relations, we can express the values of the flow quantities in the uniform flow regions behind the transmitted shock wave, the contact surfaces and the reflected wave in terms of the incident shock pressure ratio or shock Mach number.

APPENDIX B

FORMATION OF FULLY-DISPERSED SHOCK WAVES

The variation of the thickness of the shock transition region with time is shown in Fig. B1 for the case of a fully-dispersed shock wave (Figs. 21-23). The shock thickness was defined as the length of the region over which the pressure varies from 10% to 90% of the total pressure jump of the stationary shock wave (Fig. 24). The final thickness is also shown by the dashed line. It can be seen that the transition thickness increases very gradually. It is estimated from Fig. B1 that a stationary shock wave will require a formation time in excess of 11×10^{-3} sec.

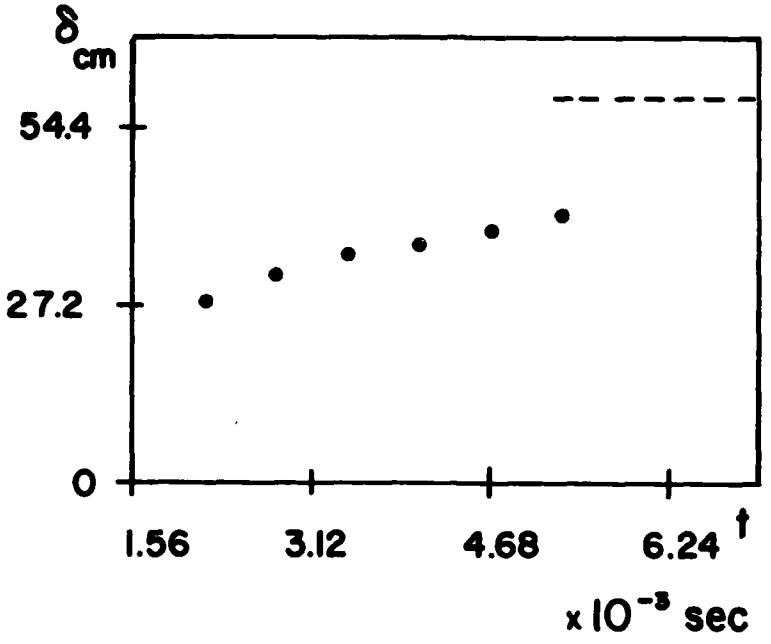

FIG. B1 VARIATION OF THICKNESS OF FULLY DISPERSED SHOCK WAVE WITH TIME. (------ FINAL VALUE).

UTIAS Report No. 252

Institute for Aerospace Studies, University of Toronto (UTIAS)
4925 Dufferin Street, Downsview, Ontario, Canada, M3H 5T6

ON THE PASSAGE OF A SHOCK WAVE THROUGH A DUSTY-GAS LAYER

Miura, H., Glass, I. I. 66 pages

1. Shock-wave refraction at a dusty-gas interface
2. Shock-wave double refraction at a dusty-gas layer
3. Dusty-gas shock waves
4. Dusty-gas shock-tube flows
5. Nonequilibrium dusty-gas flows
6. Shock-wave and contact-front transitions

I. Miura, H., Glass, I. I. II. UTIAS Report No. 252

The flow resulting from the passage of a shock wave through a dusty-air layer is studied analytically and numerically. For the cases treated here, a shock wave is always reflected at the first contact surface separating the pure gas from the dusty layer and a shock wave is transmitted into the dusty layer. The transmitted shock wave is stronger. The criteria for the reflected wave in terms of the properties of the air and dusty layer are obtained based on an idealized equilibrium-gas approximation. Working curves are presented showing the effects of the suspended particles on the resulting flow. Similarly, at the second contact front of the dusty layer, a rarefaction wave is reflected and the transmitted shock wave transmitted into the air is weakened by this nonlinear interaction. The rarefaction wave reflects at the first contact front as a compression wave and proceeds through the layer to refract at the second contact surface where it reflects as a rarefaction wave and a transmitted compression wave. This wave overtakes the transmitted shock wave in air and produces the final transmitted wave, a new contact surface and a weak reflected rarefaction wave. This final emergent shock wave from the dusty air has almost the same strength as the original shock wave entering the layer. A particular case for an initial shock wave pressure ratio of 5 has been chosen to illustrate this type of interaction in detail.

Finally, the time-dependent transition properties through the shock waves, contact surfaces and rarefaction waves were found by solving the equations of motion numerically using a modified random-choice method with an operator-splitting technique. This provides the details for the formation of the idealized equilibrium flows in the dusty-air layer and the reflected and transmitted shock waves in the air surrounding the dusty-air layer.

Available copies of this report are limited. Return this card to UTIAS, if you require a copy.

UTIAS Report No. 252

Institute for Aerospace Studies, University of Toronto (UTIAS)
4925 Dufferin Street, Downsview, Ontario, Canada, M3H 5T6

ON THE PASSAGE OF A SHOCK WAVE THROUGH A DUSTY-GAS LAYER

Miura, H., Glass, I. I. 66 pages

1. Shock-wave refraction at a dusty-gas interface
2. Shock-wave double refraction at a dusty-gas layer
3. Dusty-gas shock waves
4. Dusty-gas shock-tube flows
5. Nonequilibrium dusty-gas flows
6. Shock-wave and contact-front transitions

I. Miura, H., Glass, I. I. II. UTIAS Report No. 252

The flow resulting from the passage of a shock wave through a dusty-air layer is studied analytically and numerically. For the cases treated here, a shock wave is always reflected at the first contact surface separating the pure gas from the dusty layer and a shock wave is transmitted into the dusty layer. The transmitted shock wave is stronger. The criteria for the reflected wave in terms of the properties of the air and dusty layer are obtained based on an idealized equilibrium-gas approximation. Working curves are presented showing the effects of the suspended particles on the resulting flow. Similarly, at the second contact front of the dusty layer, a rarefaction wave is reflected and the transmitted shock wave transmitted into the air is weakened by this nonlinear interaction. The rarefaction wave reflects at the first contact front as a compression wave and proceeds through the layer to refract at the second contact surface where it reflects as a rarefaction wave and a transmitted compression wave. This wave overtakes the transmitted shock wave in air and produces the final transmitted wave, a new contact surface and a weak reflected rarefaction wave. This final emergent shock wave from the dusty air has almost the same strength as the original shock wave entering the layer. A particular case for an initial shock wave pressure ratio of 5 has been chosen to illustrate this type of interaction in detail.

Finally, the time-dependent transition properties through the shock waves, contact surfaces and rarefaction waves were found by solving the equations of motion numerically using a modified random-choice method with an operator-splitting technique. This provides the details for the formation of the idealized equilibrium flows in the dusty-air layer and the reflected and transmitted shock waves in the air surrounding the dusty-air layer.

Available copies of this report are limited. Return this card to UTIAS, if you require a copy.

UTIAS Report No. 252

Institute for Aerospace Studies, University of Toronto (UTIAS)
4925 Dufferin Street, Downsview, Ontario, Canada, M3H 5T6

ON THE PASSAGE OF A SHOCK WAVE THROUGH A DUSTY-GAS LAYER

Miura, H., Glass, I. I. 66 pages

1. Shock-wave refraction at a dusty-gas interface
2. Shock-wave double refraction at a dusty-gas layer
3. Dusty-gas shock waves
4. Dusty-gas shock-tube flows
5. Nonequilibrium dusty-gas flows
6. Shock-wave and contact-front transitions

I. Miura, H., Glass, I. I. II. UTIAS Report No. 252

The flow resulting from the passage of a shock wave through a dusty-air layer is studied analytically and numerically. For the cases treated here, a shock wave is always reflected at the first contact surface separating the pure gas from the dusty layer and a shock wave is transmitted into the dusty layer. The transmitted shock wave is stronger. The criteria for the reflected wave in terms of the properties of the air and dusty layer are obtained based on an idealized equilibrium-gas approximation. Working curves are presented showing the effects of the suspended particles on the resulting flow. Similarly, at the second contact front of the dusty layer, a rarefaction wave is reflected and the transmitted shock wave transmitted into the air is weakened by this nonlinear interaction. The rarefaction wave reflects at the first contact front as a compression wave and proceeds through the layer to refract at the second contact surface where it reflects as a rarefaction wave and a transmitted compression wave. This wave overtakes the transmitted shock wave in air and produces the final transmitted wave, a new contact surface and a weak reflected rarefaction wave. This final emergent shock wave from the dusty air has almost the same strength as the original shock wave entering the layer. A particular case for an initial shock wave pressure ratio of 5 has been chosen to illustrate this type of interaction in detail.

Finally, the time-dependent transition properties through the shock waves, contact surfaces and rarefaction waves were found uy solving the equations of motion numerically using a modified random-choice method with an operator-splitting technique. This provides the details for the formation of the idealized equilibrium flows in the dusty-air layer and the reflected and transmitted shock waves in the air surrounding the dusty-air layer.

Available copies of this report are limited. Return this card to UTIAS, if you require a copy.

UTIAS Report No. 252

Institute for Aerospace Studies, University of Toronto (UTIAS)
4925 Dufferin Street, Downsview, Ontario, Canada, M3H 5T6

ON THE PASSAGE OF A SHOCK WAVE THROUGH A DUSTY-GAS LAYER

Miura, H., Glass, I. I. 66 pages

1. Shock-wave refraction at a dusty-gas interface
2. Shock-wave double refraction at a dusty-gas layer
3. Dusty-gas shock waves
4. Dusty-gas shock-tube flows
5. Nonequilibrium dusty-gas flows
6. Shock-wave and contact-front transitions

I. Miura, H., Glass, I. I. II. UTIAS Report No. 252

The flow resulting from the passage of a shock wave through a dusty-air layer is studied analytically and numerically. For the cases treated here, a shock wave is always reflected at the first contact surface separating the pure gas from the dusty layer and a shock wave is transmitted into the dusty layer. The transmitted shock wave is stronger. The criteria for the reflected wave in terms of the properties of the air and dusty layer are obtained based on an idealized equilibrium-gas approximation. Working curves are presented showing the effects of the suspended particles on the resulting flow. Similarly, at the second contact front of the dusty layer, a rarefaction wave is reflected and the transmitted shock wave transmitted into the air is weakened by this nonlinear interaction. The rarefaction wave reflects at the first contact front as a compression wave and proceeds through the layer to refract at the second contact surface where it reflects as a rarefaction wave and a transmitted compression wave. This wave overtakes the transmitted shock wave in air and produces the final transmitted wave, a new contact surface and a weak reflected rarefaction wave. This final emergent shock wave from the dusty air has almost the same strength as the original shock wave entering the layer. A particular case for an initial shock wave pressure ratio of 5 has been chosen to illustrate this type of interaction in detail.

Finally, the time-dependent transition properties through the shock waves, contact surfaces and rarefaction waves were found by solving the equations of motion numerically using a modified random-choice method with an operator-splitting technique. This provides the details for the formation of the idealized equilibrium flows in the dusty-air layer and the reflected and transmitted shock waves in the air surrounding the dusty-air layer.

Available copies of this report are limited. Return this card to UTIAS, if you require a copy.


DATE
ILME